Merging data streams and remote sensing change detection routines for stand-replacing disturbances in Canada

Elijah Elliot Perez
Department of Natural Resource Sciences
McGill University, Montreal

A thesis submitted to McGill University in partial fulfillment of the requirements of the degree of Master of Science

Table of Contents

1 Abstract

Studying how the Earth's surface changes with time allows conservation managers a better understanding of land cover and composition for research and environmental management. Knowledge of where and when change occurs is important to land management and conservation in Canada. Satellites, like the U.S. Geological Survey's (USGS) Landsat-8, provide a regularly updated sequence of images that are used in various terrestrial monitoring approaches. In the Canadian context, Landsat-8 typically yields one or two clear images each growing season for any given location. The European Space Agency's (ESA) pair of Sentinel-2 satellites, perform marginally better in the Canadian context due to their higher resolution and more frequent revisit times. Separately, either system has limited potential to construct a time-series of clear observations for change detection. However, because of their technical compatibility combining Landsat-8 and Sentinel-2 data can enrich the total pool of clear Earth observations and make it possible to improve terrestrial monitoring approaches. This is particularly helpful for creating annual composite images to represent a growing season across an expansive region that can not otherwise be captured in one image. Using composited data, monitoring programs construct time series for trend-based detection of land-use / land-cover (LULC) change (i.e., disturbance). There are limits to constructing time series of change detection in this way, however. For example, if a method collects images from August 1st plus/minus thirty days to create a single clear image to represent peak growing season vegetation, then changes after this compositing period are not captured. Moreover, because terminal years of the time series lack a subsequent year of observations to confirm trends and values, change detection in terminal years is less certain than intermediate years. To try and resolve these issues, this thesis develops a novel classification method, dubbed Shrinking Latency in Multiple Streams (SLIMS), to combine two open-access satellite image streams (Landsat-8 and Sentinel-2). SLIMS captures the within-year spectral signature of forest disturbance and creates a sequence of near real-time classifications of forest disturbance. Subsequently, this thesis combines SLIMS with the Bayesian Updating of Land Cover (BULC) algorithm to synthesize these unpolished, individually noisy land cover classifications into a series of more accurate land cover classifications. Using a free and accessible cloud-based computing platform (i.e., Google Earth Engine), this work computes a forest change time series at a fine spatial resolution (10 metre) and very fine time slices (~5 days) to provide more detailed information concerning forest disturbances to conservation managers. This thesis discusses the opportunities and challenges of improving annual scale trend-based change detection approaches like the Canadian Forestry Service's Composite to Change (C2C) algorithm, namely in the a) time of compositing and b) the terminal years of a time series.

2 Résumé

L'étude de l'évolution de la surface de la Terre à travers le temps permet aux responsables de la conservation de mieux comprendre la couverture terrestre et la composition du sol pour la recherche et la gestion de l'environnement. Au Canada, le savoir de l'endroit et du moment où les changements se produisent est pertinent à la gestion des terres et aux prises de décisions en matière de conservation. Les satellites, comme le Landsat 8 de l'U.S. Geological Survey (USGS), fournissent des séquences d'images régulièrement mises à jour qui sont utilisées dans diverses approches de surveillance terrestre. Dans le contexte canadien, Landsat 8 fournit généralement une ou deux images claires à chaque saison de croissance pour un endroit donné. La paire de satellites Sentinel 2 de l'Agence spatiale européenne (ESA) est un peu plus performante dans le contexte Canadien en raison de sa résolution plus élevée et de ses périodes de revisite plus fréquentes. Séparément, les deux systèmes ont un potentiel limité pour construire une série chronologique d'observations claires pour la détection des changements. Toutefois, en raison de leur compatibilité technique, la combinaison des données de Landsat-8 et de Sentinel 2 peut enrichir le répertoire total des observations claires de la Terre et permettre d'améliorer les approches de surveillance terrestre. Ceci est particulièrement utile pour créer des images composites annuelles pour représenter une saison de croissance sur une vaste région, qui ne pourrait autrement pas être capturée dans une seule image. En s'appuyant sur ces données composites, les programmes de surveillance construisent des séries chronologiques qui permettent la détection de tendances des changements d'utilisation des terres/couverture terrestre (LULC) (i.e., les perturbations). Il y a cependant des limites à la construction de séries chronologiques de détection de changements de cette manière. Par exemple, si une méthode capture des images à partir du 1^er^ août plus/moins trente jours pour créer une seule image claire pour représenter la végétation de la saison de croissance maximale, les changements survenus après cette période de capture ne sont pas observés. De plus, étant donné que les années terminales de la série chronologique n'ont pas une année d'observations subséquente pour confirmer les tendances et les données, la détection des changements dans les années terminales est moins certaine que pour les années intermédiaires. Pour tenter de résoudre ces problèmes, cette thèse développe une nouvelle méthode de classification baptisée Shrinking Latency in Multiple Streams (SLIMS) pour combiner deux sources d'images satellites libre accès (Landsat-8 et Sentinel-2). SLIMS capture la signature spectrale intra-annuelle des perturbations forestières et crée une séquence de classifications en temps quasi réel des perturbations forestières. Par la

suite, cette thèse combine SLIMS avec l'algorithme Bayesian Updating of Land Cover (BULC) pour synthétiser ces classifications brutes et individuellement floues de la couverture terrestre en une série de classifications plus précises. À l'aide d'une plateforme informatique gratuite et accessible en ligne (i.e., Google Earth Engine), ce travail calcule une série chronologique de changements forestiers à une résolution spatiale fine (10 mètres) et des tranches de temps très fines (~5 jours) pour fournir des informations plus détaillées concernant les perturbations forestières aux gestionnaires en conservation. De plus, cette thèse discute des opportunités et des défis de l'amélioration des méthodes de détection de changements à l'échelle annuelle comme l'algorithme Composite to Change (C2C) du Service canadien des forêts, à savoir dans a) le temps de composition et b) les années terminales d'une série chronologique.

3 Acknowledgements

The support of my supervisor Jeff Cardille was instrumental in the completion of this thesis. Thank you for your constant enthusiasm about this work. Thanks for being so patient and understanding with me, particularly when things got bad. You got me back on track.

This project was done with the guidance of the lovely people of the Pacific Forestry Centre. Thank you, Joanne White, Mike Wulder, and Txomin Hermosilla for keeping me oriented in the right direction, moving forward, and pushing me to always be writing. Thank you, Guillaume Laroque for the crucial GIS support just when I need it. You've got a big brain and a big heart, helping everyone the way you do.

Funding from NSERC, the Pacific Forestry Centre and the McGill University Department of Natural Resource Sciences kindly supported my studies.

Thank you to all of my lab mates (in no particular order): Morgan, Talia, Sara, Bryant, Flavie, Eidan, Rylan, Patricia, Kash, Eliza. Without your company the lab would have just been that small room with computers. Once the pandemic hit, it was such a blessing to have kept in touch with video calls and virtual lab sessions. "It's just going to be another two weeks."

Thank you, Claudia Aldecoa, for that lovely hang out in that tree all those years ago. You planted the curiosity of environmental studies in my head that day.

Thank you, Emily Jacobson, for editing so much of my writing but also thanks for just always being there to talk or share a groan and a laugh over a terrible joke. You're one of my best friends.

Enormous thanks to Klara Winkler (*Doctor!*) who helped me plan, write, edit, and submit my thesis *on time*! Thank you for keeping me in my chair, at my desk, and getting those words out. It is no exaggeration to say this would have not been possible without your endless support every step of the way.

To my parents, Beverley, and Fernando, I love you so much. Thank you for all the support from way over there in Mississauga, and for driving all the way over here to visit me as often as you did and thanks for all the delicious baked goods. Thank you for encouraging me to do this and believing that I could. This is for you.

4 Preface

4.1 Thesis Format

This thesis is presented in a monograph format, as per McGill University regulations following the requirements of Library and Archives Canada. References cited are listed at the end of the thesis. Tables and figures are found within the body of the text as well as in Appendix A.

4.2 Contribution of authors

This thesis was written by Elijah Elliot Perez under the supervision of Jeffrey A Cardille. EEP and JAC wrote the SLIMS JavaScript code to run in Google Earth Engine. EEP managed data, analysed data, interpreted data, and constructed all figures and graphs. JAC created the BULC algorithm and assisted with editing the thesis.

5 Introduction

5.1 Overview

Around a third of the planet's land surface is covered by forests (Carlowicz, 2012). They are sentinel indicators of climate change such that effects are visible across a range of parameters including: stand make-up, natural disturbance rates, soil qualities, and others (Natural Resources Canada, 2015). In addition, they provide habitat for species, are the second largest carbon sink after oceans, produce natural resources for humans, and have economic and cultural significance (*Forest Ministerial Progress Report on the Pan-Canadian Framework on Clean Growth and Climate Change*, 2020). Unsurprisingly, forests have been, and continue to be, central to environmental policies and recommendations globally, such as Article 2 of the United Nations (UN) Kyoto Protocol (Kyoto Protocol to the United Nations Framework Convention on Climate Change, 1998). It compels signature parties to sustainable forest practices, afforestation, and reforestation efforts in the furtherance of their emissions limitations and reductions. Additionally, the UN Convention on Biological Diversity closely links land degradation to biodiversity loss and singles out forest conservation as critical in halting it (*UNCCD Report: LDN Contributing to Global Biodiversity Conservation Goals*, n.d.).

As forests are so important, monitoring their status is of interest for decision-makers in governments, industry, and communities in order to understand their dynamics (Gillis, 2001). Canada possesses 9% of the worlds forests (*Global Forest Resources Assessment 2020*, 2020) and within the Canadian context, the development of methods to effectively monitor and subsequently manage forests, echoes the recognition of forests' ecological, social, and economic value. Canada's international commitments are interlinked with domestic policy initiatives and agreements such as the Federal Sustainable Development Strategy (Canada & Environment and Climate Change Canada, 2021), the Pan-Canadian Framework on Clean Growth and Climate Change (Canada & Environment and Climate Change Canada, 2016) or the 2020 Biodiversity Goals and Targets for Canada (Canada & Environment and Climate Change Canada, 2019). Thus, supported by comprehensive policy frameworks, conservation managers and academics continue to question the 'where', 'when', 'why', and 'how' natural (e.g., fire) and anthropogenic (e.g., harvest) changes, also called disturbances, are occurring in forests (Schroeder et al., 2011; White et al., 2017). These policy developments are indispensable, as forests are changing at an increasing rate due to global climate change (Arneth et al., 2019), moreover forest fire disturbances are increasing, and will continue to increase due to climate change (Hall et al., 2008; Zhu et al., 2020).

Both researchers and the forest industry rely on disturbance monitoring to accurately map and quantify stand losses and forecast changes (DeFries et al., 2006; Hermosilla et al., 2016) and these changes can include the ecosystem's ability to capture and sequester carbon (Huang et al., 2010; Schroeder et al., 2011; White et al., 2017). However, the predominant method of monitoring, remote sensing, has been subject to technological limitations (DeFries et al., 2006). These can include noise inherent in every sensor, compositing issues, and time lags between a disturbance and its detection for mapping. In particular, though improvements have been made, this delay between a disturbance and its capture is a lingering problem. New technologies like synthetic satellite constellations and powerful distributed computing systems can contribute to change detection and monitoring improvements allowing for more accurate and more timely capture of forest change (Goodenough et al., 2008).

In Canada, forests cover approximately one-third of the overall land area (about 347 million hectares). These massive, protected, and often remote regions are frequently subject to dramatic natural or anthropogenic changes before they are eventually re-vegetated (Schroeder et al., 2011; White et al., 2017). Observing these dramatic changes can be costly, and difficult to monitor if they occur in remote areas, so while most of these forests are provincially and privately managed, the Canadian Forest Service works with the provinces and territories to maintain these valuable resources (Cohen et al., 2017; Natural Resources Canada, 2015).

Fires and harvest are among the most important changes in Canada's forests (Hall et al., 2008; Schroeder et al., 2011). Large-magnitude short-duration changes like crown fires (i.e., high-intensity fire that kills most vegetation as it ascends from forest floor to canopy) and logging (aka harvest) have the most dramatic effects on the forest's structure and occur relatively abruptly (Wulder et al., 2020). These are termed 'stand-replacing' changes because while they will completely remove a stand of trees, given enough time the area returns to a naturally forested state (Schroeder et al., 2011). Effective monitoring of forests requires differentiation between the causes of disturbances because aboveground biomass, carbon sequestration, and forest recovery are all affected differently by clear-cut logging as compared to fires (Schroeder et al., 2011).

Monitoring forests and their changes in Canada via satellite has been limited by image resolution (Barrette et al., 2018; DeFries et al., 2006; Wulder et al., 2019). For example, a fine spatial resolution (e.g., 10m) in satellite imagery is one way to capture forest disturbances with greater accuracy as the shape and position are truer to the phenomena on the ground (Griffiths et al., 2019). More importantly for early identification of disturbance, a fine spatial resolution (e.g., 10m instead of 30m) means smaller areas of trees are grouped together into a single pixel so each tree is a greater proportion of the total area (DeFries et al., 2006; Hall et al., 2008). Because one pixel's signal is an average representation of everything inside of it, a fewer number of trees must be disturbed before the average reflectance changes. This means that an active disturbance becomes a significant proportion of a smaller pixel more quickly, influencing its values sooner than it would for a larger one (Crowley et al., 2019; Wulder et al., 2018).

Unfortunately, creating and manipulating spatial data always involves tension between several of its inherent properties: spatial resolution, spectral resolution, total extent (and increasingly, temporal depth) (Comber & Wulder, 2019; Gorelick et al., 2017; Zhu, 2017). Each contribute to the digital size and complexity of the data, and oblige the user to use increasingly powerfully computers to manipulate it or sacrifice some desirable qualities for others (White et al., 2014). These elements can result in cost, and time limitations for analysis work performed at a global, federal, or even provincial level (Zhu, 2017).

In Canada, the Canadian Forest Service (CFS) produces annual, spatially explicit land cover classification maps. These maps have a consistent set of classes nationally while providing a spatial resolution of 30m x 30m pixels (Hermosilla et al., 2016, 2018). The CFS gathers imagery from NASA's Landsat-7 and -8 satellites from the 1st of August plus/ minus thirty days (the peak forest growing period) across Canada (White et al., 2014). Subsequently, the CFS follows a Best Available Pixel (BAP) approach, where they create a mosaic image using the clearest pixel from all images collected in the observation period. This means that for every calendar year one image is created that represents the peak growing season status of forest in Canada (Hermosilla et al., 2018). Following the trends in each pixel's spectral signatures over time, the CFS creates vast land cover maps, capable of capturing subtle inter-annual changes through their Composite to Change (C2C) algorithm (Hermosilla et al., 2016; White et al., 2017).

Classification maps have two main types of errors: commission and omission. Commission describes a reference point's inclusion in the wrong class i.e., a truly unburned location that is classified as burned. An omission error occurs when a burned location is shown on the map to be unburned. This means that a commission error in one class is an omission error from another class (*ENVI Confusion Matrix*, 2022).

Because of this single composite image per year, two kinds of omission errors arise. In the first case, large-magnitude, short-duration changes that occur after the observation period are only detected the following year. This means the change would be attributed to the wrong year. However, if there is uncertainty in *that* data then an additional year is required for confirmation. The second category of errors in classification are those caused by noise (e.g., clouds, cloud shadow), or low-confidence pixel values (e.g., pixels adjacent to noise), or have no data available and accordingly have ‘no-value’. These kinds of issues lead to uncertainty in the data and though these data ‘gaps’ can be ‘patched’ by extrapolating from prior years, this solution can also cause problems. Since it is necessary to produce high confidence classification maps, it is prudent to wait until the following year, and employ interpolation instead. This leads to delays of one to two years for important spatial data products, which is too slow to enable timely management or research (Gillis, 2001; White et al., 2014). Therefore, there is a need for rapid disturbance detection / confirmation, to enable the dating of the occurrence to be more precise than just once a year (and at the conclusion of said year) and allow managers and decision-makers to react more quickly to changes (Hall et al., 2008; Li et al., 2011).

5.2 Problem Statement

Given the limitations to the current Canadian Forest Services’ approach to forest monitoring; a) time of image compositing and b) accuracy in terminal years of time series), and the technological developments in remote sensing, there is an opportunity to improve the current method of time-series based change detection. This will help decision-makers and managers to react in a timelier fashion to forest disturbances in order to maintain forest resources and is therefore important to all stakeholders.

5.3 Thesis Objectives

The overall objective of this thesis is the improvement of a time series change-detection algorithm for forest monitoring in the Canadian context by creating an algorithm that uses Earth observation imagery from multiple satellites to shorten the effective sensor revisit time and expand the observation period to more of the Canadian forest growing period (May to October) (White et al., 2014). In this thesis, the objective is achieved through the creation of a novel algorithm that makes iterative classifications of land cover to generate a high-confidence year-end classification map of short-duration, large-magnitude forest disturbance (i.e., harvest and fire) within UTM Zone 10N in 2017. I do this by combining two algorithms: SLIMS (Shrinking Latency in Multiple Streams) and BULC (Bayesian Updating of Land-Cover). The SLIMS algorithm, which is purpose-built for this project, classifies Landsat and Sentinel data streams in real time by iteratively evaluating a typical forest status index thus rapidly creating a series of classifications. It responds to the need to expand the timeframe of Earth observation while distinguishing between the disturbance-drivers of interest in near-real time. Then an existing algorithm, BULC (Cardille & Fortin, 2016), applies Bayes' theorem to the series of SLIMS classifications and estimates a most likely class per-pixel, per-iteration, given the prior classifications as evidence. This minimizes omission and commission errors. It combines classifications derived from independent sensors thereby leveraging the highest resolution available in any sensor grouping while effectively decreasing the time between repeat observations of any point on the landscape. This combination of the SLIMS and BULC algorithms would improve an annual scale trend-based classification's ability to capture large-magnitude, short-duration change in forests in the year they occur.

5.4 Research Objective

This exploratory work focused on scripting (software development), wherein I develop an algorithm to rapidly detect forest disturbance in densely vegetated pixels. I also explore whether data from two open-access Earth observation satellites can be interwoven to increase the amount of available imagery. This would add confidence to the series of derived classification maps that distinguish harvest from fire disturbance within the same year or early in the subsequent year. This algorithm would make use of an observation timeframe of six months (May to October) up from two months (July and August). Additionally, this BULC-SLIMS intra-annual understanding of change shortens the period required to confirm national-scale synoptic annual change maps,

6 Literature Review

In this section, I will present the current academic discourse on forest environments in general terms (section 6.1), remote sensing (6.2), and how remote sensing can be leveraged for forests and disturbance observation (6.3).

6.1 Introduction to Forests

Forested lands are important to humans everywhere, either directly or indirectly. The United Nations Food and Agriculture Organization (FAO) defines forest as: "Land spanning more than 0.5 hectares with trees higher than 5 meters and a canopy cover of more than 10 percent, or trees able to reach these thresholds in situ." (*Terms and Definitions*, 2020, p. 4). Canada has 9% of the world's forests and they cover as much as two thirds of the land in the country (Natural Resources Canada, 2014a, 2015; White et al., 2017; Wulder et al., 2019). Canadian forests vary in their composition of coniferous and deciduous tree species, and can also include shrubs, and wetlands (Wulder et al., 2020). Like other forests, Canadian forests experience disturbances like fires, high wind speeds, and seasonal temperature variability (Wulder et al., 2020). These complex and dynamic ecosystems provide or have the potential to provide ecosystem services, to serve as economic resources, and to be of sociocultural importance (Wulder et al., 2020). Globally, forests are the second largest carbon sink after oceans and cover a third of the land's surface (*Forest Ministerial Progress Report on the Pan-Canadian Framework on Clean Growth and Climate Change*, 2020).

6.1.1 Forests and Humans

Humans depend on forests for the ecosystem services they provide (Dhar et al., 2016). They guard against drought, filter groundwater, contribute oxygen to the atmosphere, are a source of timber, and act as a carbon sink (Caputo et al., 2016; Felipe-Lucia et al., 2018; Lawrence et al., 2022). Trees and other woody vegetation send roots into the soil which helps mitigate erosion, and encourages interconnected webs of microscopic life, known as microbiomes, to develop (Baldrian, 2017; Hua et al., 2022). These microbiomes help cycle nutrients and water in the soil which further enhances the soil's capacity to support vegetation (Baldrian, 2017; Lawrence et al., 2022; Schoenholtz et al., 2000). That vegetation can then provide nutrients and support faunal species of all kinds which in turn promotes the resilience of the ecosystem those creatures rely on.

Forests are a major part of the global carbon cycle because they both capture carbon from the atmosphere as they grow and develop (i.e., photosynthesis), and release carbon to the atmosphere as they undergo natural processes like wildfires (Lawrence et al., 2022; Wulder et al., 2020). If forests are managed in a way that encourages their growth, then this management approach is helpful to mitigating climate change by better capturing carbon (Felipe-Lucia et al., 2018; Hua et al., 2022; Wulder et al., 2020).

In Canada, forests are a part of the idealized image of the country. Forests are a part of popular culture, featured in music, television, and film. Enjoying their esthetics and recreational activities is part of what it means to 'be Canadian' (Natural Resources Canada, 2014a). Indigenous communities across the country have lived on and shared a spiritual connection with the land for generations before colonization (Alper & Salazar, 2000, p. 124). For example, on the Pacific coast First Nations have used the forest floor as a source of many traditional foods like wild berries. They also use forest species such as large red cedar trees (*Thuja plicata*), for traditional tools and cultural / artistic expression (Sutherland et al., 2016).

The Canadian forestry sector employs over 200,000 people and in 2014 was 1.2% of Canada's GDP, or $22 billion CAD (Statistics Canada, 2018). The forestry sector is composed of three main sub-sectors. (i) Forestry and logging, which cut and move trees to lumber facilities, (ii) solid wood manufacturing which includes lumber for both domestic and export consumption, and (iii) pulp and paper industries which produce all manner of processed fiber products e.g., paper or cardboard (Natural Resources Canada, 2020; Statistics Canada, 2018). While the majority of exports go to the United States, Canadian lumber products are used all over the world (Natural Resources Canada, 2014b).

Depending on management, one might create favourable conditions for severe fire, diseases, and pests (Dhar et al., 2016; Felipe-Lucia et al., 2018). Since the early 2000's, mountain pine beetles have expanded exponentially in western Canada as historical forest management led to a higher overall proportion of pine trees (*Pinus* spp.) in the forest composition (Dhar et al., 2016). The increase of mountain pine beetles led to extensive tree mortality to such an extent that other aspects of the forest, like soil quality, may have been disturbed or negatively impacted (Baldrian, 2017; Hall et al., 2008).

6.1.2 Forest Disturbance

Forests undergo changes in their vegetative status in response to changes in climate and disturbances such as varying levels of precipitation from annual cycles in large weather systems (Cohen et al., 2017; Natural Resources Canada, 2013). Forest disturbances can have a great impact on the ecosystem's cycles and species composition. Despite this, disturbances in the landscape are not generally negative and do not necessarily result in a loss of vegetation volume

(Whitman et al., 2018; Zhu et al., 2020). Forest disturbances can be described by the rate at which they occur, and the magnitude of their impact on a forest's status (Hermosilla et al., 2015). Here I group disturbances in terms of their progression as either slow or fast, and as having a small or large impact on altering the ecosystem. Large magnitude disturbances are considered 'stand-replacing' changes because they completely remove a stand of trees, though the area typically returns to a vegetated state (Schroeder et al., 2011).

Table 1 Examples of forest disturbances organized by their magnitude or size of their impact, and their rate of change or how quickly they occur.

		Rate of Change	
		Slow	Fast
Magnitude of Change	Small	Annual shift in precipitation	Small fire, selection harvest
	Large	Bark beetle infestation	Crown fire, clearcut harvest

Consider a gradual decrease in annual precipitation as an example of slow disturbance with a small impact. Less precipitation year after year might mean that less total water is available to plants in the soil. If some plants have shallower root systems than others, they may receive less water (Lawrence et al., 2022; Schoenholtz et al., 2000). Plants that do not receive as much water as others may not thrive as well as those that do and may have less stored resources for the following year. This difference in water availability can bring about a gradual change in forest health such that it may only be perceived at an annual scale over many years.

In contrast, a pest species invasion is a slow-acting disturbance that can impose a large change to a forest landscape. Bark beetles, for example, can severely harm tree health over a large area but do so gradually over the course of years (Dhar et al., 2016; Ministry of Forests, n.d.). An infestation can kill entire stands of trees and even make them unusable as lumber products. Despite this damage these insects are still a part of an ecological cycle that can help a forest stand by opening gaps in an established forest canopy, allowing the understory to receive more sunlight.

In the forest landscape, fires are abrupt changes but vary in their intensity and impact i.e., crown fires which are large disturbances and smaller understorey fires, which are small disturbances (Hall et al., 2008; Holsinger et al., 2021). Crown fires exhibit much higher temperatures compared to small fires, burning from the understory to the tree-tops where their more intense flames consume the tree canopy (Holsinger et al., 2021; Whitman et al., 2018). Small fires can move through areas of forests consuming fuels like woody debris without damaging the bark of the more mature trees. Wildfires are the most common disturbance agent in forests and play a large part in altering carbon cycles, patterns of succession, and species composition (Crowley et al., 2019; Hall et al., 2008; Whitman et al., 2018). Like beetles, wildfire can leave behind standing deadwood (snags) and these snags can serve as habitat for some types of birds, like woodpeckers, become the home of communities of many small invertebrates, or substrate for fungal growth (Dhar et al., 2016).

Fires do more than just consume and remove various amounts forest vegetation allowing a similar stand to eventually return but can change the composition and distribution of species (Hall et al., 2008). Serotinous plant species like lodgepole pine rely on fire to open their cones and spread their seeds (Whitman et al., 2018). Aspen and birch trees also benefit, propagating more quickly than other species following a fire and gaining an advantage in the altered landscape. Small fires tend to alter the structure of, and remove, forest floor fuel much more than they alter tree stand species composition (Hall et al., 2008). Unfortunately, climate change is expected to increase the rates of fire occurrence as well as their magnitude while also hampering a forest's ability to recover from fire events (Schroeder et al., 2011; White et al., 2017; Zhu et al., 2020).

Like fires, harvests (the removal of trees by humans) are another fast disturbance common in forests that can be both less and more impactful. Depending on the forest management approach the method of removal can be selective or clearcut, but in either case harvests occur over a short duration from an ecological perspective. Unsurprisingly, clearcutting has more dramatic effects on the forest's structure and is a large-magnitude change (Wulder et al., 2020). Management decisions to allow either method of resource extraction are influenced by resource needs and the provisioned areas available based on the forest's capacity to provide trees (Caputo et al., 2016; Dhar et al., 2016; Hall et al., 2008). Despite increases in more selective harvesting of trees, clearcutting remains the more common method of forest harvest in Canada and some argue what remains is a landscape more similar to natural activities like high-intensity fires (Schroeder et al., 2011).

While they may be large disturbances to forest ecosystems, harvests stand in stark contrast to forest fires that can disrupt forest management activities such as resource provisioning, extraction, and forecasting. The sudden loss of trees to fire may lead to industrial operational shifts to salvage harvesting (i.e., recovery of remaining lumber material post-disturbance), economic shortfalls, or both, in addition to a loss of greenhouse gas regulation capacity and pollution removal capacity (Caputo et al., 2016; Dhar et al., 2016). Fortunately, both fire and harvest sites continue to play an important role in the ecosystem, since these areas return to a vegetated and even treed state. Whereas the paving of a road would mean the area becomes deforested, regrowth following fires and harvest contribute to the ecosystems natural functions including habitat creation and carbon sequestration (Wulder et al., 2019).

Because climate change is affecting all of Canada's forests and changing disturbance processes, it is important to understand where and how disturbances have impacted this important natural resource (Canada & Environment and Climate Change Canada, 2016; Hall et al., 2008; Natural Resources Canada, 2015). Unfortunately, there is evidence that forest fires are already occurring more frequently (Zhu et al., 2020). Only by continuing to monitor and gather evidence about the Earth's forests can managers and decision-makers gain a better understanding of disturbance characteristics and cycles to support sustainable natural resource management of forests (Canada & Environment and Climate Change Canada, 2021; Comber & Wulder, 2019).

6.1.3 Forest Monitoring and Management

Different stakeholder groups are interested in information about forests in the Canadian context (Gillis, 2001). Lumber and pulp/paper industries are often concerned with the amount of biomass available for extraction as well as the kinds of trees and where they are found. The locations of severe canopy fires is of interest to loggers because often it presents opportunities for salvage harvests (Dhar et al., 2016; Hall et al., 2008; Whitman et al., 2018). Local communities may be interested in maintaining healthy forests as a way of preventing soil erosion, for flood control, and for the ability of healthy, robust soil structures in forests to purify water that might be drawn from the ground (Caputo et al., 2016; Felipe-Lucia et al., 2018). Climate watchdog agencies are interested in forests as providers of a variety of ecosystem services including water quality regulation, greenhouse gas regulation, pollution removal, and carbon capture and storage (Caputo et al., 2016). Responding to these needs, the Canadian National Forest Inventory produces a suite of maps, reports, statistical datasets and other resources that can be freely accessed by anyone (*NFI*, n.d.).

In general terms, forest monitoring means regularly collecting data and recording changes in forest status (Comber & Wulder, 2019; Natural Resources Canada, 2013). The parameters monitored vary depending on the interested party and their specific needs, nevertheless forest monitoring is critical to management, planning, and sustainability (Hall et al., 2008; Wulder et al., 2019). A typical inventory performed in Canada involves interpreting aerial and satellite photography and combining this information with field measurements of the vegetation, its distribution, volume, and species present in an area (Gillis, 2001; Natural Resources Canada, 2013; Wulder et al., 2019). These inventories are performed by forest managers from federal and provincial agencies as each province is responsible for managing its own forests (Gillis, 2001; White et al., 2017) while Canada's international environmental agreements are federal affairs. Circa 1960 managers might have used different metrics or measurement standards that could vary from province to province, thus a federal inventory meant converting each of these disparate data sets, collected at different times, to a national standard in order to make data inter-comparable (Gillis, 2001). Canada's modern National Forest Inventory (NFI) is a collaborative effort between the provinces and territories, and the Canadian Forest Service (*NFI*, n.d.; Wulder et al., 2019). A well-defined set of practices from survey design through data collection and processing to reporting, the NFI incorporates a network of field plots where aerial and on-site sampling is done, and a network of plots for aerial surveying in more remote locations where site visits are not feasible (*NFI*, n.d.).

Through regular monitoring one can detect and track disturbance in forests. As mentioned, regular periodic gathering of on-site data can be costly and for some locations impossible, because they are remote and not easily accessed (Cohen et al., 2017). Thus, one of the promising aspects of remote sensing is the potential extension of in-situ knowledge collected to-date (DeVries et al., 2015). By finding relationships between remotely sensed data and concurrent on-site data, it is possible to infer forest status and parameters (like stand age, or soil quality) via optical and structural elements (like leaf-area, or greenness) of a forest ecosystem. Retrospective analysis and synthesis is crucial in establishing these relationships and baseline values for the wide range of parameters central to forest change monitoring and forecasting (Cohen et al., 2017; White et al., 2017).

Thus, humans use and depend on forests for a multitude of ecosystem services. Natural and human induced forest disturbances must be monitored to support sustainable management decisions and practices that allow forests to exist and humans to continue benefiting from them over the long term. Satellite-based Earth observation is a critical tool for monitoring because a large portion of the earth, and in particular Canada, is covered by forests, many of which are too remote and difficult to assess otherwise.

6.2 Remote sensing

Remote sensing, in the strictest sense, is the act of collecting information from a subject without making physical contact. Within the Earth sciences remote sensing technology like cameras (optical), radio detection and ranging (RADAR), and light detection and ranging (LIDAR), allow us to acquire information (reflectance values) about any part of the Earth's surface and atmosphere using air-borne and satellite-born sensor platforms.

6.2.1 Earth Observation Satellites

Satellites have proven an effective way to regularly gather information about the surface of the entire Earth because they capture data across large areas as they complete each orbit. (Comber & Wulder, 2019; DeFries et al., 2006). Satellites orbit the earth in a predictable way, with polar low-earth-orbit satellites able to photograph every spot on the Earth's surface repeatedly. The optical sensors on satellites are much like cameras that passively receive the reflection of sunlight off the Earth's surface and their orbits are structured such that they pass over the sun-lit side of the planet at a regular period of each orbit. This behaviour means observations occur at regular intervals, clouds or other atmospheric obfuscations notwithstanding, and thus satellites are well suited for monitoring forest changes and stability (DeFries et al., 2006).

Two widely-used satellites for Earth observation are NASA's Landsat-8 and the Sentinel-2 satellites of the European Space Agency (ESA) (DeVries et al., 2015; Gómez et al., 2016; Griffiths et al., 2019; Huang et al., 2009; Schroeder et al., 2011; Wulder et al., 2020; Zhu & Woodcock, 2014). They are popular for forest monitoring in no small part because their data is open access but crucially, their sensors have resolutions on the ground that are suitable for observing forest changes like fires and harvests (DeFries et al., 2006; Gómez et al., 2016; Wulder et al., 2018). Landsat-8 has 30 metre pixels, which we can understand as a square on the ground whose sides are 30 metres in length, with an area of 900 square metres. The Sentinel-2 satellite pair provide images of the ground with 10 metre resolution or only 100 metres square which contributes to greater accuracy in disturbance detection (Barrette et al., 2018; Wulder et al., 2019). Because 10 metre pixels represent a smaller area of trees, any one tree represents more of the total signal reflected to the satellite. A disturbance affecting 50 metres square represents half of a Sentinel-2 pixel but only 5% of a Landsat-8 pixel. While one pixel is too large to observe any single tree this resolution has been shown to be sufficient for studying forests, especially at a national scale (DeFries et al., 2006) and the complementary nature of these satellites supports using them together.

Landsat-8 and Sentinel-2 are known as multispectral sensors because they receive optical wavelengths (a.k.a. bands) of not only red, green, and blue light the way our eyes do, but also shorter and longer wavelengths. Landsat-8, for example, captures eight bands of light that human eyes cannot see. This ability to acquire bands of the electromagnetic spectrum beyond the capability of human sight means satellites collect more data and thus provide more information about the Earth's forests with every photograph.

6.2.2 What Can Satellites Tell Us About Forests?

Forest structure and vegetation health cannot be directly observed or measured via satellite imagery, but they can be revealed by understanding the relationships between parameters of interest, such as canopy cover, and its spectral responses or 'signature' (Gómez et al., 2016; Hall et al., 2008; Wulder et al., 2018). This is based on the underlying principle of remote sensing of land surface cover: surface reflectance values of a subject are consistent if its physical characteristics are consistent (Hermosilla et al., 2018). Indeed, the relative strength of the reflectance bands makes it possible to distinguish the presence of different kinds of targets, like vegetation or human development, and separate similar kinds of those targets, (e.g., separating shrubs from trees or roads from buildings).

The spectral reflectance is only part of the information necessary for the remote detection of vegetation dynamics, however. Confounding factors from the natural environment such as elevation, sloping topography and its orientation, or seasonal variation, add variability to the reflected energy leading to increases or decreases in the overall signal (Rouse et al., 1974). By applying transformations to the signal bands and understanding their ratios or relative strengths, one can derive indices that are sensitive to subjects of interest (e.g., trees) (Whitman et al., 2018). In this way, a subject can be detected more reliably regardless of whether they are found on level terrain or a slope, which direction that slope faces, or whether the study period is in the spring or fall (Rouse et al., 1974).

Given the number of bands provided by any one satellite, it is helpful to compare and contrast bands and band combinations (indices) for vegetation monitoring, including some bands specifically designed to monitor forest fires and logging (Barati et al., 2011; Schroeder et al., 2011; Xue & Su, 2017; Zhu, 2017). Among these bands and indices, some are more sensitive to changes in the physical structure of the forest (e.g., the density of the understory), and others respond more to the green leaf area, or the amount and 'greenness' of leaf area visible from above. Examples include the Forestness Index (FI), the Leaf Area Index (LAI), the Normalized Difference Vegetation Index (NDVI), the Enhanced Vegetation Index (EVI) and the Normalized Burn Ratio (NBR), the last of which I have used with SLIMS. The Forestness Index is a z-score measure of how likely a pixel is to be forested using the mean and standard deviation values of other pixels known to be forested (Huang et al., 2009). The FI can use any band sensitive to vegetation cover (e.g., red, or infrared) and integrating the results from multiple useful bands, can produce a robust Integrated Forestness z-score (IFZ). The Leaf Area Index (LAI) developed by Jordan in (1969), is an index that correlates the density of forest canopy to the strength of near-infrared divided by the signal of the red band. This is because the relative intensity of infrared light to red is much greater reflected from the forest floor than from the canopy (Jordan, 1969). Unfortunately, it does not perform well in areas where sandy soils are prevalent under thin canopy, because reflections from this substrate has high confounding impact (Barati et al., 2011). One of the most used indices for tracking vegetation cover is NDVI (Normalized Difference Vegetation Index), which has been used to infer biomass, vigor, and other characteristics (Rouse et al., 1974; Xue & Su, 2017). It uses the near-infrared and red bands but, as the name implies, it normalizes these values using the total signal strength in both bands. This improves upon LAI's underperformance in sparse areas of vegetation somewhat, as well as corrects for variations in incident light because of sun-object angle or atmospheric interference (Rouse et al., 1974). Unfortunately, among other issues, a difficulty with NDVI is that the correlation between vegetation density and NDVI values break down in areas of more dense vegetation and reaches saturation too quickly (Hall et al., 2008). In an effort to specifically address the influence of soil, vegetation density, atmosphere, and total illumination on NDVI, Liu and Huete (1995), developed the Enhanced Vegetation Index (EVI). It uses red and infrared bands but also introduces the blue band, new terms, and coefficients to account for the atmosphere, soil, and other confounding factors.

An important index for fires and logging that is wildly popular, used by C2C, Crowley et al., (2019), and the one I have decided to here, is the Normalized Burn Ratio (NBR) which is sensitive to burned areas in forests (García & Caselles, 1991; Hall et al., 2008; Hermosilla et al., 2016; Li et al., 2011; Parker et al., 2015; Schroeder et al., 2011; Whitman et al., 2018). The NBR can serve as a measure of burn severity by using the proportion of the near infrared band (NIR) to the second shortwave infrared band (SWIR2) both of which are present in the Landsat and Sentinel-2 satellites. The index calculates the difference between the two bands divided by the total strength of both bands (Eq. 1)

$$NBR = \frac{NIR - SWIR2}{NIR + SWIR2}$$

Eq 1: Formula to calculate NBR

The index varies between vegetation types, meaning that there is no fixed number for an intact forest, but rather it depends on the forest type and condition so nominal values for healthy or disturbed vegetation will vary (Hall et al., 2008). Once disturbed, this index value decreases so comparing NBR indices for the same location at two different times, (i.e., a differenced Normalized Burn Ratio (dNBR)), can distinguish burned and harvested areas. Crowley et al. (2019) use dNBR to refine identified burned areas in the Canadian Rockies. Selection harvesting can be more difficult to detect via satellite-based remote sensing because it tends to disrupt less of the total canopy cover and leaf area (Schroeder et al., 2011). Although sensors with finer resolutions may overcome this to some extent (Crowley et al., 2019; Wulder et al., 2018). Smaller fires that only burn the understory are also more difficult to detect with satellites like selection harvesting (Whitman et al., 2018). Because clearcut harvesting can appear spectrally similar to fire, distinguishing one from another using this index poses a challenge (Schroeder et al., 2011). Fortunately, there is a notable difference; where both fire and harvest can remove the forest canopy, harvests tend to leave behind more live vegetation on the forest floor.

It is important to differentiate between harvests and fires as disturbance agents in forest monitoring because the recovery of vegetation biomass, carbon sequestration, and forest recovery are all affected differently for clear-cuts compared to fire (Schroeder et al., 2011). Satellite-based remote sensing provides several avenues and opportunities to address this issue (Cohen et al., 2017). The first shortwave infrared band (SWIR1) has elevated spectral values when there is more live vegetation left behind compared to areas that experience fires. SWIR1 can also be used to identify changes in vegetation and soil moisture (Whitman et al., 2018).

The Landsat series of satellites, the longest running Earth observation program, has been accumulating imagery of the Earth's surface for 50 years providing an impressive and important temporal depth to the collection of data (White et al., 2017; Wulder et al., 2019). This long-running monitoring project is proving invaluable for establishing historical trends and norms, improving the usefulness of current findings (DeFries et al., 2006; Kennedy et al., 2010). Thanks to the increasing number of space borne Earth observation sensors, it is becoming easier to monitor the health and structure of enormous areas of forest in a nearly continuous manner (Wulder et al., 2020).

6.2.3 Satellites Used in This Thesis

Two major space agencies provide free and publicly available imagery that allow us to monitor any part of the Earth's surface. The spatial resolutions of these two satellite systems can be considered medium (White et al., 2014) or fine (Griffiths et al., 2019) scale for forestry, depending on monitoring context. The U.S. Geological Survey's (USGS) Landsat-8 satellite is currently the penultimate satellite in a legacy of Earth observing satellites that began with Landsat-1 in 1972. The Landsat-8 satellite launched in February of 2013 carrying its then-state-of-the-art sensor pair, the Operational Land Imager (OLI) and Thermal Infrared Sensor (TIRS) (U.S. Geological Survey, 2022). The OLI is capable of providing visible, near infrared, and short-wave infrared imaging bands at 30 metre resolution. The satellite platform orbits the Earth in such a way that it revisits a given location every 16 days.

The European Space Agency (ESA) has operated Sentinel-2 since June 23rd, 2015, when the first of a twin pair of satellites was launched. Launched on March 7th, 2017, the second satellite joined its twin to form what is known as a 'constellation' (European Space Agency, 2022). These orbital platforms both carry the same onboard sensors to capture spectrally consistent images at 10 to 20 m resolution. Thanks to the pair orbiting 180 degrees out of phase, Sentinel-2 A and B give a combined revisit time of 5 days or better at higher latitudes.

The development of Landsat-8 and Sentinel-2 involved the close collaboration of scientists from both agencies and as a result their data products are largely compatible. This is because their Earth observation missions were always conceptually similar: to observe changes to the landscape and support forestry, agriculture, and disaster relief (*ESA–NASA Collaboration Fosters Comparable Land Imagery*, 2013). Thus, it made sense to develop the hardware in collaboration to extend the usefulness of both missions.

6.3 Remote Sensing, Forests, and Disturbance

6.3.1 Land Cover and Disturbance

Classifications of land use / land cover (LULC) through remote sensing assign a single category to a given pixel in a study area (Zhu, 2017). Classifications can represent many different attributes (e.g., species, ecosystems, or stage of post-fire recovery) of interest, which is why many different classifications of land cover exist (Olofsson et al., 2014). Someone who is interested in forest vegetation structures might begin by determining one or more attributes they wish to classify, perhaps a region's dominant vegetation by family or species. Another classification could differentiate between levels of human interference (natural vegetation vs agriculture vs urban). Next, they establish a set of criteria by which to measure said attribute(s), using novel parameters or those established in the relevant literature (Hall et al., 2008). After choosing the appropriate methods and tools, and collecting data (e.g., visiting sites to survey or collect samples, flying transects with drone-mounted hyperspectral imaging devices, or examining satellite imagery), they can evaluate the study area according to these criteria to create a classification map.

In the Canadian forest context, potentially interesting LULC classes go beyond differentiation between classes like 'forest' or 'bare ground'. Maps of change that identify areas of vegetation that have been burned versus having been harvested are as important as maps that indicate 'what can be harvested'. Understanding and classifying changes and change drivers, as well as patterns of change enriches our knowledge of land cover classes, though every classification has limitations (White et al., 2017; Wulder et al., 2019). For example, change classes might not differentiate between causes; areas classified as burned do not reveal if it was a natural or anthropogenically induced fire. Areas classified as regrowing or undisturbed forest can not indicate a natural grown forest or one that was planted.

6.3.2 Methods for Forest Disturbance Detection

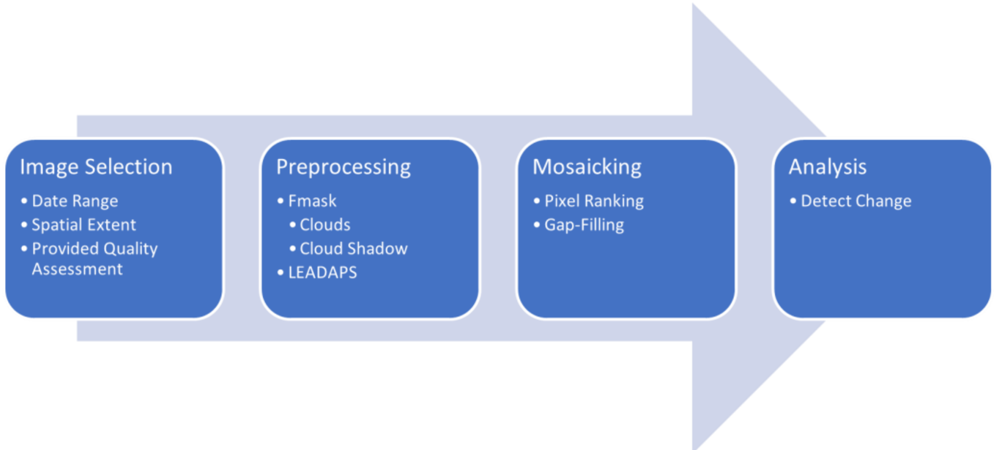

Figure 1. A generalized change detection workflow. In order to extract information from satellite images we must prepare selected images and occasionally fill data gaps that can occur due to noise removal. Only after these operations are complete can analysis be undertaken. The mosaicking step is particularly important for algorithms accumulating sets of images in order to give a single, synthetic, 'best' representation for a desired time period.

In monitoring land cover using satellite imagery, algorithms are used to detect disturbance (i.e., change detection algorithms) and there are many different change detection algorithms available to choose from, depending on the ecosystem of interest (Barati et al., 2011; Gómez et al., 2016). Almost all algorithms will have in common the main conceptual phases shown in Figure 1, with the possible exception of mosaicking which may not be necessary. Algorithms can differ in their temporal resolution, the bands or indices they operate on, the satellites they support, the kinds of disturbances they can detect, and in their mathematical terms (Gómez et al., 2016; Zhu, 2017). In general, change detection algorithms have to cope with three different kinds of changes, a) seasonal changes that are periodic in nature, b) gradual changes like soil degradation or afforestation, and c) abrupt changes like fires and harvest. For the sake of comparison, I present in more detail five common change detection algorithms: continuous monitoring of land disturbance (COLD), break detection for additive season and trend (BFAST), Landsat-based detection of Trends in disturbance and recovery (LandTrendr), vegetation change tracker (VCT), and composite to change (C2C).

All five of these change detection methods use a time series of Landsat data, either Landsat Time Series Stacks (LTSS) or Landsat Analysis-Ready Data (ARD). LTSS are a sequence of perfectly co-registered images from the same satellite path-row, and ARD are individual images that have had many pre-processing steps performed by the USGS to meet a quality level suitable for analysis, minimizing further preprocessing. These change detection methods all operate at the pixel scale (they operate on each pixel separately), instead of first constructing larger multi-pixel objects, or attempting to decompose a pixel's spectral properties to interpret 'sub-pixel' information. Even if a 'moving-window' averaging process is applied, where for each pixel in the image, the values of its surrounding four or eight connected neighbours are averaged with it, the principal calculations are only applied to a single pixel's values at a time. Some trend detection methods like COLD, and BFAST programmatically construct what they use as historical stability in a preceding period, to find deviations from this stability, and they achieve this in different ways, but both processes are computationally expensive due to their iterative nature. Of these five automated change detection algorithms, BFAST does not capture recovery or gradual degradation like VCT, COLD, C2C and LandTrendr do.

BFAST: The break detection for additive season and trend (BFAST) algorithm can detect both trends as well as abrupt changes (Verbesselt et al., 2010). As the name suggests, the algorithm is based on a method called 'additive season and trend' which has been previously established by Verbesselt et al. (2010). The algorithm builds a mathematical model of stability including slope, intercept, and error terms, to establish within- and between-year stability of cover from *n* observations. To automatically build this model of stability, the algorithm searches for a period free from disturbances by working backwards, known as reverse-ordered-cumulative sum of residuals. Beginning at $t=n$ (where t is time), then $n-1$ (the entire period less one observation), $n-2$, and so forth, a cumulative prediction error term for the linear trend harmonic season is assessed. This stops when a predefined error limit is exceeded, or a predefined maximum number of events are evaluated. If no changes occur over a user-defined number of events, this is considered a period of stability. Elements like solar illumination angle or precipitation will follow regular seasonal patterns whose effect on the reflectance can be described mathematically. What remains is a value indicative of the vegetation status, and an error term. This approach is sometimes referred to as de-trending. By modelling the elements of the detected signal that are the result of regularly occurring events, these trends are accounted for and 'removed'. New observations can be compared to a predicted range of values defined by these cycles and if the value falls outside of this range, then a possible change has occurred.

COLD: The continuous monitoring of land disturbance (COLD) algorithm uses all Landsat imagery available transformed into an arbitrary spectral index, so long as the index is responsive to forest status changes, in order to detect forest change (Zhu et al., 2020). Like BFAST, COLD builds its initial model of stable condition, described by three harmonic terms, from twelve clear images. Unlike BFAST, the COLD algorithm is capable of detecting land cover change aside from forest change by using most or all of the spectral bands available in each image. Once 15 clear images are collected the algorithm can evaluate the last three to look for outliers, because it requires at least three images to detect and confirm change. The model of stability then shifts along with the intake of new observations (this is known as a 'moving window') to reduce the impact of subtle, undetected changes influencing the fit of the model. The model has three component terms so it can describe overall reflectance, within-year trends, and between-year trends. In doing this, it can capture both gradual and abrupt changes. Changes are detected by evaluating new data against the stability model plus or minus three times the root mean square error. If two consecutive outlying points are detected, then it is labeled as a possible change, until a third consecutive value confirms it, otherwise it is considered noise. While COLD can produce a change map at any point using all the available imagery up to that moment, the map has a time delay of three data points.

LandTrendr: The Landsat-based detection of trends in disturbance and recovery (LandTrendr) algorithm is a popular trend-based algorithm that makes use of both signal trends, as well as breaks, to detect changes that are either gradual or abrupt in nature, over an annual timescale (Kennedy et al., 2010). The core of the method is a temporal segmentation process, and it can be applied to an arbitrary index, so long as they reflect some relationship to the forest cover and its changes. To that end, LandTrendr can be used with the normalized burn ratio, or normalized difference vegetation index. Segmentation begins after image normalization and cloud masking. First, transient values (called 'spikes') are removed and the segmentation process constructs a spectral trajectory with the first and last pair of vectors connecting values across years. Creating a regression through the first and last points and searching for the maximum absolute deviation value will identify a new point as an additional vertex that will serve as an anchor for the next iteration of the segmentation. That is, two new regressions are performed with this vertex becoming the new first point with the *original* final point, and the point that preceded it as the new last point and begins with the original *first* value. This process is repeated until a minimum residual error remains for each regression where the total number of subset regressions does not exceed a user-defined maximum number. This now-complex vector is then iteratively simplified, by removing vertices until a statistically best-fitting vector is defined with the smallest residual values between the original set of values and the vector model. This model can describe both sudden change and gradual change with meaningful breaks and good-fit (minimal mean-squared errors) regressions respectively.

VCT: The vegetation change tracker (VCT) algorithm is another annual-scale algorithm that isolates suspect forest pixels before assigning each of them a score in its primary index, the integrated forest z-score (IFZ) (Huang et al., 2010). The IFZ assigns very low values to pixels most likely to be treed, and higher values suggest the presence of other land covers. This spectral transformation takes advantage of several bands, red, short-wave infrared one (SWIR1), and short-wave infrared two (SWIR2), because these are most sensitive to both fire and non-fire forest disturbances. To detect changes in a time series, the algorithm searches for breaks in the IFZ score that both exceed a minimum threshold in magnitude and persist longer than a minimum predetermined duration in the time series to exclude transient noise signals. Gaps due to cloud and shadow masking are interpolated a year after they occur; however, if a true change follows a false one, the interpolation can raise the IFZ value and lead to change class commission error.

C2C: The composite to change (C2C) algorithm is both an annual interval classification method as well as change detection method (Hermosilla et al., 2014). C2C uses a single gap-free composite image per year to obtain radiometrically-consistent representative images over large areas (method explained in further detail in 6.3.3). Before analysis can begin, noise removal must be performed and C2C uses the transient nature of noise to detect and eliminate it. Once the series of seamless images of the study area is established, a Normalized Burn Ratio (NBR) time series is evaluated per-pixel in search of breakpoints in the series to identify trends and change events. Starting from the beginning, all values in the series are paired up to create a series of line segments, then these segments are merged if the 'cost' of merging them does not exceed a pre-determined root-mean-square error value. The pair of segments with the smallest error are merged first, the segments are paired again, and the process is repeated until the cost of merging any two segments would exceed the maximum error value. What remains are sequences of trend lines that, when combined with breakpoints can be sorted into four broad groups: 1) trends that have no breaks 2) trends with multiple breaks and all the slopes are positive 3) trends with one breakpoint followed by a negative slope and 4) trends with multiple breakpoints, and one or more negative slopes. Combining these trends, breakpoints, and slopes, a variety of change metrics can be derived that describe landscape classes and their fluctuations through time.

6.3.3 Representative Images in Annual Interval Methods

Examining a location year after year at an annual scale provides several advantages (Hermosilla et al., 2018; White et al., 2017; Wulder et al., 2018). Because the Earth is the same distance and orientation relative to the sun after completing an orbit, the sun-Earth-sensor geometry will be similar in every observation. This minimizes the effect of seasonal shifts in surface and atmospheric temperature, solar illumination and albedo that would otherwise need to be accounted for in pre-processing (DeFries et al., 2006). Additionally, and perhaps most importantly vegetation phenological effects are minimized. If the vigor of vegetation growth is of interest, then deviations from a nominal state will be more easily detectable. Gradual changes to plant health like the harm caused by illness or the invasion of pest species such as mountain pine beetle can be detected, as is soil quality or deterioration (Kennedy et al., 2010).

In remote sensing for Earth Sciences research, multiple images are often available for a region of interest within a suitable window of time. If a study area is smaller than (and falls within) the geometry of the desired sensor's imagery, it can be appropriate to simply select the clearest image for analysis (Huang et al., 2010). For larger regions or regions that experience persistent cloud cover as can be the case during active fire periods, creating a pixel-level composite image from all available images within an observation period may be necessary or simply desirable (Barrette et al., 2018; Hermosilla et al., 2015; Kennedy et al., 2010).

An obvious property for organizing satellite images is where they are, formally called their spatial index, and it indicates the portion of the surface of the Earth an image covers. For the Landsat program this index is named World Reference System (WRS) (now in its second version, WRS-2) and it is composed of two elements, a 'path' (the flight-line taken from the north to the south pole) and a row (a roughly latitudinal division). Historically, compositing images was achieved by choosing the least cloudy image available in each path/row (White et al., 2014). Sometimes referred to as 'mosaicking' or creating an image mosaic, a single pixel could be selected for overlapping or side-lapping portions of images based on a single ranking, like highest normalized difference vegetation index (NDVI). Now, for workflows involving extensive creation of composite images from chronologically proximate observations, developments in computing capabilities facilitate more elaborate compositing methods that can improve the signal to noise ratio beyond what was possible with early methods.

A single cloud-free composite image for each interval is sometimes referred to as a Best Available Pixel (BAP) composite and represents a season or time interval (Hermosilla et al., 2014, 2015). It is important to examine how a BAP is constructed to understand how errors may manifest in the change detection process. For example, one contemporary approach begins preprocessing satellite imagery by applying the Landsat Ecosystem Disturbance Adaptive Processing System (LEDAPS) and Fmask (Function of mask) algorithms to address atmospheric complications (Huang et al., 2010; Zhu & Woodcock, 2014). First, the Fmask algorithm identifies pixels suspected of being cloud and cloud shadow and outputs a masking layer to remove them from the input image. Then LEDAPS calibrates data from the Optical Land Imager (OLI) sensor so it can generate surface reflectance values for each image, correcting for the effects of the atmosphere between the ground and the sensor. Importantly, LEDAPS constructs a layer qualifying atmospheric opacity for every pixel. The lower the value, the clearer the reflectance from the ground. Once these two steps (LEDAPS and Fmask) are complete, an overall score can be generated for every pixel.

This overall score determine which pixel value will be included in the BAP image and in this example it consists of four sub-scores that are calculated and summed (White et al., 2014). Two of these scores are image-based (every pixel in one image gets the same score) and two are per-pixel. The first image-based score is related to the sensor, so that if one sensor is less desirable than another, it can be discriminated against. The second image-wide score is assigned based on the date the image is taken. Images captured nearer to an ideal date can be rated more highly than those captured at other times of the year. The third and fourth pixel-scores draw on the preprocessing steps. Based upon the distance between a given pixel and those of clouds and cloud shadows as calculated by Fmask, pixels are given a better score if they are farther from these areas. Finally, using the LEDAPS opacity values, clearer pixels are scored higher than those which are hazy or darker (White et al., 2014).

For algorithms operating on an annual interval, two types of problematic change events (that is, a disturbance such as fire occurring in the world, not their representation in imagery) are identified. The first are partially captured change events -changes beginning during the observation period, often closer to the end, and continuing past the end of the observation period. The second are post-season changes -changes occurring entirely following the conclusion of the most recent observation period.

For the first issue, partially captured disturbances, error correction may incorrectly identify these true changes as errors, during processing or pre-processing, leading to omissions of detection. Even after pooling images from an observation period and from multiple satellites, it is possible there are pixel locations with no clear observations or which contain unusual values since cloud masking and haze scoring algorithms are imperfect and forest fires are often accompanied by persistent haze and smoke (White et al., 2014). If the pool of pixels for such a disturbance contains both clear observations and cloud masked or outlying (perhaps darker) values, then the clear images may be incorrectly preferred (Hermosilla et al., 2014). In other words, if the algorithm obtains a reflectance signal within a nominal range and does indeed obtain some observations that meet those criteria, they may be chosen in error. These kinds of pixels represent sources of uncertainty despite proxy values providing a means of gap filling for these locations using information from spatial neighbours, prior years or ensuing years, if they are available. Late season changes, those that occur after the observation window, will simply not be detected until the following year and a disturbance in year *n* will be detected in year *n+1*.

In both cases, partially captured change events and post-season changes, the potential detection is confirmed by an additional data point but in the latter case the confirmation of change arrives almost 2 years after the true change occurs on the ground, and the year assigned to the change is wrong. Using C2C as an example, it includes two years ahead of, and following, the time series being classified because without these, there can be no proxy value assignment in the case of data gaps, they "enable trends to be based upon pre- and post-period evidence" (Hermosilla et al., 2014, p. 222). Still, it can be difficult to have a high degree of confidence in values across all locations for the most recent image, which is the image at the end of the time series, despite all of these compositing steps (Barrette et al., 2018; Hermosilla et al., 2015). Kennedy et al. (2010) describe this temporal-dependency shortcoming succinctly: *"if each year's spectral deviation is judged entirely with regard to the years before and after it, the spectral deviations of the first and last years of the trajectory are by definition more difficult to judge than deviations in all other years" (p. 2905)*.

Indeed, time-based error correction methods are a common feature of trend-based classification methods. Abrupt deviations from normal or expected values can indicate the presence of persistent clouds or shadows, however they may also indicate true change like fires and harvest. These anomalous pixels are often evaluated against values in the subsequent intervals. For example, if a pixel's value increases or decreases dramatically at time *t*, but at *t+1* is again similar to its antecedent value (*t-1*), then this deviation is likely classified as noise (Hermosilla et al., 2015; Huang et al., 2010; Kennedy et al., 2010). However, in the absence of the next image (*t+1*), uncertainty remains as to whether this deviation is signal or noise. The design of a change detection algorithm must therefore account for such values in some manner, by flagging these values as potential change or ignoring the value and continuing to label a location as 'treed' or 'undisturbed'.

Despite these issues annual-interval algorithms that make use of multiple images per year, construct image mosaics, and use spatial and temporal error-correction methods, are powerful tools for change detection (Holsinger et al., 2021). End users accept that the most recent classification that can possibly be created is one no sooner than the minimum number of confirmatory data points required (Wulder, personal communication, 2019).

Modern approaches to mosaicking such as the one elaborated above, combined with the growing demand for expansive, synoptic data products, necessitate the use of increasingly powerful computer systems (Claverie et al., 2018; White et al., 2014). Distributed computing platforms, sometimes referred to as 'cloud computing' or simply 'the cloud', make it possible to produce maps that cover large spatial extents without sacrificing a fine spatial resolution.

6.3.4 Cloud Computing for Remote sensing

Cloud computing is the distribution of computation among a cluster of computer servers, in a remote location. Without user intervention, the machines in that remote location allocate their computing time among all concurrent users in a dynamic fashion. A user can submit tasks that are broken down into constituent instructions and carried out simultaneously on separate machines, with the size of the cluster of machines scaling (within predefined limits) according to the needs of the task (Gorelick et al., 2017). This allows a user to perform calculations that would otherwise require more computational power and time than is typically available to an individual (Comber & Wulder, 2019; Gorelick et al., 2017). In the context of remote sensing, analytical transformations to produce results are included under this umbrella term as are the preprocessing steps like image collection, and pixel selection using elaborate criteria (E.g., that of Best Available Pixel). Importantly, a user does not need to understand how to operate or manage a server 'farm', only obtain access, and understand how to submit tasks. Afterwards, the results of the various component calculations are merged automatically and sent back to the user (Gorelick et al., 2017).

Google's Earth Engine platform provides a powerful, accessible suite of tools intended for remote-sensing studies on a global scale. Distributing calculations across networks of server farms provides enormous computational power and data storage capacity (Gorelick et al., 2017). Conveniently, massive catalogues of satellite imagery (on the order of petabytes) and their derivative products provided by the USGS, ESA, and many other organizations, are already stored on Google's data servers and new imagery is always being ingested at a variety of processing levels. Both the data and service are freely accessible as is storage space for user-created files. This enables the user to create many datasets (e.g., maps of disturbed vs undisturbed forest) for different classification-data subsets (e.g., by time-period and/or sensor) and enables them to perform classifications, accuracy measurements, and comparisons more quickly than they otherwise could (Claverie et al., 2018). This workflow, in the broad strokes, is the new norm, where the user can call up images using multiple temporal and spatial criteria, rather than seeking specific observations constrained by any single sensor (White et al., 2014).

7 Methodology

In this thesis, I develop an algorithm to detect forest disturbance based on Earth observation imagery from multiple satellites, effectively increasing the amount of available imagery for added confidence in within-year forest change classification. In addition, I extend the observation period from July and August, the two-month peak growing season of Canada's forests (White et al., 2014), to six months, May to October.

The following sections describe the change detection and attribution methods of the study period and the available imagery for the chosen location (7.1). It also describes the web-based platform used to carry out the work (7.2), the image pre-processing and compositing (7.3), the algorithm development (7.4), the regression analysis and thresholding for change detection (7.5), the per-sensor assessments (7.6, 7.7), and lastly, the bolstered change estimates using both sensors (7.8).

7.1 Study Area and Period

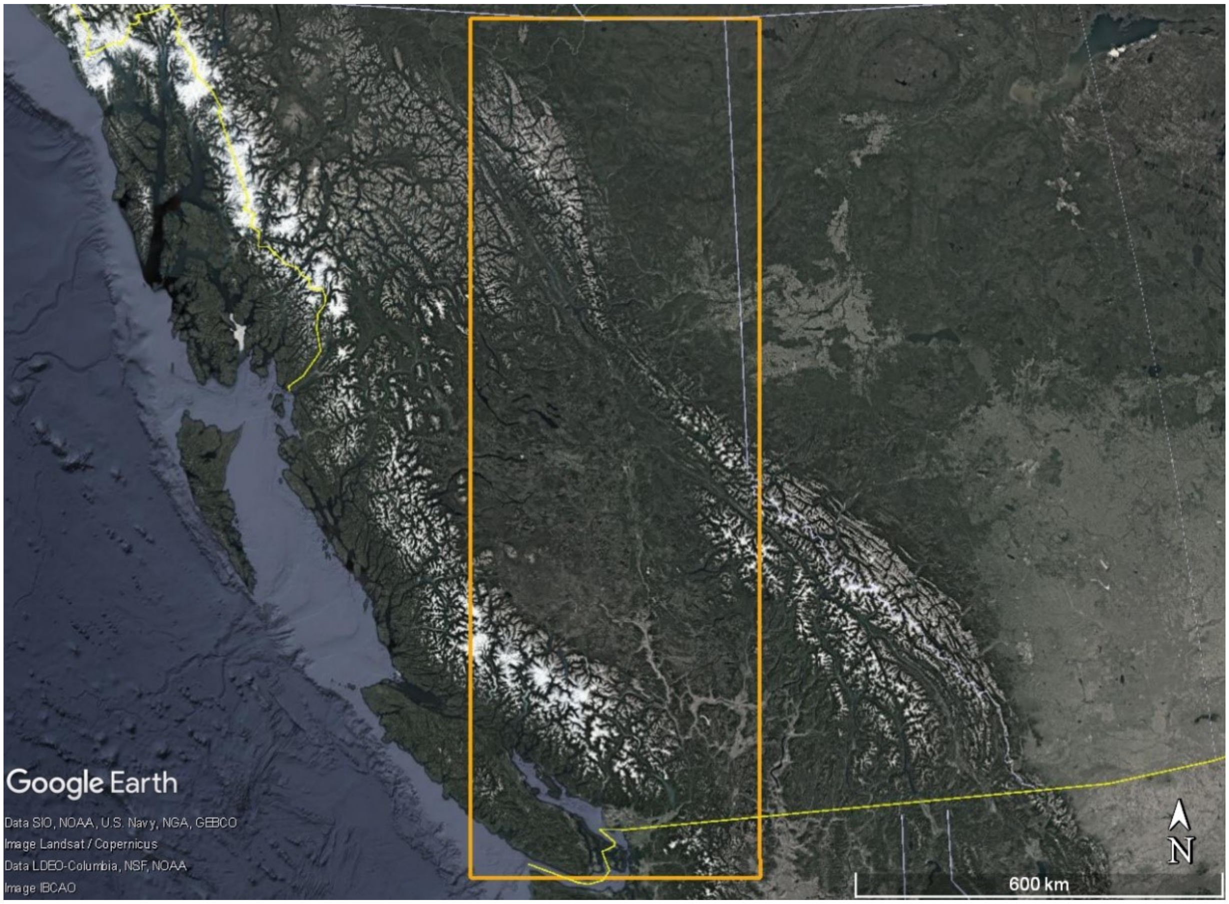

Figure 2. The study area was the entirety of UTM Zone 10N the majority of which is situated over British Columbia, Canada. Outlined in orange.

The study area was the entirety of the Universal Transverse Mercator (UTM) Zone 10N (Figure 2). This region was selected because it contains a mix of land cover types found in the northern forests of Canada, it features harvest disturbance events and in 2017 experienced a massive wildfire (Crowley et al., 2019). Common LULC types in the study area include forest, grassland, regrowing forest, human settlement, rocky outcroppings, agriculture, and wetlands. The study period was from May until October (inclusive) in 2017, so as to include the nominal best available pixel image collection period used by the CFS (August 1st +/- 30 days) and extend the period by four months. The study area, UTM Zone 10N, is covered by 45 Landsat-8 image footprints (i.e., the total extents of one image, where multiple image extents form a contiguous grid), and 84 image footprints of Sentinel-2.

7.2 Google Earth Engine

All images for this work were sourced from the catalog of Earth observation data stored on Google's Earth Engine servers and retrieved and processed at the time of each algorithm run. Earth Engine also hosts the code repository for the algorithm and visualized the results of processing which helped create the figures presented in this thesis.

7.3 Sensors and Imagery

For each satellite, I collected data from May 1st to Oct 31st for both 2016 and 2017. With these date limits, I obtained a total of 518 and 2,910 scenes for Landsat-8's Operational Land Imager (OLI) and Sentinel-2 Multispectral Imagers (MSI), respectively. Then, I used mosaicking to stitch together all the images collected by one sensor on one day and was left with 185 composite-image days between both sensors: 91 for Landsat-8 and 94 for Sentinel-2. In this five-month study period in 2017, I secured at least one image on 125 of the 153 days, about 82% of the days available. Across all images, pixels were masked individually if they met the built-in Quality Assessment band criteria for cloud, cloud shadow, or haze. For pixels that passed the masking criteria, each image's values were transformed into the Normalized Burn Ratio (NBR), which is suitable for monitoring fire and harvest which are the disturbance types of interest (Schroeder et al., 2011).

I focused on four scenes that illustrate the stand-replacing forest changes of interest that occur in Canadian northern forests:

- Harvest: An area representative of clearcut harvest conditions in Western Canada.
- Early Fire: A part of the Elephant Hill fire studied by Crowley et al., (2019) among others. This section burned sometime between July 2nd and July 10th, 2017. This was relatively early in the season, and I expected a substantial number of 2017 images both before and after the fire for this scene.
- Late Fire: A part of the Elephant Hill fire that burned late in the season, after the nominal C2C date of early August.
- Stable Forest: An area near the Elephant Hill fire that was neither harvested nor burned in 2017.

7.4 Algorithm Development

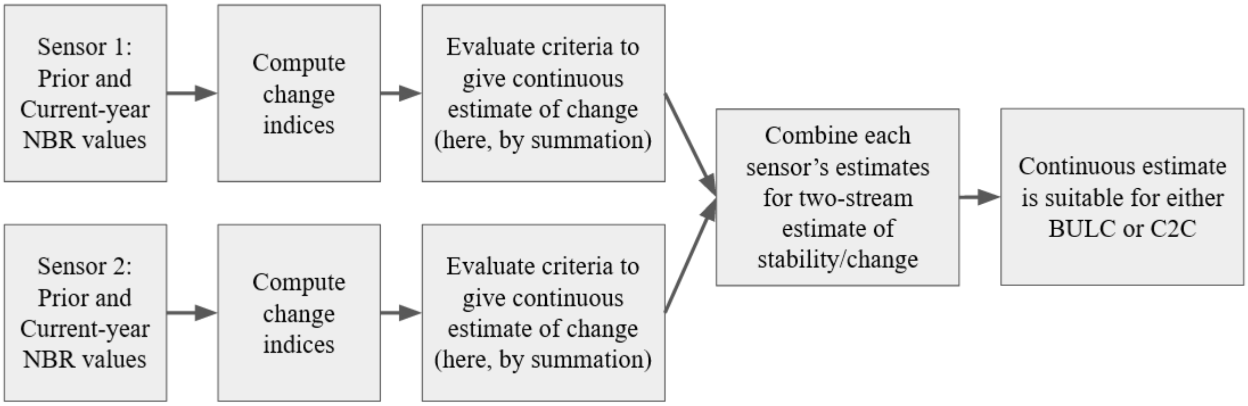

Figure 3. The SLIMS process flow chart. The data streams are analysed separately before being interwoven into a single story of stability and change. This allows the use of thresholds relevant to a given sensors characteristics, while the overall method produces comparable classifications that can be used either for the BULC algorithm or as a complement to an annual scale change algorithm such as C2C.

I developed an algorithm called SLIMS (Shrinking Latency in Multiple Streams) for assessing and labeling change and stability in Canadian forests. SLIMS (Figure 3) sequentially ingests imagery, assesses the state of each pixel and the information about expected NBR values synthesised and stored from the previous year, and updates the estimated state of the pixel in light of new data. The algorithm is designed to be run every time a new observation is available to produce a time series of estimated change throughout a growing season which may then be used repeatedly in Bayesian Updating of Land Cover (BULC), or once at the end of a growing season to produce a final estimate of LULC change and stability suitable for integration with C2C. The processing steps of the algorithm are the following:

1. Receive a new image, set of images, or mosaic image for the study area. At present, these images are Landsat-8 and Sentinel-2 imagery, but the general approach can be used for any sensor.
2. Screen pixels in the image for noise such as clouds, cloud shadows, scan-line errors, and other potential errors that result in pixels that should not be considered.
3. Compute the NBR for valid pixels in the image.
4. For the first year (here, 2016), SLIMS develops an expected NBR value for every pixel in the study area. SLIMS tracks the mean and standard deviation for each pixel, updating them at each time step. After a season of images are acquired, these two values are stored per-pixel, and then used for comparison with the second year (sometimes called 'current year' or 'target year') here, 2017. N.B. there exists the capacity to collect a time series of means and standard deviations, but the current implementation only uses the final values.

5. Five SLIMS parameters are calculated and assessed for all valid pixels (See 7.5). The sequences used can be either all images to date in the current year (if run repeatedly throughout a summer) or the summer season's images (if run once at the end of the growing season). In this thesis, I used all images for the period May-October 2017. At each step, NBR values are compared against the previous year's mean (producing a dNBR value), marked as anomalous or not (using the mean and standard deviation of the previous year's values), and along with across-years and within-year slope calculations, form the five criteria described in 7.5.

7.5 Criteria for Change Detection

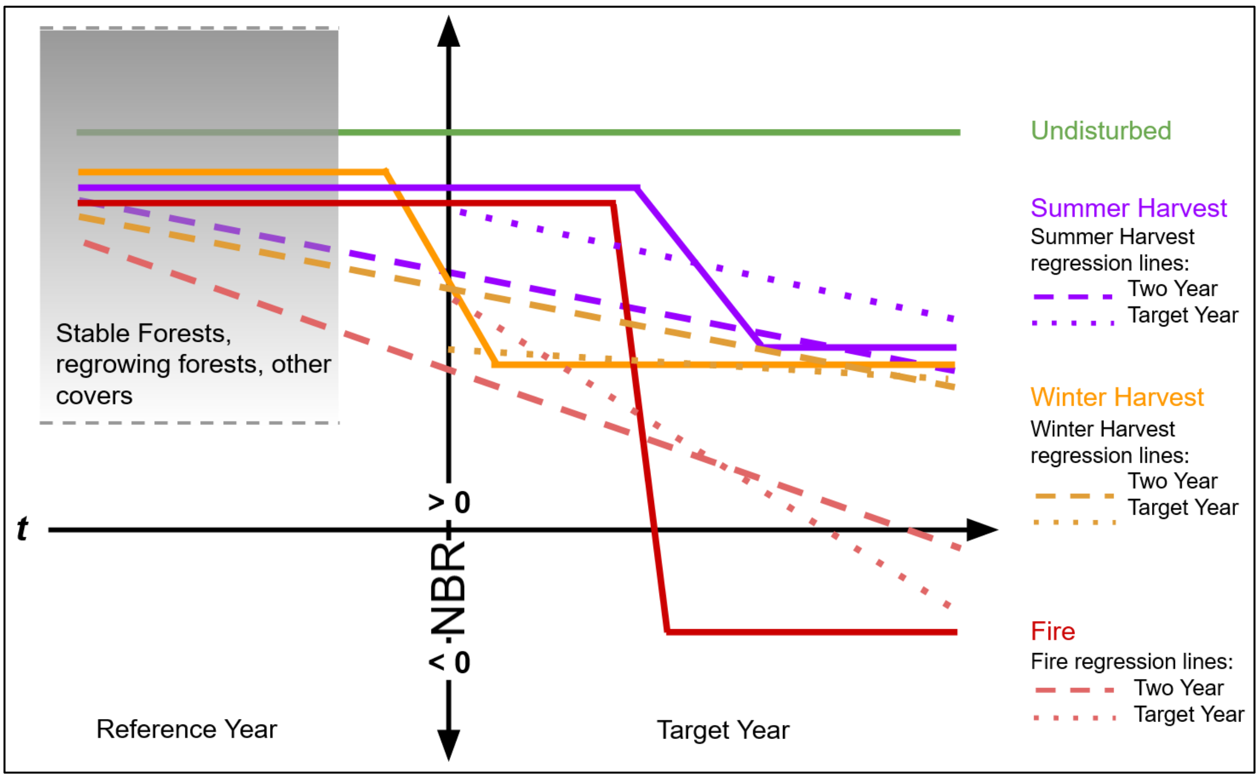

Figure 4. A schematic view of stability and change of forest Normalized Burn Ratio (NBR) pixel values and regression lines at the conclusion of a two-year period (although the data can be continuously collected). Two separate regressions are created iteratively throughout the target year with the addition of each clear observation. One regression line describes the vector trend of NBR values for only the target year, and the other describes a trend that includes the values of the reference year. The characteristics of the pairs of regression lines supports the separation of fire from harvest as does the magnitude and timing of the change in NBR values.

To detect stand-replacing change in Canadian forests, I selected five criteria for evaluating and distinguishing each sensor's time series. These criteria for change detection were validated in discussions with members of the Canadian Forest Service (CFS) (M. Wulder, J. White, T Hermosilla, 2020-02-25). The selected criteria capture facets of the NBR signals, which vary both within and between LULC histories (Figure 4, Figure 5, Figures 13 – 15).

1. **Mean NBR in prior year.** This measure identifies pixels in which there is the potential for stand-replacing forest change in a target year (*i*). This is shown in Figure 4 as a shaded grey rectangle in the upper left. Values that indicate treed cover in reference year (*i-1)* are then eligible to be reported as stand-replacing change in year *i*. This metric is good because NBR is a tried and reliable way to detect dense vegetation cover, however it can sometimes consider clouds and snow cover as vegetation.
2. **Two-year slope**. The series of NBR values from reference year *i-1* and target year *i* are considered jointly, and the slope is calculated for the combined series. In Figure 4 they are the thick dashed lines. Substantially negative slopes (qualification established by manually inspecting images with trial and error) indicate change. This allows the slope of the regression line to have a damped response to transient signals (e.g., NBR values) that can often represent false positives (e.g., clouds) and makes use of all data points over the longer observation period. A shortcoming is that this can sometimes cause a delayed response to events (true positives) that occur late in the observation period.
3. **Current-year slope**. The series of NBR values from the current year are considered, with the slope calculated for the series; represented by the thin dashed lines in Figure 4. Where harvest occurs between years, the current-year slope would be expected to be near 0. Where fire occurs mid-season, the current-year slope would be substantially negative (again, this threshold is established through trial and error). This ability to separate fire from harvest is excellent but with too few images it may be susceptible to noise.
4. **dNBR series**. The dNBR series records the dNBR of each image using a given image's NBR and the mean estimated from the previous year. The timing of a sustained drop in dNBR can be used to pinpoint the date of change. With this metric, the mean of this series in the current year can be captured. This produces an image close to that of a dNBR using a Best Available Pixel for each year but will struggle to capture disturbances that are mid to late in the season.
5. **Anomaly dNBR (adNBR**). This limits the dNBR series to those observations that were outside the expectation established in the prior year. I use a z-score to evaluate whether a value has significantly dropped outside expectation. The mean or median of this selective series should be less driven by the timing of any disturbance and more by the

mean of the full dNBR series (criteria 4) criteria, which is strongly influenced by the number of images before and after a disturbance.

Each of the criteria has a function, strengths, and weaknesses (Table 1).

Table 2 Criteria for SLIMS and indices for change detection.

SLIMS Criteria				
Index	**Criterion**	**Function**	**Strengths**	**Weakness**
1	**Mean NBR Prior Year**	Initial Treed State	Identifies stands that could be replaced in current year	Cloud, snow cover both bright; lower bound unclear
2	**Two-year slope**	Change / No Change	Employs all data, resilient against transient noise	Susceptible to cloud/shadows; late occurring events may not have enough power
3	**Current-year Slope**	Fire vs. Harvest vs. No Change	Distinguishes harvest (flat line) vs. fire (sloped line) in pixels that changed in target year	Where there are a small number of images in the target year, a fitted line with few images is susceptible to noise
4	**dNBR time series: mean of dNBRs in current year**	Change / No Change	Approximates dNBR of BAP	Fires mid-season and later can be produce varied data that is harder to parse: with some values small and some large, a true late fire can go undetected
5	**"Anomaly dNBR": dNBR mean in current-year images lying outside last year's mean and SD**	Change / No Change	Like #3, but only for dNBR established as outside expectation. Gets true end-state value (e.g., gathers up post-fire values)	Too-tight distribution of NBR values in prior year could mark many as outside expectation. Susceptible to cloud shadows and overreacting to a few low values

7.6 Synthetic (Preliminary) Assessments

I composed two synthetic assessments (Table 2) of the time series that enhanced the contrast between changed and unchanged pixels. These facilitated visual inspection to evaluate the power and behaviour of individual criteria in detecting change. A synthetic assessment arranges individual criteria (from Table 1) into informative three-band combinations for inspection by assigning each criterion to either the red, green, or blue band (Table 2). For synthesis A, criteria 2 was assigned to the red band, criteria 5 to green, and 3 to blue, this allows to draw the result as a colored picture. Criteria 4 was omitted from the synthetic assessments because while it can differentiate between disturbed and undisturbed pixels, it did not perform as well as Criteria 2, 3, or 5. With synthesis A any type of disturbance can be displayed, while Synthesis B is specific to harvest and fire (stand replacement) in forests.

Table 3 Landscape views built from individual criteria, channelled to RGB respectively.

Synthetic RGB Assessments		
Index	**Criteria**	**Function**
Synthesis A	2, 5, 3	Disturbance of any type, with distinction of harvest and fire
Synthesis B	2, 1, 3	Stand replacing disturbance, with distinction of harvest and fire

7.7 Composite Assessment

I sampled and examined the resulting data layers and classification in order to create thresholds per-criterion and make a binary assessment of disturbed versus undisturbed. I present here four scenes of different land cover disturbance that demonstrate the performance and capture of change. I summarize the five criteria as a simple sum of binary assessments to produce a range of values between 0 and 5. This is referred to in the figures as the Sum of Five, where 5 represents having satisfied all five of the characteristic criteria, and the more criteria satisfied, the more confidence in the change detection. This has the effect of weighing each criterion (Table 1) equally. Taking these values as proportions provides an estimate of the probability that a stand-replacing change has occurred in the target year.

7.8 Estimates of stand-replacing change using both data streams

The five criteria summarizing each sensor's data stream can be combined in any number of ways that might be sensitive to each sensor's image quality or timing, spatial resolution, or image frequency. Here, I computed the mean value of the Sum of Five criteria for each sensor, producing a multi-sensor assessment of the likelihood that stand-replacing change has occurred in a pixel. In combining the data streams in this way, it weighs the information from each sensor equally.

8 Results

The visual examination of the study area, in particular of the four exemplar scenes, reveals SLIMS ability to capture harvest and fire disturbance. The iterative process of SLIMS yields several time sequences: NBR, two-year slope, study-year slope, dNBR and adNBR for both sensor's data streams which are each sufficient to capture changes to different extents on their own. When used in various combinations (as in synthetic assessment, more so in Sum of Five) their change capture ability is enhanced.

The presentation of results here is divided by disturbance type exemplar scene and then each section is presented following the structure of the methods: the Five Criteria, synthetic assessment, and the Sum of Five composites for each sensor separately. Finally, the estimates of stand-replacing change are considered with both sensors combined. In this way the contribution of each sensor and each change criterion is examined separately and then together.

8.1 Detection of Harvests

In 2016, the harvest region (Figure 6) comprised a mostly forested area. The signal for a pixel typical of a stand that is harvested, drops significantly between the end of the previous year and the start of the monitoring period in the later year illustrated by the bold orange line in Figure 4. This is reflected in the negative trend in the Two-Year Slope (lighter Trend Lines in Figure 4). This drop is shown in Figure 6 Panel 2 as lighter regions. In the later year the NBR values, while noisy, produce a non-negative trend (the teal line in Figure 5).

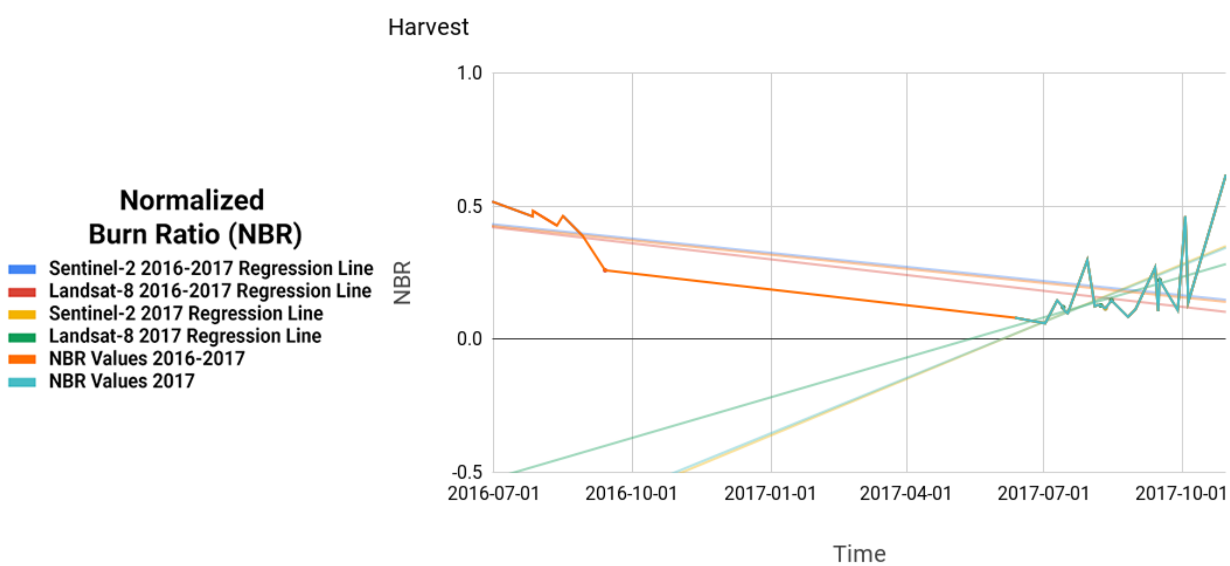

Figure 5 The Two-year and one-year slopes for pixels typical of harvests in the study area and corresponds to the schematic of Figure 4. In orange and then teal (left to right) is a single, sensors-merged, NBR series with corresponding two-year regression lines and one-year regression lines (one each considering only the points for Landsat-8 and Sentinel-2).

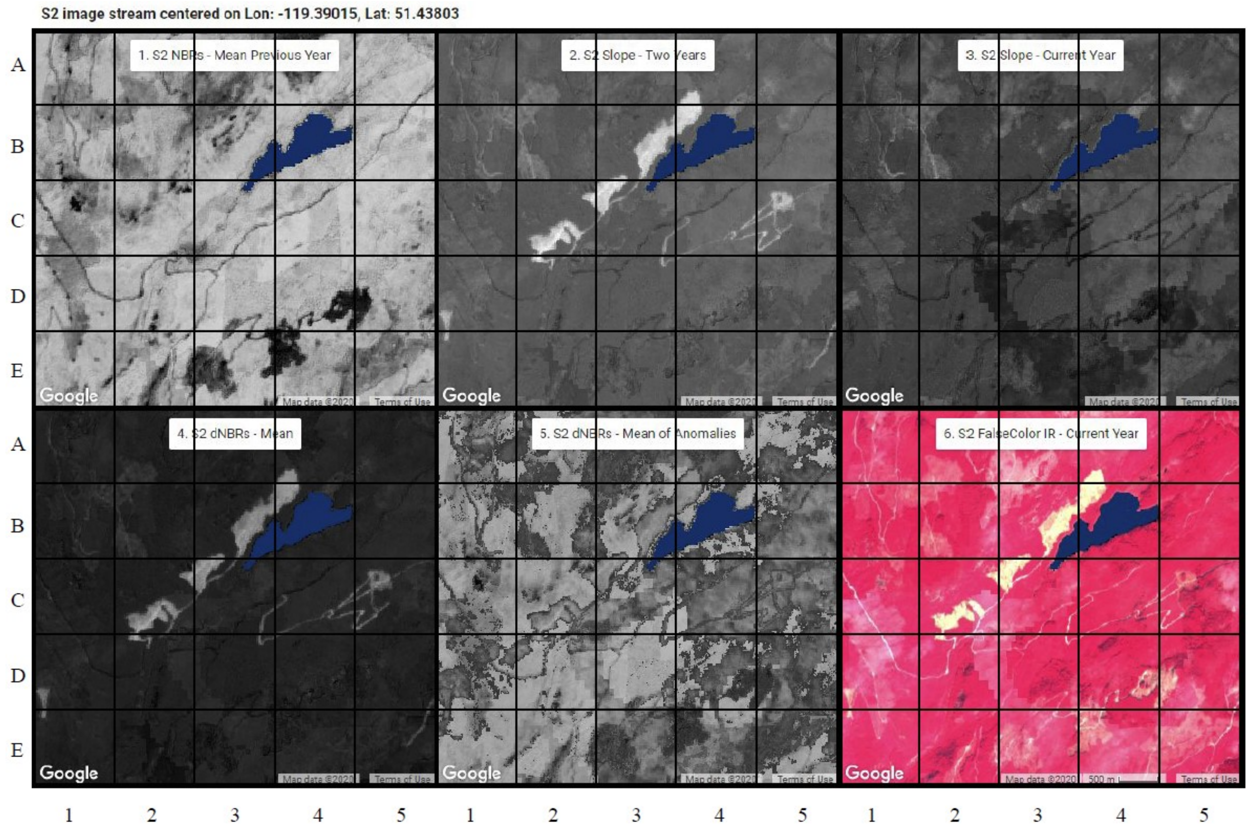

Figure 6. Five criteria and a false-colour infrared representation of the target year for ***Sentinel-2*** *in the Harvest area. Panel 1 (top left): the NBR for the previous year (2016) with dark areas showing low NBR values. Panel 2 (top centre): slope of the two-year regression line with values inverted such that more negative values are lighter in colour. Panel 3 (top right): slope of the one-year (2017) regression line, also inverted so that positive sloping trend lines are darker. Panel 4 (bottom left): the difference between average NBR values of 2016 and 2017, colour scale inverted such that a negative value (indicating loss of vegetation) is lighter in colour. Panel 5 (bottom centre): the anomalous NBR values of 2017 subtracted from the mean NBR values of 2016. Harvest is visible when comparing cells with those of other panels, but the overall image is quite noisy. Panel 6 (bottom right): false colour infra-red image of the scene with RGB channels using infrared, red, and green, such that lighter areas are exposed terrain and red areas are vegetation cover.*

The harvest scene features a lake in sector B4; a road in sector D1 traveling to the southeast; three areas of apparent harvest that were already evident in 2016, in sectors D4, D5, E3 and E4; possible logging road in sector C1 and D1, as revealed in the mean NBR value for 2016 (Figure 6, Panel 1) and a color-IR view of the area in a representative 2017 growing season image (Figure 6, Panel 6). The sequence of NBR values across the two years indicated a drop between 2016 and 2017 (due to overwinter harvesting) and a steady, low signal in 2017 (sectors C2 or B3 in Figure 6, Panel 3 show no features, for example). Between 2016 and the end of the growing season of 2017, the fitted slope of NBR values indicated a large drop in sectors C2, C3, B3, and B4, with logging roads joining them in C2 and C3 (Figure 6, Panel 2). There is also an indication of logging activity in sectors C4 and C5.

It is noteworthy that the slope in 2017 in the apparent harvest areas (Figure 6, Panel 3) is at or near 0, as expected in harvest areas. The mean dNBR values for the 2017 growing season show harvest between sectors C2 and A4, with road building activity in C3 to C5 (Figure 6, Panel 4). For this harvest area, the mean of anomalous dNBR values is an uninformative criterion (Figure 6, Panel 5), and does not show any meaningful distinction between harvest and non-harvest sectors. Although the harvest is somewhat visible as mid-tone regions with darker outlines, overall disturbance has no predominant presentation and appears patchy throughout the scene.

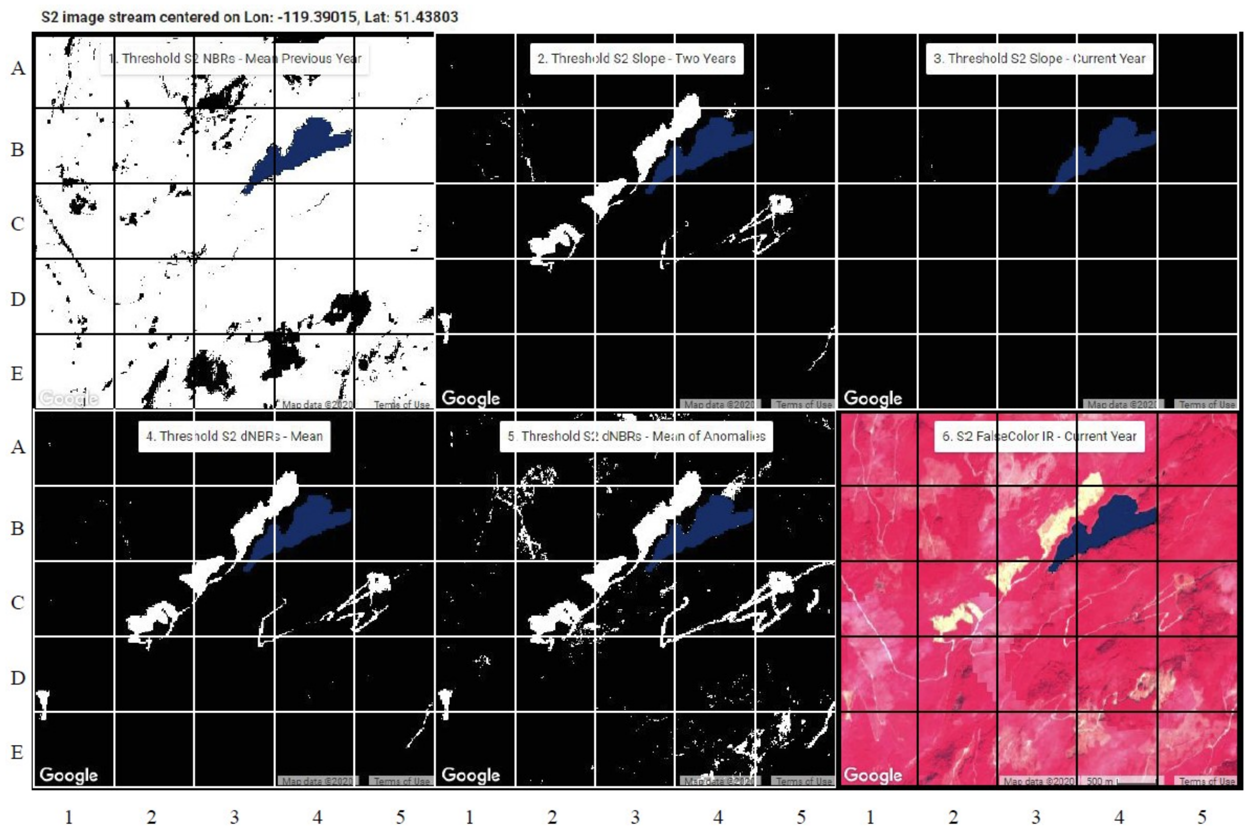

*Figure 7. Panels 1 to 5 (bottom centre, left; top left, centre, right): Thresholds of the five criteria (7.5 Table 1) for **Sentinel-2** in the Harvest area. Everywhere the threshold criterion is met the figure is white. Panel 1 (top left): Illustrating NBR values exceed that of a user-adjustable threshold of NBR and can be considered forest land cover. Panel 2 (top centre): the slope of the regression line for two years is sufficiently negative in areas where reference data suggest is harvest. Panel 3 (top right): a black image satisfies expectations that no change occurs during the target year. Panel 4 (bottom left): the differenced Normalized Burn Ratio identifies areas of vegetation loss between prior year and target year, in white. Panel 5 (bottom centre): thresholding the captured anomalous dNBR values reveals a sensitivity to linear disturbance objects. Panel 6 (bottom right): false colour infra-red image of the scene with RGB channels using infrared, red, and green, such that lighter areas are exposed terrain and red areas are vegetation cover.*

The first five panels in Figure 7 illustrate locations in white where their respective criteria in Figure 6 satisfy threshold values. For example, in Panel 1 the region is almost completely white as most pixels in this region met the criteria for forest in the mean NBR value of 2016. Panels 2, 4, and 5 reveal apparent harvest sites in white as well as other smaller features while Panel 3 is empty because the slope value in 2017 is close to zero. The anomalous dNBR criterion (Panel 5) surprises with its sensitivity to fine-scale linear objects e.g., the road network in A2 and B2 as well as capturing increased noise in regions such as D4, when compared against Panel 4, the simple difference of NBR means which does not show the noise.

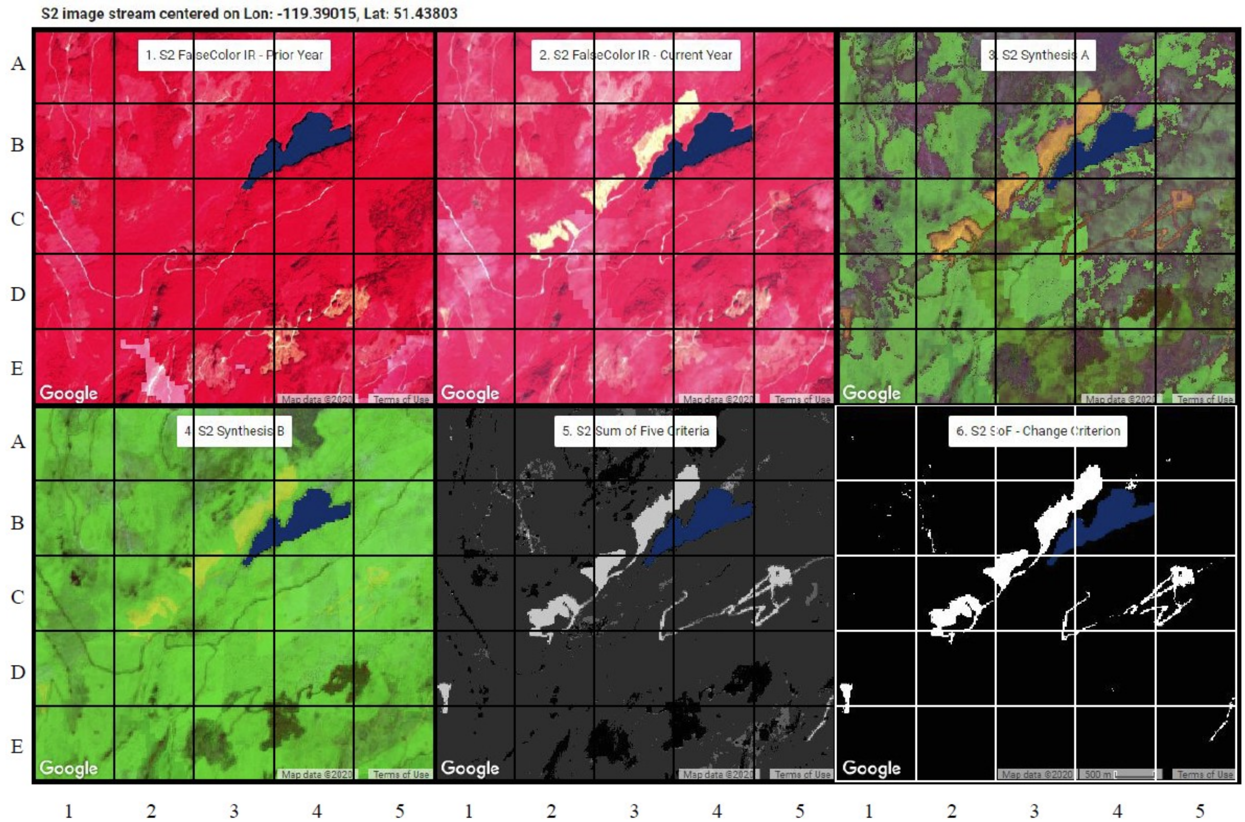

Figure 8. Panels 1 & 2 (top left, top centre): Harvest area, ***Sentinel-2*** *representative images for the earlier and later years respectively, in NIR false colour. Panel 3 (top right): RGB composite for Synthesis A. RED: Two-Year Slope inverse values; GREEN: anomalous NBR values from 2017 differenced from 2016; BLUE: Target-Year Slope inverse values. Panel 4 (bottom left): RGB composite for Synthesis B. RED: Two-Year Slope inverse values; GREEN: Target-Year mean NBR values; BLUE: Target-Year Slope inverse values. Panel 5 (bottom centre): summation of the 5 criteria. Panel 6 (bottom right): indicates areas of agreement between 3 or more criteria.*

The first Panel in Figure 8 is a false colour infrared illustration of the harvest region in the year prior to the investigation. Existing logging work is visible in cells such as D4 and E4. Those and other persistent features remain visible in Panel 2, the false colour infrared illustration of the harvest region in 2017, the target year. The Synthesis Product A in Panel 3 reveals the two-year line-of-best-fit slope values as the image's red band. The green intensity is representative of areas that do not have anomalous dNBR values in 2017, and the blue channel is the slope in 2017 and thus almost entirely absent, (apart from water features like the one in B3 and B4 which are not products of these 3 bands). Exchanging the anomalous dNBR for the NBR values of the 2016 year, in the green visualization band yields Synthesis B in Panel 4. The intensity of the colour green is thus low in areas of existing logging like E2 to E5. Summing the binary layers of Panels 1 to 5 in Figure 7 give a single score between 0 and 4 (not 5) everywhere, and I show that in Figure 8, Panel 5 as a monochrome gradation with higher scores in lighter grey indicating more agreement between the change criteria. The maximum score for harvest is 4 because the slope in the target year (here 2017) should *not* cross a threshold of significant steepness (see Change Criteria 2 & 3 in section 7.5). Harvest areas near the centre of the frame are lighter in colour indicating stronger agreement between criteria while weaker agreement can be seen in the heterogeneous regions in E4 and E5. Finally, in Panel 6 white areas in the binary layer represent an agreement between 3 or more criteria.

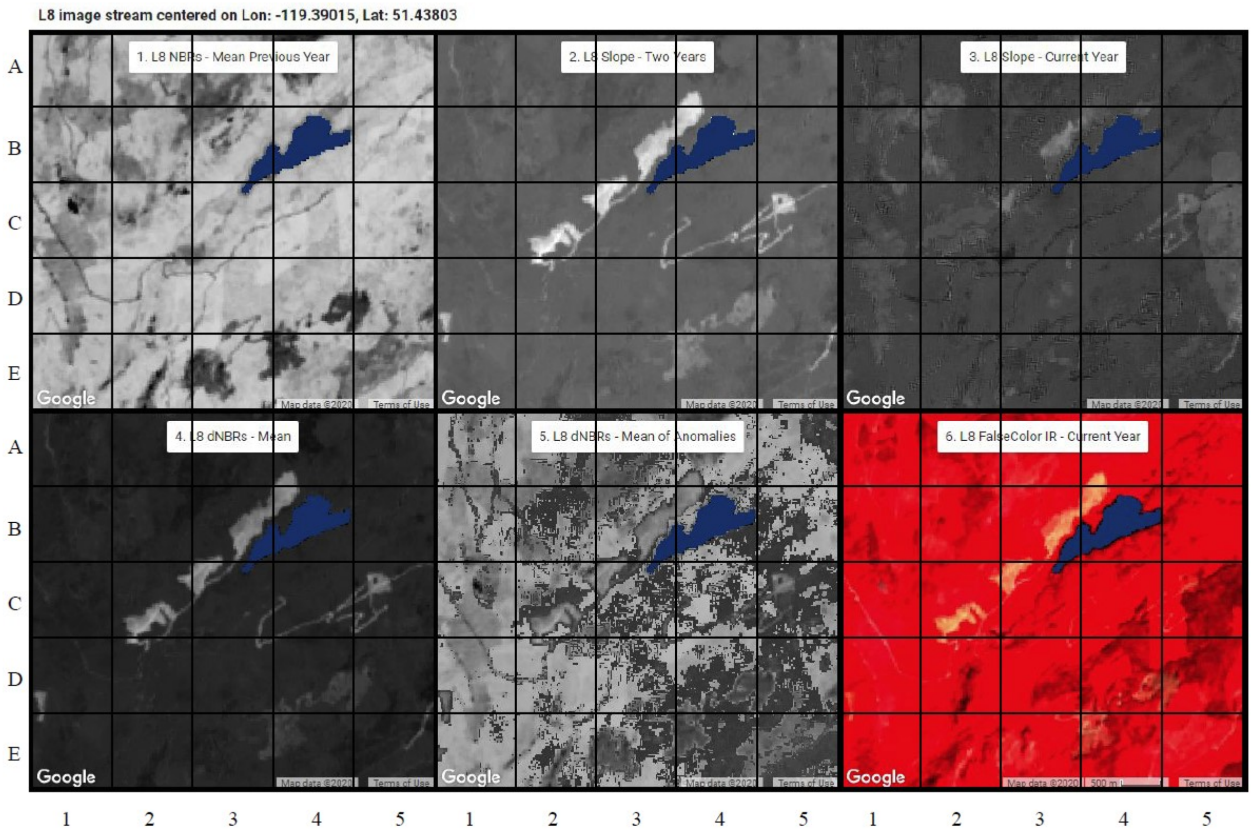

Figure 9. Five criteria and a false-colour infrared representation of the target year for ***Landsat-8*** *in the Harvest area, like that for Sentinel-2 in Figure 6. Panel 1 (top left): the NBR for the previous year (2016) with dark areas showing low NBR values. Panel 2 (top middle): slope of the two-year regression line with values inverted such that more negative values are lighter in colour. Panel 3 (top right): slope of the one-year (2017) regression line, also inverted so that positive sloping trend lines are darker. Panel 4 (bottom left): the difference between average NBR values of 2016 and 2017, colour scale inverted such that a negative value (indicating loss of vegetation) is lighter in colour. Panel 5 (bottom middle): the anomalous NBR values of 2017 subtracted from the mean NBR values of 2016. Again, harvest is visible in a fashion when comparing cells with those of other panels, but the overall image is quite noisy. Panel 6 (bottom right): false colour infra-red image of the scene with RGB channels using infrared, red, and green, such that lighter areas are exposed terrain and red areas are vegetation cover.*

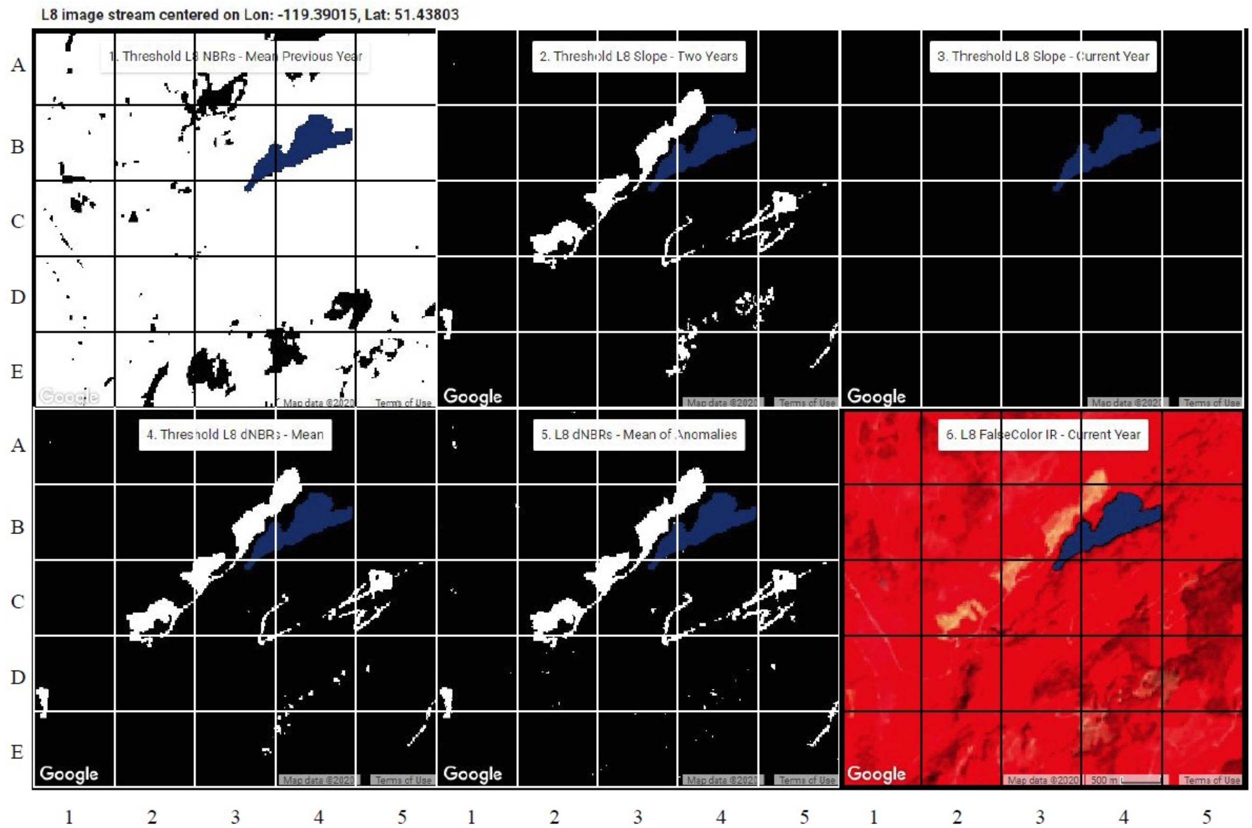

Figure 10. Panels 1 to 5 (bottom centre, left; top left, centre, right): Thresholds of the five criteria (7.5 Table 1) for ***Landsat-8*** *in the harvest area. Everywhere the threshold criterion is met the figure is white. Panel 1 (top left): Illustrating NBR values exceed that of a user-adjustable threshold of NBR and can be considered forest land cover. Panel 2 (top centre): the slope of the regression line for two years is sufficiently negative in areas reference data suggest is harvest. Panel 3 (top right): a black image satisfies expectations that no change occurs during the observation period. Panel 4 (bottom left): the differenced Normalized Burn Ratio identifies areas of vegetation loss between prior year and target year, in white. Panel 5 (bottom centre): thresholding the captured anomalous dNBR values reveals a sensitivity to linear disturbance objects. Panel 6 (bottom right): false colour infra-red image of the scene with RGB channels using infrared, red, and green, such that lighter areas are exposed terrain and red areas are vegetation cover.*

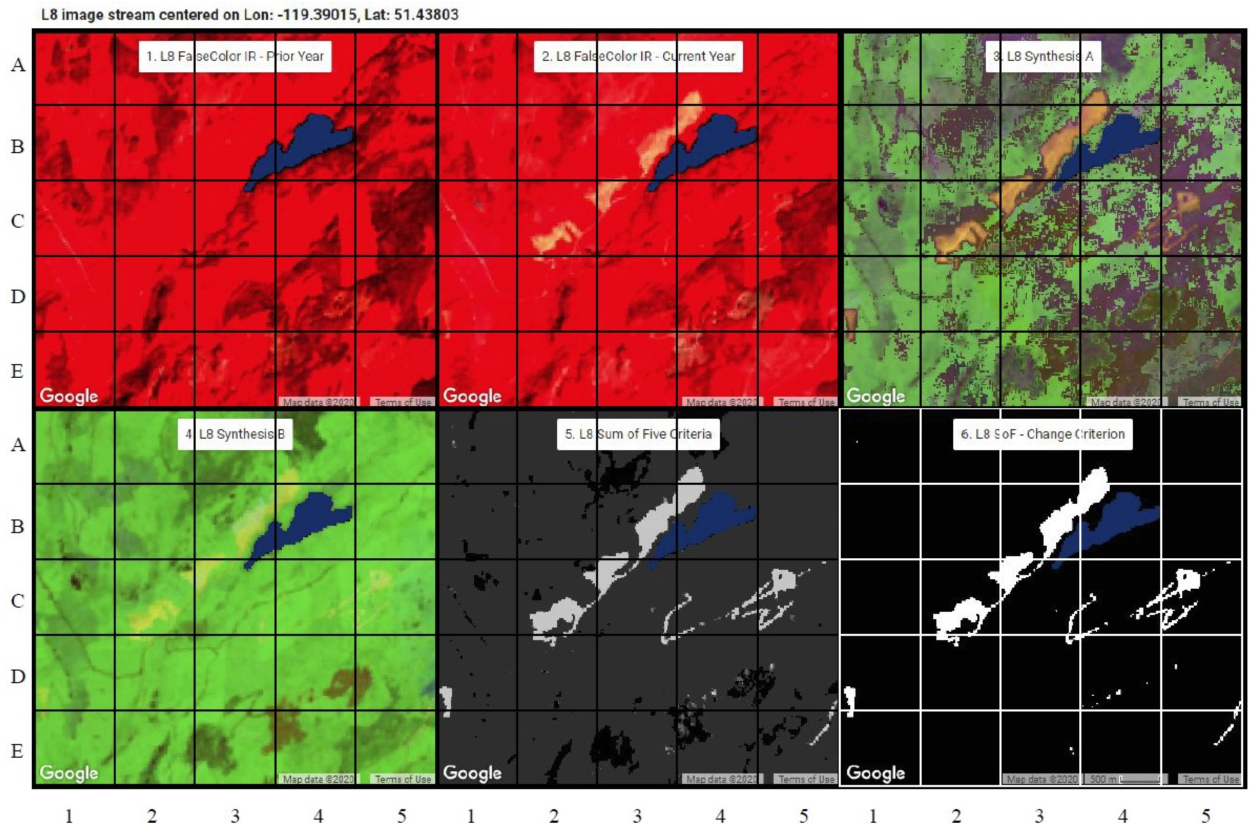

*Figure 11. **Landsat 8** representative images for the earlier and later years, in NIR false colour, panels 1 and 2 respectively. Panel 3 (top right): RGB composite for Synthesis A. RED: Two-Year Slope inverse values; GREEN: anomalous NBR values from 2017 differenced from 2016; BLUE: Target-Year Slope inverse values. Panel 4 (bottom left): RGB composite for Synthesis B. RED: Two-Year Slope inverse values; GREEN: Target-Year mean NBR values; BLUE: Target-Year Slope inverse values. Panel 5 (bottom centre): summation of the 5 criteria. Panel 6 (bottom right): indicates areas of agreement between 3 or more criteria.*

Figure 9, Figure 10, and Figure 11 provide the same information as Figures 6, 7, and 8 respectively but for the Landsat-8 data stream. Such that figures 6 and 9, figures 7 and 10, and figures 8 and 11 are directly comparable. Generally speaking, because of the lower spatial resolution of Landsat-8, there are fewer narrow linear features (e.g., the cut in Figure 7-2-B2 is entirely absent in Figure 10-2-B2) and the edges of these features tend to be coarser. In Figure 11 Panel 5, areas like D4, D5, and E4 highlight a bit of noise in lighter grey colours which might end up as noise in a final classification but when combined with Sentinel-2, areas like this are eliminated.

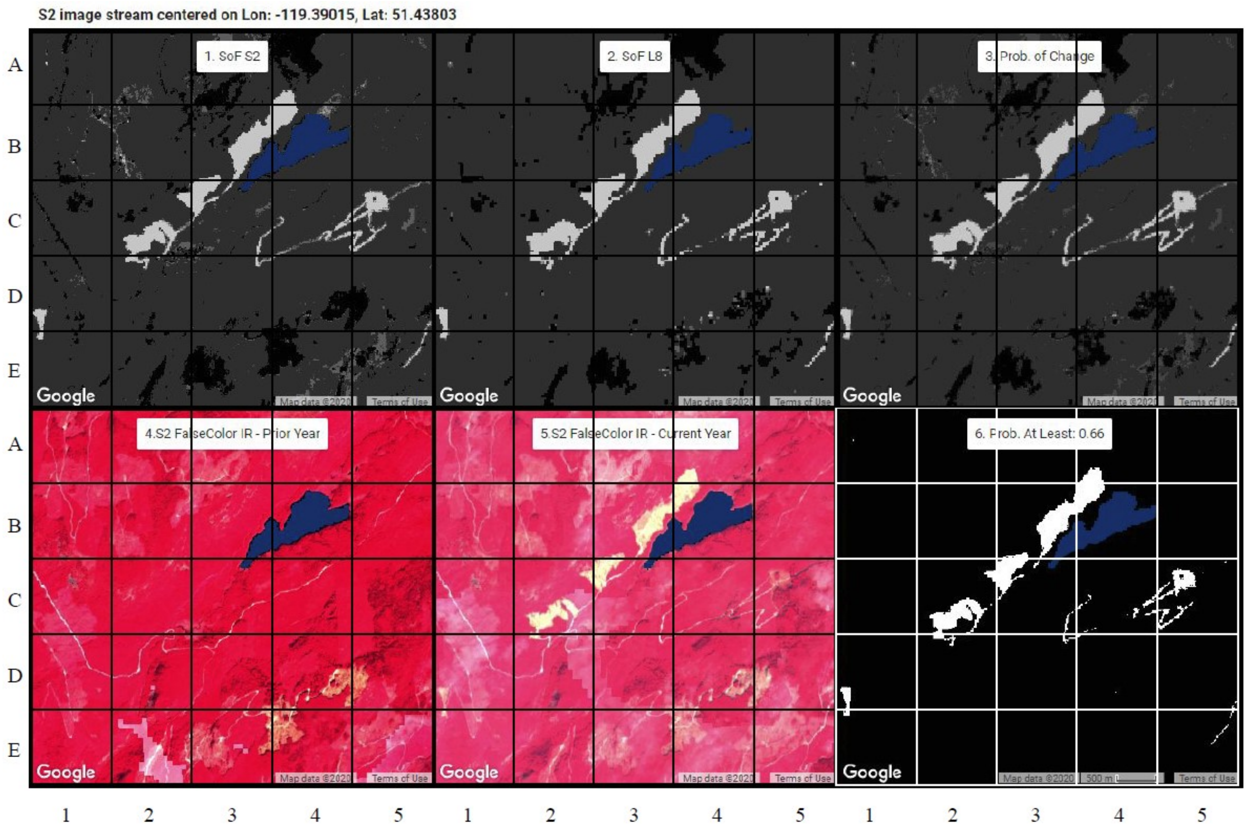

Figure 12. Panels 1 & 2 (top left, top centre): an estimated probability of change from ***Sentinel-2*** *and* ***Landsat-8*** *separately, and in panel 3 (top right) their jointly considered probability of change. Lighter areas are more likely change than darker areas. Panel 6 (bottom right): a 'thresholded' view of said estimate of change at 66% likelihood or greater, that a change has occurred in the Harvest area (white is disturbed, black is undisturbed). Panels 4 & 5 (bottom left, bottom centre): representative NIR false colour for both years; red areas are vegetation cover and yellower areas are bare ground.*

Panels 1 and 2 illustrate the sums of the five criteria for each sensor in Figure 12. Due to the finer spatial resolution of Sentinel-2 as compared with Landsat-8, areas of increased heterogeneity are revealed (lighter colours represent more likely disturbed areas) in Panel 1 (e.g., sector B2) that are absent from Panel 2. The jointly considered estimated probability of change, i.e., the mean of the probabilities reported over both sensors is visualized in Panel 3, rendered in greyscale like the first two Panels but with additional gradations. In Panel 6, white pixels indicate areas where the probability of change is greater than, or equal to 66% (a threshold obtained through subjective interpretation) using both sensors. This reveals the large areas of harvest, and wider linear elements that change by the end of the 2017 growing season.

8.2 Detection of Early Fire

The next series of seven figures, beginning with Appendix A Figure 16, represent the same criteria, synthetic assessments, and downstream calculations as with harvest, in a region where fire occurred early in the nominal monitoring period. Three small bodies of water are visible in this scene in sectors A4, A5, and D2.

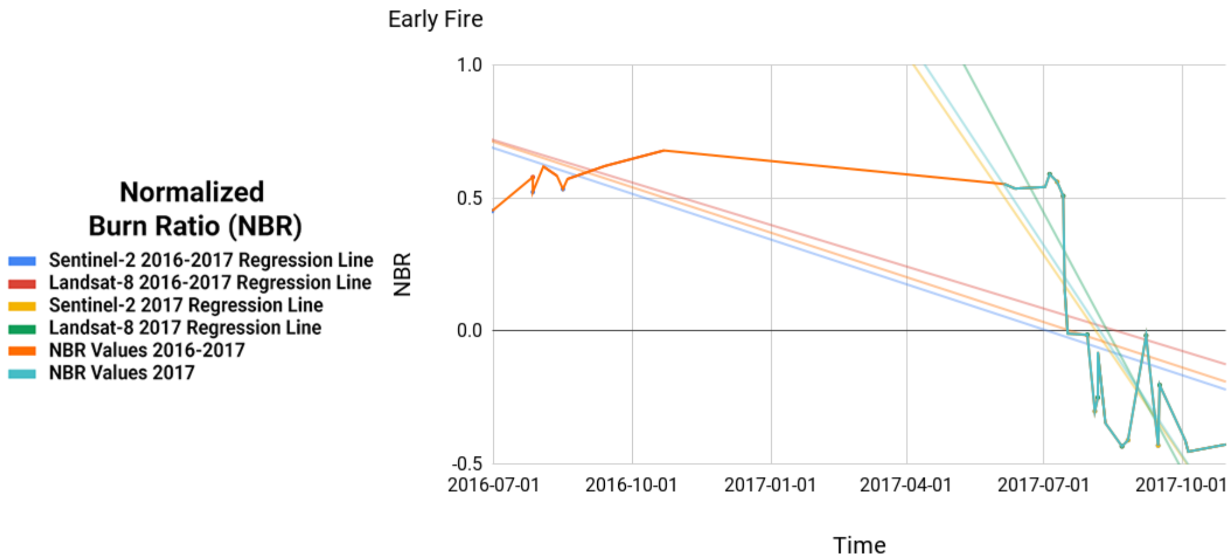

Figure 13 Two-year and one-year slopes for pixels typical of an early-season the study area, corresponding to the schematic of Figure 4. In orange and then teal (left to right) is a single, sensors-merged, NBR series with corresponding two-year regression lines and one-year regression lines (one each considering only the points for Landsat-8 and Sentinel-2).

For early fire areas, the graph (Figure 13) of a representative pixel's NBR values visualized indicates that a stable, positive NBR sequence in the first year (here 2016) shifts to a negative one in the early part of the second year. In this area, the shift occurs in July 2017 (Figure 13, teal portion of the bold line). As a result of this drop, the trend line spanning both years of the data stream is more negative compared to the trend line of a pixel interpreted as harvest (Figure 5). Panel 2 in Appendix A Figure 16 shows these types of pixels, assumed burned area, in light grey. The negative NBR values in the second year translate into a negative slope of the corresponding trend lines (light yellow, blue, and green on the right-hand side of Figure 13) - the lighter portions of Panel 3 in Appendix A Figure 16 represent these negative values.

In the early fire scene, prominent features include a network of vegetation extending from the northwest to the south and southeast; the largest patch of cultivated land in this scene is centered in E3. These pixels demonstrate NBR values sufficiently high to count as 'treed' in the 2016 observation period but remain largely undisturbed by fire in 2017 as seen in e.g., Panel 6 of Appendix A Figure 22 where the area appears in black.

There are notable differences between the Sentinel-2 (Appendix A Figure 16) and Landsat-8 (Appendix A Figure 19) second-year slope values in their respective Panel 3, and a larger area is captured as change by Landsat that is missed by Sentinel e.g., sectors B4 or C2 in Appendix A Figures 17 and 20 respectively. These elevated values are prominent in the threshold figures as white regions, and higher levels in the blue band of Synthesis B (Appendix A Figures 18 and 21 Panel 4).

Looking again at Appendix A Figures 16 and19 (Sentinel-2 and Landsat-8 respectively) panel 3, Sector C1 sees similar drops in NBR values. Although for each individual sensor there is an estimated 60% likelihood of stand-replacing change for the majority of the area within C1 (Appendix A Figures 18 and 21 Panel 5) when the sensors are considered jointly however, the area in C1 does not meet the final elevated criteria (66% agreement between all indicators) for stand replacing change shown in Appendix A Figure 22, Panel 6.

Comparing the change criterion panels, Panel 6 of Appendix A Figure 18 and Appendix A Figure 21, shows less agreement for Landsat-8 than Sentinel-2, as in sector B2 or E5 for example. Many more fields of vegetation in Synthesis A (Panel 3) exhibit a green quality for Sentinel-2 suggesting a greater proportion of anomalous NBR values in those areas (B1, B2, E3, etc.). However, Landsat-8 has more agreement between its evaluation criteria than Sentinel-2, seen in Panel 5 as more light-grey and more white, sectors E1 and E2.

8.3 Detection of Late Fire

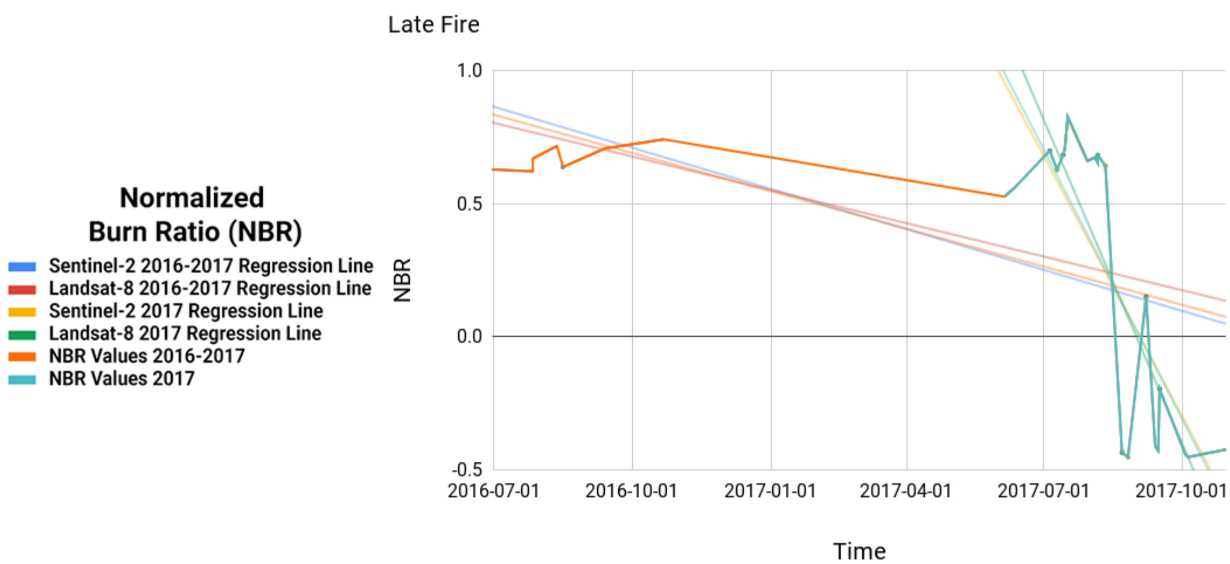

Figure 14 Two-year and one-year slopes for pixels typical of late-season fire in the study area and corresponds with the schematic of Figure 4. In orange and then teal (left to right) is a single, sensors-merged, NBR series with corresponding two-year regression lines and one-year regression lines (one each considering only the points for Landsat-8 and Sentinel-2).

In Appendix A Figure 23 and Appendix A Figure 26 a late-season fire is apparent in Panels 2 through 6 in sectors C1 southwards to E1 and diagonally to the northeast sector B1 and a bit beyond. A lower 'arm' of the fire runs parallel southwest-to-northeast from E2. While there are few obvious roads at this scale, this scene features numerous valleys with lakes and rivers e.g., sectors A1, A2, D2, etc. and the scenes are largely the same for both sensors. This LULC focus region was included to determine the feasibility of capturing the signal of forest fire with fewer images compared with an early-season fire occurrence (Appendix A Figures 16 – 22). The smaller number of NBR values emblematic of a fire occurrence, exert less influence on the Two-Year trend line, though they still weigh heavily on the Later-Year slope. The late fire is illustrated by the delayed drop in NBR values on the teal line compared to that in the upper right quadrant (Figure 14). With fewer available images post-fire than for an early fire, the one-year slope criterion for the second year might be shallower, yet it is still possible to leverage the Anomalous dNBR values (Appendix A Figure 23, Panel 5) in areas with late fires.

Comparing the results of the Sentinel-2 (Figure 24) and Landsat-8 (Figure 27) data, the thresholds for the criteria (NBR values in their respective 1st panels and dNBR values in their 4th panels) suggest additional fine-scale change detail for Sentinel-2 not captured in the Landsat-8 data, such as the vertical striations in sector A5. For Landsat-8, the slope of the two-year trend line, the mean dNBR values and the anomalous dNBR values all capture less apparent change than their Sentinel-2 equivalents and the Landsat-8 panels (Appendix A Figure 27 Panels 1 – 5) are overall darker images. It appears that Appendix A Figure 24 Panel 5 for Sentinel-2 is polluted with commission error for change which can occur when the NBR trajectory in the prior year has very little variation, creating a small standard deviation. For both sensors, the 'thresholded' mean dNBR values are the most restrained and between the sensors the slopes for the current year are most alike.

A greater gradation in the Sum of Five Panels for Sentinel-2 (Appendix A Figure 25) when compared to Landsat-8 (Appendix A Figure 28) suggests greater inter-criterion disagreement for Landsat-8. In the northeastern sectors A4 to B5 the lower overall agreement for Landsat-8 leads to less white in the same area for the five change criterion. As before, the Anomalous dNBR criterion is more fragmented for Sentinel-2 than Landsat-8 and the green band of Synthesis A reflects this fact. A prominent example of this effect is sector B1. When the two Sums of Five layers are averaged together, they behave as expected and produce a reasonable estimated change probability threshold map for Appendix A Figure 29, Panel 6.

8.4 Detection of Forest Stability

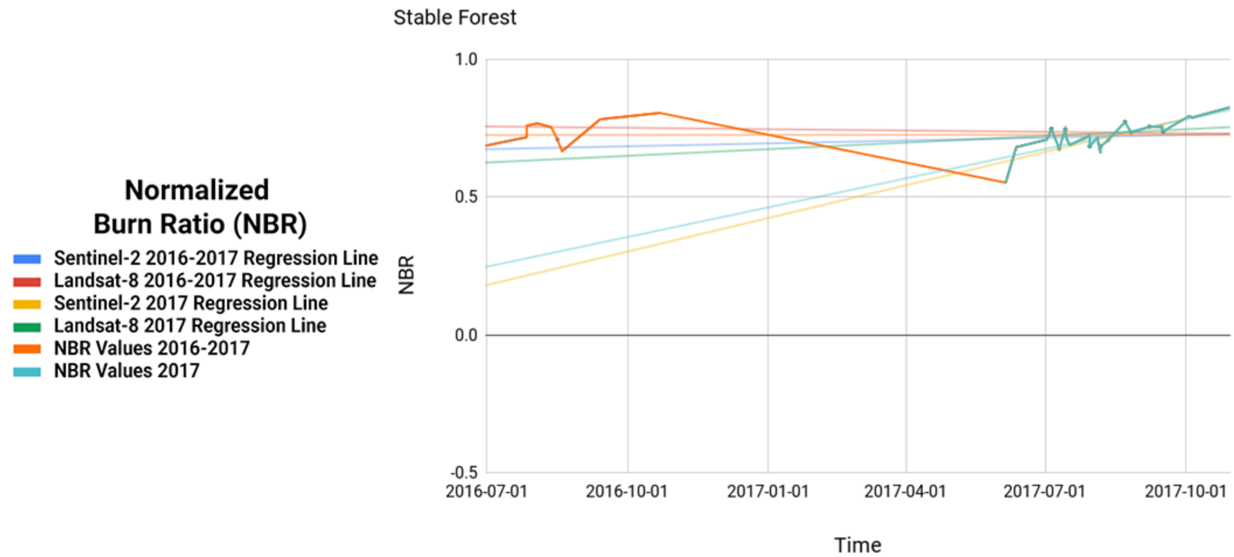

Figure 15 Two-year and one-year slopes for pixels typical of undisturbed forest the study area, corresponding to the schematic of Figure 4. In orange and then teal (left to right) is a single, sensors-merged, NBR series with corresponding two-year regression lines and one-year regression lines (one each considering only the points for Landsat-8 and Sentinel-2).

In 2016, the selected forest region lacks remarkable features aside from bodies of water in A4, C3, D5, E4 and remains largely unchanged in 2017. The area displays a steady series of NBR values spanning both years (Figure 15), correspondingly flat two-year trend lines, and non-negative trend lines in the later year slopes. Contrasting Landsat-8 and Sentinel-2, the two-year slope of the former is less dynamic over the extent of the scene in Appendix A Figure 33, Panel 2. Examining the later year slope shows that the opposite is true, and that Sentinel-2 has less dynamic range in Appendix A Figure 30.

As described in Table 2, the Anomalous dNBR index is susceptible to noise if the NBR values from the prior year are exceptionally stable. This index contributes substantial noise for Sentinel-2 in Appendix A Figure 31 Panel 5 and for Landsat-8 it contributes to Synthesis A in Appendix A Figure 35 Panel 3. By evaluating the sensors in conjunction, a stable and change-free region appears as expected in Appendix A Figure 36, Panel 6. This reveals that there is stability in the vegetations reflectance in these regions and not simply a lack of indication of disturbance.

8.5 Separation of Fire and Harvest

As suggested by the schematic of Figure 4 the NBR vectors for fire and harvest are unlike one another, and the target-year slope can be used to discriminate them. Harvests that occur over the winter or in the target year produce a shallower line of best fit than fires do yet Figures 5, 13, & 14 reveal an additional trait. There is separability of harvest from fire using their residual NBR values as well, which is captured in the adNBR.

9 Discussion

In this thesis, I found that even in cloudy and smoke-filled areas (e.g., areas that experienced fire), there were enough images to consider and classify land cover independently within the Landsat-8 and Sentinel-2 streams. In some pixels that were either persistently cloudy or smoky in 2017, the estimated probability is lower, which could be quantified by considering the results in each pixel and the number of images used to produce and evaluate the criteria developed. In the Sentinel-2 stream, there were fewer images available for regression-fitting in 2016 due to the sensor pair's launch and calibration schedule; having only 2A and not 2B did not affect the results in most pixels, though some pixels were only imaged once or twice in 2016, which created noise in those areas. With both Sentinel-2A and -2B in operation, as has been the case since 2017, an increase in total imagery is to be expected. This would result in a corresponding increase in clear observations, leading to greater confidence in every pixel overall.

Prior to this work, the characteristics of each sensor's signals (e.g., approximate upper and lower bounds, mean values for various land covers, etc.), in all their variety, across such a large area were unknown to me. My initial efforts to replicate simple dNBR thresholding was unsuccessful on individual images. Large swaths of the unchanged study area (e.g., natural grasslands, bare rock) exhibited NBR or dNBR values on a given day that mimicked those of recently harvested forest. This meant that earlier work like that by Crowley et al. (2019) in tracing severe fires with a single dNBR threshold could not be repeated exactly as done before when working with about a hundred times more pixels beyond known fire boundaries. More within-year and between-year context was needed to classify stability and change across the large area, a contributing factor that led to the development of the SLIMS algorithm.

The SLIMS algorithm developed in this thesis interprets characteristics of the NBR signal series, in short increments of two years. SLIMS is as an algorithm which is able to discard nearly all of the information it receives (e.g., all but the most recent mean and standard deviation values) and hold only a two-year buffer of NBR values as it interprets the NBR signal, thereby decreasing its overall memory requirements. With this implementation of SLIMS, I used the five criteria: (1) mean of the previous year's NBR values, (2) slope of NBR values between years, (3) slope of NBR values within the target year, (4) mean of the series of dNBR values, and (5) the mean of the series of dNBR values that were 'anomalous', (i.e., considerably outside expectation). The use of five possible criteria instead of only one provides greater confidence in the detection and interpretation of change from satellite imageries.

The NBR value streams for Sentinel-2 and Landsat-8, though highly compatible, were treated as two separate streams rather than being combined to a single stream. Images from each sensor were, with some exceptions, frequent enough for the SLIMS criteria to be evaluated in each pixel. This allowed me to produce two complementary assessments of change, which could be combined in any way desired e.g., by using BULC. In this thesis, I used the average SLIMS score across the two streams to classify change – though it would be equally possible to use the maximum score, the minimum score, or require a pixel to be estimated to have changed in both streams before reporting it as likely change.

Across an area as large as UTM Zone 10N, there is a substantial computational cost to generating and evaluating many thousands of individual-day LULC classifications to prepare for ingestion into BULC. Before the development of SLIMS, testing and assessing different classification parameters was especially time-consuming given that classifications were error-prone when prepared for BULC outside of known fire perimeters. This situation led to the development of SLIMS, which permits on-the-fly trial-and-error assessment of change at large extents. The SLIMS algorithm can be run at year's end in a few minutes in Earth Engine but can also run at any time upon receiving new imagery.

Importantly, I am able to refine the SLIMS outputs by adding value to the probability surface in several ways. Most immediately, SLIMS reliably distinguishes harvest from fire by using the criterion of the target-year slope (as described above), which differs between the two LULC change types. Beyond the difference between the target-year slope values for separating these LULC classes, which I did here, it is also feasible that the mean of the final NBR, or adNBR values could be used to make this distinction, as preliminary inspections showed that a clearcut leaves a higher residual NBR signal than that of a stand replacing fire. Future work will involve the inclusion of additional spectral information to enhance their separation. Because the approach of summing criteria in a point-style system is another way that the SLIMS criteria can be combined, the absolute NBR value of the anomalous-value pixel group is another dimension that could be incorporated. Additionally, the use of Synthesis B recombination slope-driven red, green, and blue bands, illustrates another way the criteria could be easily and usefully combined.

SLIMS can be run throughout a growing season, not just at the end. In this thesis, I show the results of SLIMS running only at the end of the year when a year's worth of images is available to researchers. However, the algorithm is designed to be run on any day with new observations, ingesting that imagery, and updating the probability of change in each pixel. The end-year results shown in this thesis are the same whether SLIMS is run iteratively all summer or not. The result of the design of SLIMS is that it can be used equally to produce a daily, weekly, or monthly time series, as well as an end-of-year assessment layer. Each of the criteria is assembled throughout the season and can be output at each time step either individually or as the summed SLIMS surface.

From a processing standpoint, the fact that only a two-year buffer is needed for calculating slopes is helpful. At each new year, most of the earlier year's information can be forgotten. If needed, it is also possible to diminish memory growth entirely within a year by writing each day's result to disk and assembling a new day's inputs from existing outputs. Importantly, the algorithm does not demand mathematically complex reanalysis at each time step, but rather depends on means, standard deviations, and line-fitting. Still, the SLIMS algorithm pushed up against the limits of what Google Earth Engine could achieve, when applied across the entire UTM zone. It is likely additional performance could be gained through refactoring of the code, or perhaps making use of more efficient intermediate data structures like array images.

End-of-year output from SLIMS is useful as a provisional change estimate product as-is. Given the overall goal of producing a credible estimate of changed pixels using intra- and inter-year dynamics of only two years, the SLIMS output is useful for generating and initial analysis or posterior check for an annual time step classification method. In addition to a classification map, SLIMS outputs a continuous probability surface that estimates, for each pixel, the probability that a pixel was changed in the growing season of the target year according to the two sensor data streams. I illustrated estimated probabilities of change from SLIMS for four characteristic areas of the UTM Zone 10N study region in the results. Brighter pixels are higher probabilities of change as assessed by SLIMS (e.g., Figure 12, panels 1 – 3 show estimated probabilities of change per sensor and then combined).

Though SLIMS change probability estimates or classifications can be input directly to an algorithm like C2C, SLIMS was developed as a means of enabling rapid prototyping of classifications of change surfaces for use with BULC, without needing to manually create hundreds of LULC classifications for BULC to ingest. SLIMS has been developed in anticipation of the BULC algorithm being made native to the Earth Engine platform, which should bring performance enhancements and public availability. In case BULC is not implemented to instantly run across vast areas from the outset, SLIMS can produce a product directly for use in C2C as a provisional product while BULC runs are processing. Thus, the algorithm is able to produce a capstone product for immediate consideration in, for example, C2C and value-added output after processing with BULC. Processing SLIMS output in BULC will dampen remaining stray errors of omission and commission that will inevitably occur during SLIM's evaluation of an entire growing season.

The individual criteria developed for the implementation of SLIMS perform well but the current methods of combining them leave room for further development. There is clearly sufficient information contained in the criteria (as seen in the figures showing the individual criteria, and their joint viewing in the Synthesis indices), but their combination can be further developed.

Future development could include the inclusion of (or substitution for) other change indices, like the Integrated Forest Z-Score (IFZ) allowing the user to select their desired bands based on the vegetation of interest and the particulars of its spectral responses. A modified version of SLIMS that evaluates the first short-wave infrared (SWIR1) band of both Landsat and Sentinel sensors could improve discrimination between fire and harvest changes based on Schroeder et al. (2011) which shows promise.

9.1 Context for Approach

It is worth noting the differences and similarities between the work presented in this thesis and that of Crowley et al. (2019). While highly demanding and advanced in its own right, Crowley et al. (2019) addressed a problem substantially different from what is addressed in this thesis and an itemized comparison of that paper to this thesis is presented below in Table 4. This thesis uses pixels of multiple LULC types and histories and is not limited to known fire perimeters. A major challenge in my work compared to Crowley et al. (2019) was that large parts of my study areas did not experience change and thus often created errors. I included a much larger area than the predefined fire boundaries and used moderated signals in the form of the slope of lines of regression through a time series of NBR values, instead of the NBR values themselves. The past-year information is essential for my work as the context of a pixel is important for its classification.

Table 4 Comparing this thesis against (Crowley et al., 2019)

Factor in consideration	**BULC fire detection work (Crowley et al., 2019)**	**This thesis**
Study area constraints	Pixels within known fire perimeters	All pixels of multiple cover types and histories
Principal challenge	Identifying the timing of fire that was very likely to have occurred in each pixel	Balancing omission and commission errors in pixels, the vast majority of which did not experience change in a given year
Type of disturbance	Forest fire	Forest fire and harvest
Type of signal	Pronounced signal of severe fires from established forests (large NBR change)	Moderated signal: new harvest can look like regrowing forest, bare rock, etc. Less-severe fire can look like other LULC types.
Utility of past-year information	Useful for NBR of BAP for dNBR	Crucial to establishing expectation to understand variation in the large majority of pixels that were not disturbed
What is needed to create events of suitable quality	dNBR adequate	dNBR on a single image can be greatly confused with other LULC for non-severe fires; context necessary to adequately classify pixels to prevent enormous confusion, esp. between harvest and other LULCs

9.2 Complementarity of Sensor Streams in Assessing Change

This thesis considered Landsat-8 and Sentinel-2 as complementary but distinct data sources and used the two to increase confidence and steer away from the commission and omission errors that are occurring when only a single sensor's information is assessed. At the outset of this thesis, it was unclear whether the sensor limitations and data constraints would hamper the blending of information from the two data streams. I found that Sentinel-2's data sparseness in 2016 due to having only one of the twin satellites in operation was not a hindrance to the SLIMS assessment. Further, I found that the relatively infrequency of Landsat-8 data did not prohibit the assessment with SLIMS. Additional imagery from the second Sentinel-2 sensor should only serve to steady the regression's temporal evolution and clarify the resultant classification.

9.3 Strengths of Approach

SLIMS is efficient, demanding only limited memory and processor speed at each time step. Of the criteria presented here, three are computationally efficient (Criteria 3, 4, and 5) and two are slightly less so (Criteria 1 and 2). It is possible to record a dynamically changing mean and standard deviation without holding every item in memory at each time step. Given a current mean and standard deviation and a new observation, it is straightforward to update the sample's new mean and standard deviation without needing to revisit all observations to that point. It is worth noting that there are several ways of combining the information from the streams, and I was able to examine only the NBR in this thesis.

It is worth noting that the present implementation of SLIMS in Earth Engine demands no more than two years of observations (with each image's information compressed into a single band) be stored at any point in time. That is, to store the information from 50 multi-band images over a two-year period, only 50 NBR values would need to be stored. In contrast, if an algorithm needed all bands to be stored for each image, this would be hundred bands of information.

9.4 Weaknesses and Limitations

Although it was largely successful, the work exhibits several weaknesses. First, because landscapes can change across such large areas, any classification system can break down at larger extents. For example, while an NBR threshold for treed cover might be 0.4 in one large region, forest composition or abiotic factors might cause this value to vary in other regions. To combat this, SLIMS builds an expectation in each pixel and carries it forward between years. The intended effect is to track whether a pixel's NBR or dNBR values move substantially outside expectation. Computation of the two-year slope and within-year slope (Criteria 1 and 2) are less efficient than the mean and standard deviation and they require (for the moment) storing the observation set from the two years in order to compute the slope at each time step. I think it could be useful to explore dNBR variation and perform a geographically weighted regression to record how the threshold value should vary across space.

Second, as study areas grow larger, every new composite image day will cover proportionally less of the total landscape. For a year-end classification this should have no impact, but it will have the effect of repeating the last impression for longer and longer periods of time as the interval between image days grows. This must be accounted for when moving to a near-real-time classification sequence, as any transient noise will linger for longer stretches.

Third, other non-stand-replacing changes can be confused with stand-replacing forest change. In this thesis, I found for example that I systematically labeled several agricultural areas as stand-replacing change. Visual inspection suggests that the agricultural areas might be confused for harvest, in that the NBR differs between years due to crop differences or image timing. I expect that crops could be removed from the provisional product by paying particular care to the predictably high variation in those pixels, and that a few years of data could be marshaled to screen those pixels out relatively quickly. It may be beneficial to integrate known LULC in a pre-screening step, disqualifying pixels from further evaluation. This may carry the added benefit of reducing computational cost if fewer pixels are considered for change overall.

9.5 Future Work

Currently slope thresholds must be adjusted manually which limits spatial transferability. The SLIMS algorithm would benefit greatly from the adjustment of the regression slope thresholds based on ground context/data. Perhaps factors like ecozones, latitudes, or a priori vegetation classifications could adjust thresholds in a more comprehensive manner than the current user-set method.

A regression performed on a rolling window of data points from the time series could provide noise damping while still allowing the slope to respond to true changes. The number of points considered at once should be tested to balance sensitivity against specificity and as with thresholds, might depend on ground context.

Future work could examine methods for incremental re-estimation of slopes given new data if the slope-fitting component is expensive to run in either speed or, especially, memory. For example, an absolute magnitude difference between two successive data points might be a helpful check before triggering a regression re-computation.

The Short-Wave Infrared band 1 (SWIR1) may hold promise for discriminating harvest from fire and could be used iteratively (computationally expensive, more robust) or once following the interpretation of the slopes (less expensive, less resilient to noise).

9.5.1 SLIMS time series

This thesis describes a single retrospective estimate computed at the end of the growing season and using minimal data to produce a high-quality change estimate map. Though run once, the SLIMS criteria are designed to be able to be computed at individual time steps, with the whole-year retrospective estimate being equivalent to the estimation at year's end. Future work could involve implementing SLIMS in such a way that a new 'final' classification is produced at regular update intervals or on demand. Because the criteria can be computed efficiently at each time step with little overhead, it might be possible to produce estimated change maps throughout a season of interest. The outcome could be a continuously updated change detection map across the entire study area for a single growing season, ending with the results as shown in this thesis.

9.5.2 Aiding BAP Construction

As part of the operation of SLIMS, anomalous dates with respect to the NBR values are identified. This information might be useful in BAP construction: where the anomalous dates are confirmed to contain real change, the band values from the later dates could be adopted for the BAP calculation in that location. That was not done in this work but would be a straightforward extension of the methodology.

9.5.3 Accuracy Assessment

I would perform an accuracy assessment to establish an objective measurement of SLIMS performance. While these exemplar regions (Detection of Harvests, Detection of Early Fire, Detection of Late Fire, and Detection of Forest Stability) were chosen because they demonstrate the ability of SLIMS to detect change without much 'salt and pepper' noise or commission error, a statistical understanding would greatly aid future development. Perhaps a relationship exists between the number of observations on average for a given class, and the accuracy in that class and whether there exists a lower or upper bound beyond which the performance of SLIMS may degrade. For example, it may not be possible for the algorithm to reject noise with less than 3 clear observations, because transient signals may have an overpowering influence on the regression.

9.6 Significance of This Work

It is possible the SLIMS algorithm combined with BULC could augment existing trend-based techniques (like LandTrendr and VCT) by providing a confirmatory 'look' at the study area after the data collection window has passed, with little computational cost (as implemented in Google's Earth Engine). This may increase confidence in end-of-series images and decrease the need for proxy-value assignment to fill gaps (pixels with no observations) at the end of the series via linear extrapolation. The linear extrapolation uses the values of the two nearest years that have observations to compute a predicted value for the gap, per pixel (Hermosilla et al. 2015). SLIMS with BULC could provide an updated NBR image (in the case of the C2C method) and these NBR values could then be compared with, or replace, the extrapolated values, closing gaps and/or identifying change. The combination of SLIMS and BULC should complement the detection of gradual changes with trend analysis and provide an earlier signal (n(SLIMS + BULC) vs n+2) that a large magnitude change has occurred, even if at that moment the other qualities of the disturbance cannot be described (cause, duration, severity). The harmonization with SLIMS and BULC may therefore have knock-on benefits in subsequent years, increasing series confidence and reducing reliance on gap-filling techniques.

10 Conclusion

In this thesis, I developed the Shrinking Latency in Multiple Streams (SLIMS) algorithm demanding little reanalysis or memory growth, that is suitable to be run with little information carried between iterations. The SLIMS algorithm presented in this thesis is not only a LULC classification system but also a skeleton for combining data streams for LULC change detection. It is flexible in that one can rapidly change thresholds, add, or drop criteria of interest, explore different ways of combining criteria, and see results over a large area extremely quickly. The implementation in Earth Engine across a large portion of western Canada was successful and points the way toward future extensions of the methods and analyses to larger portions of Canada. Given development time, the derivation of thresholds with spatial variation would promote the spatial extensibility of SLIMS. Threshold values might be modeled as varying abruptly (as at ecozone limits) or gradually (and could be modeled per-pixel provided appropriate ground-based evidence). In this setting of enormous, but still ultimately limited, processing power, the SLIMS algorithm is a useful, practical approach to providing a high-quality year-end assessment of change across a very large area in a timely manner.

Compared to the Best Available Pixel approach for Canadian forest, the SLIMS algorithm can incorporate multiple satellite instruments and expand the observation period for data collection. Through improved coverage and reduced delays between images, classifications can include a much larger observation period, incorporating imagery from May to the end of October. By expanding the observation period, forest harvests and fires occurring earlier and later in the summer are more likely to be captured in a shorter amount of time. Simply filtering non-growing-period images for clouds and then masking the noise reduces SLIMS classification error and this classification can then be used to improve the C2C process, creating a high-confidence map with little delay.

11 References

Alper, D. K., & Salazar, D. J. (2000). *Sustaining the Forests of the Pacific Coast: Forging Truces in the War in the Woods*. UBC Press.

Arneth, A., Barbosa, H., Benton, T., Calvin, K., Calvo, E., Connors, S., Cowie, A., Davin, E., Denton, F., & van Diemen, R. (2019). IPCC special report on climate change, desertification, land degradation, sustainable land management, food security, and greenhouse gas fluxes in terrestrial ecosystems. *Summary for Policy Makers. Geneva: Intergovernmental Panel on Climate Change (IPCC)*.

Baldrian, P. (2017). Forest microbiome: Diversity, complexity and dynamics. *FEMS Microbiology Reviews*, *41*(2), 109–130. https://doi.org/10.1093/femsre/fuw040

Barati, S., Rayegani, B., Saati, M., Sharifi, A., & Nasri, M. (2011). Comparison the accuracies of different spectral indices for estimation of vegetation cover fraction in sparse vegetated areas. *The Egyptian Journal of Remote Sensing and Space Science*, *14*(1), 49–56. https://doi.org/10.1016/j.ejrs.2011.06.001

Barrette, J., Paré, D., Manka, F., Guindon, L., Bernier, P., & Titus, B. (2018). Forecasting the spatial distribution of logging residues in Canada's managed forests. *Canadian Journal of Forest Research*. https://tspace.library.utoronto.ca/handle/1807/91227

Canada & Environment and Climate Change Canada. (2016). *Pan-Canadian framework on clean growth and climate change: Canada's plan to address climate change and grow the economy.* http://www.deslibris.ca/ID/10065393

Canada & Environment and Climate Change Canada. (2019). *Summary of Canada's 6th national report to the Convention on Biological Diversity.* http://publications.gc.ca/collections/collection_2019/eccc/CW66-167-1-2019-eng.pdf

Canada & Environment and Climate Change Canada. (2021). *Achieving a sustainable future: A federal sustainable development strategy for Canada 2019 to 2022.* https://epe.lac-bac.gc.ca/100/201/301/weekly_acquisitions_list-ef/2021/21-14/publications.gc.ca/collections/collection_2021/eccc/En4-136-2021-1-eng.pdf

Caputo, J., Beier, C. M., Groffman, P. M., Burns, D. A., Beall, F. D., Hazlett, P. W., & Yorks, T. E. (2016). Effects of Harvesting Forest Biomass on Water and Climate Regulation Services: A Synthesis of Long-Term Ecosystem Experiments in Eastern North America. *Ecosystems*, *19*(2), 271–283. https://doi.org/10.1007/s10021-015-9928-z

Cardille, J. A., & Fortin, J. A. (2016). Bayesian updating of land-cover estimates in a data-rich environment. *Remote Sensing of Environment*, *186*, 234–249. https://doi.org/10.1016/j.rse.2016.08.021

Carlowicz, M. (2012, January 9). *Seeing Forests for the Trees and the Carbon: Mapping the World's Forests in Three Dimensions*. NASA Earth Observatory; NASA Earth Observatory. https://earthobservatory.nasa.gov/features/ForestCarbon

Claverie, M., Ju, J., Masek, J. G., Dungan, J. L., Vermote, E. F., Roger, J. C., Skakun, S. V., & Justice, C. (2018). The Harmonized Landsat and Sentinel-2 surface reflectance data set. *Remote Sensing of Environment*, *219*(August 2017), 145–161. https://doi.org/10.1016/j.rse.2018.09.002

Cohen, W. B., Healey, S. P., Yang, Z., Stehman, S. V., Brewer, C. K., Brooks, E. B., Gorelick, N., Huang, C., Hughes, M. J., Kennedy, R. E., Loveland, T. R., Moisen, G. G., Schroeder, T. A., Vogelmann, J. E., Woodcock, C. E., Yang, L., & Zhu, Z. (2017). How Similar Are Forest Disturbance Maps Derived from Different Landsat Time Series Algorithms? *Forests*, *8*(4), 98. https://doi.org/10.3390/f8040098

Comber, A., & Wulder, M. (2019). Considering spatiotemporal processes in big data analysis: Insights from remote sensing of land cover and land use. *Transactions in GIS*, *23*(5), 879–891. https://doi.org/10.1111/tgis.12559

Crowley, M. A., Cardille, J. A., White, J. C., & Wulder, M. A. (2019). Generating intra-year metrics of wildfire progression using multiple open-access satellite data streams. *Remote Sensing of Environment*, *232*(October 2018), 111295. https://doi.org/10.1016/j.rse.2019.111295

DeFries, R., Achard, F., Brown, S., Herold, M., Murdiyarso, D., Schlamadinger, B., & de Souza, C. (2006). Reducing greenhouse gas emissions from deforestation in developing countries: Considerations for monitoring and measuring. *Report of the Global Terrestrial Observing System (GTOS) Number*, *46*, 23.

DeVries, B., Verbesselt, J., Kooistra, L., & Herold, M. (2015). Robust monitoring of small-scale forest disturbances in a tropical montane forest using Landsat time series. *Remote Sensing of Environment*, *161*, 107–121. https://doi.org/10.1016/j.rse.2015.02.012

Dhar, A., Parrott, L., & Heckbert, S. (2016). Consequences of mountain pine beetle outbreak on forest ecosystem services in western Canada. *Canadian Journal of Forest Research*, *46*(8), 987–999. https://doi.org/10.1139/cjfr-2016-0137

ENVI Confusion Matrix. (2022). https://www.l3harrisgeospatial.com/docs/enviconfusionmatrix.html

ESA–NASA collaboration fosters comparable land imagery. (2013, February 13). The European Space Agency. https://www.esa.int/Applications/Observing_the_Earth/Copernicus/ESA_NASA_collaboration_fosters_comparable_land_imagery

European Space Agency. (2022). *Sentinel-2*. https://www.esa.int/Applications/Observing_the_Earth/Copernicus/Sentinel-2

Felipe-Lucia, M. R., Soliveres, S., Penone, C., Manning, P., van der Plas, F., Boch, S., Prati, D., Ammer, C., Schall, P., Gossner, M. M., Bauhus, J., Buscot, F., Blaser, S., Blüthgen, N., de Frutos, A., Ehbrecht, M., Frank, K., Goldmann, K., Hänsel, F., … Allan, E. (2018). Multiple forest attributes underpin the supply of multiple ecosystem services. *Nature Communications*, *9*(1), 4839. https://doi.org/10.1038/s41467-018-07082-4

Forest Ministerial progress report on the Pan-Canadian Framework on Clean Growth and Climate Change (No. 4; Forest Ministerial Progress Report, p. 48). (2020). Canadian Council of Forest Ministers. https://www.ccfm.org/releases/forest-ministerial-progress-report-on-the-pan-canadian-framework-on-clean-growth-and-climate-change-2020/

García, M. J. L., & Caselles, V. (1991). Mapping burns and natural reforestation using thematic Mapper data. *Geocarto International*, *6*(1), 31–37. https://doi.org/10.1080/10106049109354290

Gillis, M. D. (2001). Canada’s National Forest Inventory (Responding to Current Information Needs). *Environmental Monitoring and Assessment*, *67*(1), 121–129. https://doi.org/10.1023/A:1006405820244

Global Forest Resources Assessment 2020. (2020). FAO. https://doi.org/10.4060/ca9825en

Gómez, C., White, J. C., & Wulder, M. A. (2016). Optical remotely sensed time series data for land cover classification: A review. *ISPRS Journal of Photogrammetry and Remote Sensing*, *116*, 55–72. https://doi.org/10.1016/j.isprsjprs.2016.03.008

Goodenough, D. G., Niemann, K. O., Dyk, A., Hobart, G., Gordon, P., Loisel, M., & Chen, H. (2008). Comparison of Aviris and AISA Airborne Hyperspectral Sensing for Above-Ground Forest Carbon Mapping. *IGARSS 2008 - 2008 IEEE International Geoscience and Remote Sensing Symposium*, *2*, II-129-II–132. https://doi.org/10.1109/IGARSS.2008.4778944

Gorelick, N., Hancher, M., Dixon, M., Ilyushchenko, S., Thau, D., & Moore, R. (2017). Google Earth Engine: Planetary-scale geospatial analysis for everyone. *Remote Sensing of Environment*, *202*, 18–27. https://doi.org/10.1016/j.rse.2017.06.031

Griffiths, P., Nendel, C., & Hostert, P. (2019). Intra-annual reflectance composites from Sentinel-2 and Landsat for national-scale crop and land cover mapping. *Remote Sensing of Environment*, *220*(October 2017), 135–151. https://doi.org/10.1016/j.rse.2018.10.031

Hall, R. J., Freeburn, J. T., De Groot, W. J., Pritchard, J. M., Lynham, T. J., & Landry, R. (2008). Remote sensing of burn severity: Experience from western Canada boreal fires. *International Journal of Wildland Fire*, *17*(4), 476–489. https://doi.org/10.1071/WF08013

Hermosilla, T., Wulder, M. A., White, J. C., Coops, N. C., & Hobart, G. W. (2014). An integrated Landsat time series protocol for change detection and generation of annual gap-free surface reflectance composites. *Remote Sensing of Environment*, *158*, 220–234. https://doi.org/10.1016/j.rse.2014.11.005

Hermosilla, T., Wulder, M. A., White, J. C., Coops, N. C., & Hobart, G. W. (2015). Regional detection, characterization, and attribution of annual forest change from 1984 to 2012 using Landsat-derived time-series metrics. *Remote Sensing of Environment*, *170*, 121–132. https://doi.org/10.1016/j.rse.2015.09.004

Hermosilla, T., Wulder, M. A., White, J. C., Coops, N. C., & Hobart, G. W. (2018). Disturbance-Informed Annual Land Cover Classification Maps of Canada's Forested Ecosystems for a 29-Year Landsat Time Series. *Canadian Journal of Remote Sensing*, *44*(1), 67–87. https://doi.org/10.1080/07038992.2018.1437719

Hermosilla, T., Wulder, M. A., White, J. C., Coops, N. C., Hobart, G. W., & Campbell, L. B. (2016). Mass data processing of time series Landsat imagery: Pixels to data products for forest monitoring. *International Journal of Digital Earth*, *9*(11), 1035–1054. https://doi.org/10.1080/17538947.2016.1187673

Holsinger, L., Parks, S., Saperstein, L., Loehman, R., Whitman, E., Barnes, J., & Parisien, M.-A. (2021). Improved fire severity mapping in the North American boreal forest using a hybrid composite method. *Remote Sensing in Ecology and Conservation*. https://doi.org/10.1002/rse2.238

Hua, F., Bruijnzeel, L. A., Meli, P., Martin, P. A., Zhang, J., Nakagawa, S., Miao, X., Wang, W., McEvoy, C., Peña-Arancibia, J. L., Brancalion, P. H. S., Smith, P., Edwards, D. P., & Balmford, A. (2022). The biodiversity and ecosystem service contributions and trade-offs of forest restoration approaches. *Science*. https://doi.org/10.1126/science.abl4649

Huang, C., Goward, S. N., Masek, J. G., Thomas, N., Zhu, Z., & Vogelmann, J. E. (2010). An automated approach for reconstructing recent forest disturbance history using dense

Landsat time series stacks. *Remote Sensing of Environment*, *114*(1), 183–198. https://doi.org/10.1016/j.rse.2009.08.017

Huang, C., Goward, S. N., Schleeweis, K., Thomas, N., Masek, J. G., & Zhu, Z. (2009). Dynamics of national forests assessed using the Landsat record: Case studies in eastern United States. *Remote Sensing of Environment*, *113*(7), 1430–1442. https://doi.org/10.1016/j.rse.2008.06.016

Jordan, C. F. (1969). Derivation of Leaf-Area Index from Quality of Light on the Forest Floor. *Ecology*, *50*(4), 663–666. https://doi.org/10.2307/1936256

Kennedy, R. E., Yang, Z., & Cohen, W. B. (2010). Detecting trends in forest disturbance and recovery using yearly Landsat time series: 1. LandTrendr — Temporal segmentation algorithms. *Remote Sensing of Environment*, *114*(12), 2897–2910. https://doi.org/10.1016/j.rse.2010.07.008

Lawrence, D., Coe, M., Walker, W., Verchot, L., & Vandecar, K. (2022). The Unseen Effects of Deforestation: Biophysical Effects on Climate. *Frontiers in Forests and Global Change*, *5*. https://www.frontiersin.org/article/10.3389/ffgc.2022.756115

Li, A., Huang, C., Sun, G., Shi, H., Toney, C., Zhu, Z., Rollins, M. G., Goward, S. N., & Masek, J. G. (2011). Modeling the height of young forests regenerating from recent disturbances in Mississippi using Landsat and ICESat data. *Remote Sensing of Environment*, *115*(8), 1837–1849. https://doi.org/10.1016/j.rse.2011.03.001

Liu, H. Q., & Huete, A. (1995). A feedback based modification of the NDVI to minimize canopy background and atmospheric noise. *IEEE Transactions on Geoscience and Remote Sensing*, *33*(2), 457–465. https://doi.org/10.1109/TGRS.1995.8746027

Ministry of Forests, L. (n.d.). *Bark beetles—Province of British Columbia*. Province of British Columbia. Retrieved 4 March 2022, from https://www2.gov.bc.ca/gov/content/industry/forestry/managing-our-forest-resources/forest-health/forest-pests/bark-beetles

Natural Resources Canada. (2013, January 23). *Forest inventory*. Natural Resources Canada. https://www.nrcan.gc.ca/our-natural-resources/forests/sustainable-forest-management/measuring-and-reporting/forest-inventory/13417

Natural Resources Canada. (2014a, August 25). *How do forests benefit Canadians*. Natural Resources Canada. https://www.nrcan.gc.ca/our-natural-resources/forests/state-canadas-forests-report/how-do-forests-benefit-canadians/16509

Natural Resources Canada. (2014b, August 26). *How does the forest sector contribute to Canada's economy?* Natural Resources Canada. https://www.nrcan.gc.ca/our-natural-resources/forests/state-canadas-forests-report/forest-industry-contribute/16517

Natural Resources Canada. (2015, September 10). *Forest change indicators*. Natural Resources Canada. https://www.nrcan.gc.ca/climate-change-adapting-impacts-and-reducing-emissions/climate-change-impacts-forests/forest-change-indicators/17768

Natural Resources Canada. (2020). *Overview of Canada's forest industry*. https://www.nrcan.gc.ca/our-natural-resources/forests-forestry/forest-industry-trade/overview-canadas-forest-industry/13311

NFI. (n.d.). Retrieved 18 March 2022, from https://nfi.nfis.org/en/faq

Olofsson, P., Foody, G. M., Herold, M., Stehman, S. V., Woodcock, C. E., & Wulder, M. A. (2014). Good practices for estimating area and assessing accuracy of land change. *Remote Sensing of Environment*, *148*, 42–57. https://doi.org/10.1016/j.rse.2014.02.015

Parker, B. M., Lewis, T., & Srivastava, S. K. (2015). Estimation and evaluation of multi-decadal fire severity patterns using Landsat sensors. *Remote Sensing of Environment*, *170*, 340–349. https://doi.org/10.1016/j.rse.2015.09.014

Rouse, W., Haas, R. H., Schell, J. A., & Deering, D. W. (1974). *Monitoring vegetation systems in the Great Plains with ERTS*. *1*, 9. NASA STI Repository.

Schoenholtz, S. H., Miegroet, H. V., & Burger, J. A. (2000). A review of chemical and physical properties as indicators of forest soil quality: Challenges and opportunities. *Forest Ecology and Management*, *138*(1), 335–356. https://doi.org/10.1016/S0378-1127(00)00423-0

Schroeder, T. A., Wulder, M. A., Healey, S. P., & Moisen, G. G. (2011). Mapping wildfire and clearcut harvest disturbances in boreal forests with Landsat time series data. *Remote Sensing of Environment*, *115*(6), 1421–1433. https://doi.org/10.1016/j.rse.2011.01.022

Statistics Canada. (2018, March 14). *Forests in Canada*. https://www150.statcan.gc.ca/n1/pub/16-201-x/16-201-x2018001-eng.htm

Sutherland, I. J., Bennett, E. M., & Gergel, S. E. (2016). Recovery trends for multiple ecosystem services reveal non-linear responses and long-term tradeoffs from temperate forest harvesting. *Forest Ecology and Management*, *374*, 61–70. https://doi.org/10.1016/j.foreco.2016.04.037

Terms and Definitions (Working Paper No. 188; Forest Resources Assessment). (2020). Food and Agriculture Organization. http://www.fao.org/forests/en/

UNCCD Report: LDN contributing to global biodiversity conservation goals. (n.d.). Retrieved 8 February 2022, from https://www.unccd.int/news-events/report-ldn-contributing-global-biodiversity-conservation-goals-0

Kyoto Protocol to the United Nations Framework Convention on Climate Change, (1998).

U.S. Geological Survey. (2022). *Landsat 8*. https://www.usgs.gov/landsat-missions/landsat-8

Verbesselt, J., Hyndman, R., Zeileis, A., & Culvenor, D. (2010). Phenological change detection while accounting for abrupt and gradual trends in satellite image time series. *Remote Sensing of Environment*, *114*(12), 2970–2980. https://doi.org/10.1016/j.rse.2010.08.003

White, J. C., Wulder, M. A., Hermosilla, T., Coops, N. C., & Hobart, G. W. (2017). A nationwide annual characterization of 25 years of forest disturbance and recovery for Canada using Landsat time series. *Remote Sensing of Environment*, *194*, 303–321. https://doi.org/10.1016/j.rse.2017.03.035

White, J. C., Wulder, M. A., Hobart, G. W., Luther, J. E., Hermosilla, T., Griffiths, P., Coops, N. C., Hall, R. J., Hostert, P., Dyk, A., & Guindon, L. (2014). Pixel-Based Image Compositing for Large-Area Dense Time Series Applications and Science. *Canadian Journal of Remote Sensing*, *40*(3), 192–212. https://doi.org/10.1080/07038992.2014.945827

Whitman, E., Parisien, M.-A., Thompson, D. K., Hall, R. J., Skakun, R. S., & Flannigan, M. D. (2018). Variability and drivers of burn severity in the northwestern Canadian boreal forest. *Ecosphere*, *9*(2), e02128. https://doi.org/10.1002/ecs2.2128

Wulder, M. A., Coops, N. C., Roy, D. P., White, J. C., & Hermosilla, T. (2018). Land cover 2.0. *International Journal of Remote Sensing*, *39*(12), 4254–4284. https://doi.org/10.1080/01431161.2018.1452075

Wulder, M. A., Hermosilla, T., Stinson, G., Gougeon, F. A., White, J. C., Hill, D. A., & Smiley, B. P. (2019). Satellite-based time series land cover and change information to map forest area consistent with national and international reporting requirements. *Forestry: An International Journal of Forest Research*.

Wulder, M. A., Hermosilla, T., White, J. C., & Coops, N. C. (2020). Biomass status and dynamics over Canada's forests: Disentangling disturbed area from associated aboveground biomass consequences. *Environmental Research Letters*, *15*(9), 094093. https://doi.org/10.1088/1748-9326/ab8b11

Xue, J., & Su, B. (2017). Significant Remote Sensing Vegetation Indices: A Review of Developments and Applications. *Journal of Sensors*, *2017*, e1353691. https://doi.org/10.1155/2017/1353691

Zhu, Z. (2017). Change detection using landsat time series: A review of frequencies, preprocessing, algorithms, and applications. *ISPRS Journal of Photogrammetry and Remote Sensing*, *130*, 370–384. https://doi.org/10.1016/j.isprsjprs.2017.06.013

Zhu, Z., & Woodcock, C. E. (2014). Automated cloud, cloud shadow, and snow detection in multitemporal Landsat data: An algorithm designed specifically for monitoring land cover change. *Remote Sensing of Environment*, *152*, 217–234. https://doi.org/10.1016/j.rse.2014.06.012

Zhu, Z., Zhang, J., Yang, Z., Aljaddani, A. H., Cohen, W. B., Qiu, S., & Zhou, C. (2020). Continuous monitoring of land disturbance based on Landsat time series. *Remote Sensing of Environment*, *238*, 111116. https://doi.org/10.1016/j.rse.2019.03.009

12 Appendix A

12.1 Early Fire

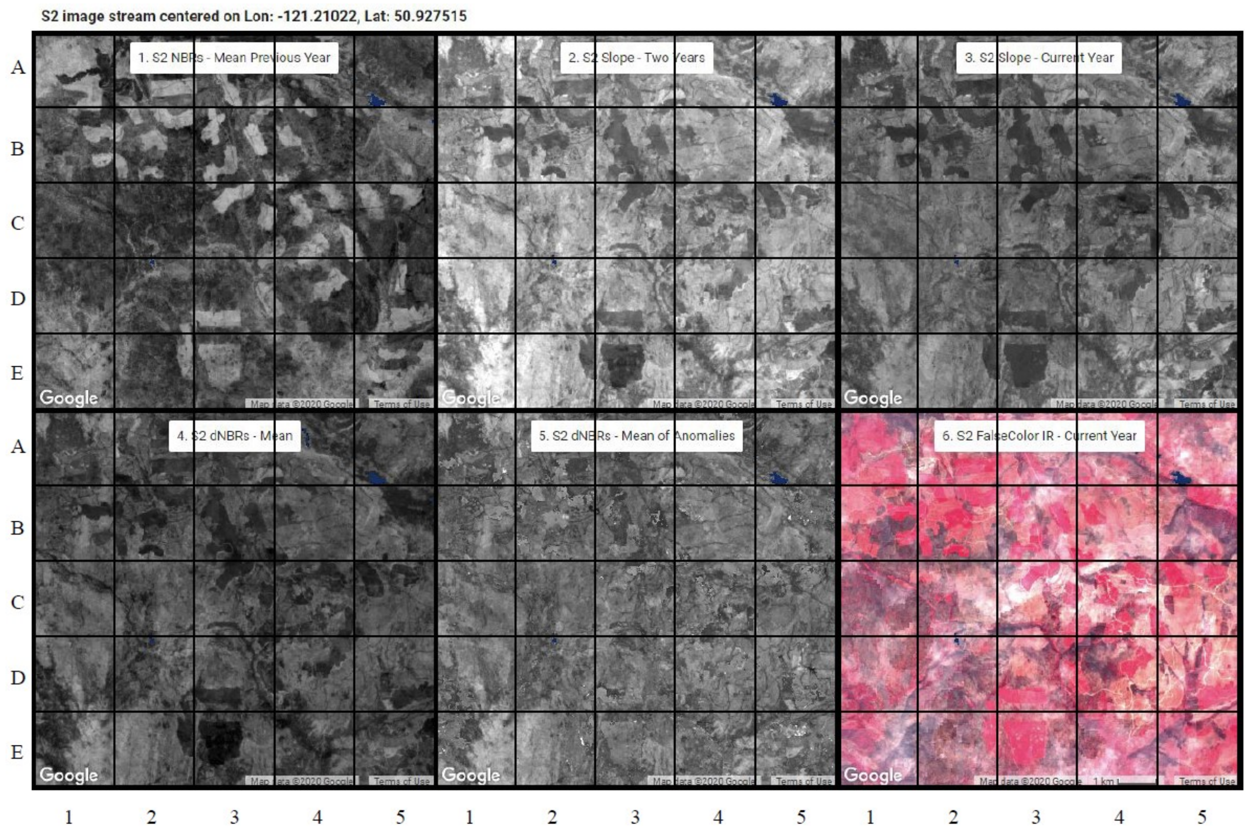

Figure 16 Five criteria and a false-colour infrared representation of the target year for ***Sentinel-2*** *in the Early Fire area. Panel 1 (top left): the NBR for the previous year (2016) with dark areas showing low NBR values. Panel 2 (top centre): slope of the two-year regression line with values inverted such that more negative values are lighter in colour. Panel 3 (top right): slope of the one-year (2017) regression line, also inverted so that positive sloping trend lines are darker. Panel 4 (bottom left): the difference between average NBR values of 2016 and 2017, colour scale inverted such that a negative value (indicating loss of vegetation) is lighter in colour. Panel 5 (bottom centre): the anomalous NBR values of 2017 subtracted from the mean NBR values of 2016. Panel 6 (bottom right): false colour infra-red image of the scene with RGB channels using infrared, red, and green, such that lighter areas are exposed terrain, deeper, brown-tinged red indicated burned areas like cells C1 or E2 and brighter red areas are vegetation cover (e.g., centre of E3).*

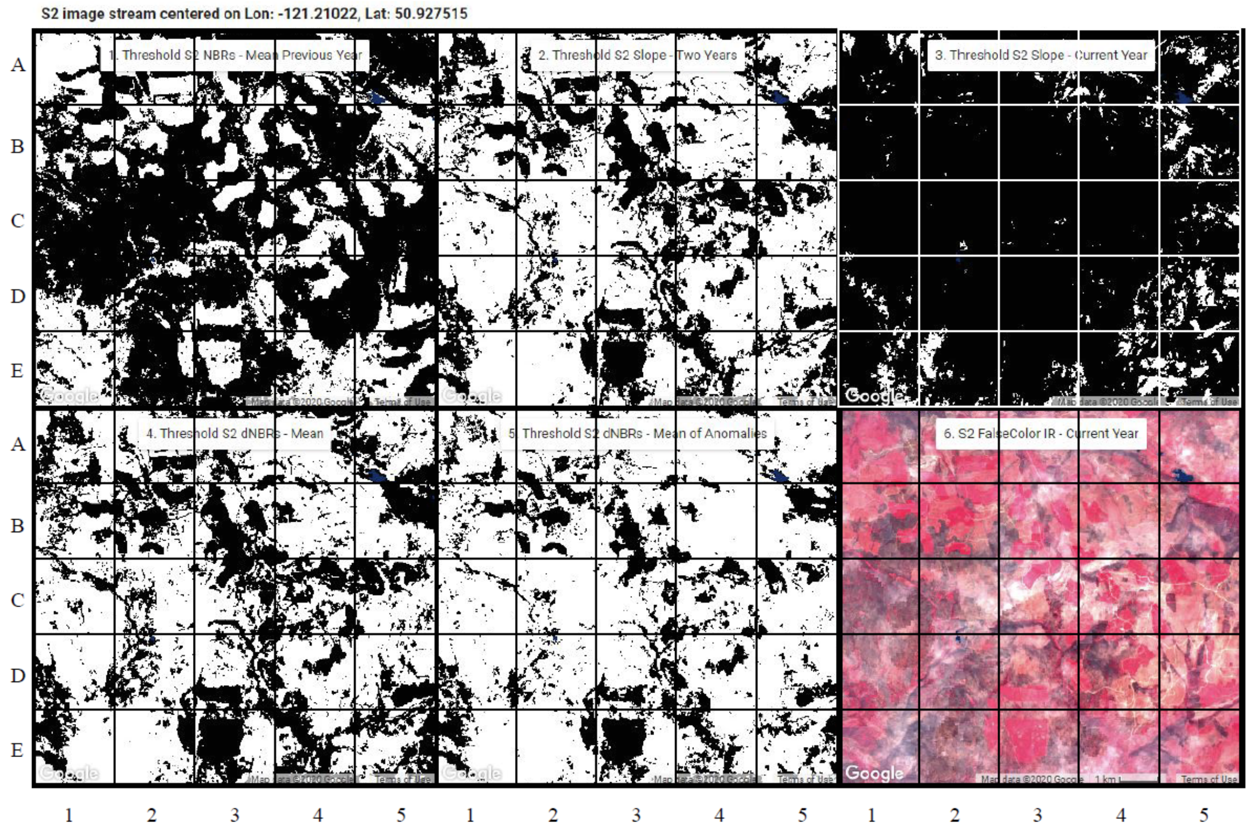

Figure 17 Panels 1 to 5 (bottom centre, left; top left, centre, right): Thresholds of the five criteria (7.5 Table 1) for ***Sentinel-2*** *in the Early Fire area. Everywhere the threshold criterion is met the figure is white. Panel 1 (top left): Illustrating NBR values exceed that of a user-adjustable threshold of NBR and can be considered forest land cover. Panel 2 (top centre): the slope of the regression line for two years is sufficiently negative in areas reference data suggest is harvest. Panel 3 (top right): black areas indicate that no change occurs during the year 2017. Panel 4 (bottom left): the differenced Normalized Burn Ratio identifies areas of vegetation loss between prior year and target year, in white. Panel 5 (bottom centre): thresholding the captured anomalous dNBR values. Panel 6 (bottom right): false colour infra-red image of the scene with RGB channels using infrared, red, and green, such that lighter areas are exposed terrain, deeper, brown-tinged red indicated burned areas like cells C1 or E2 and brighter red areas are vegetation cover (e.g., centre of E3).*

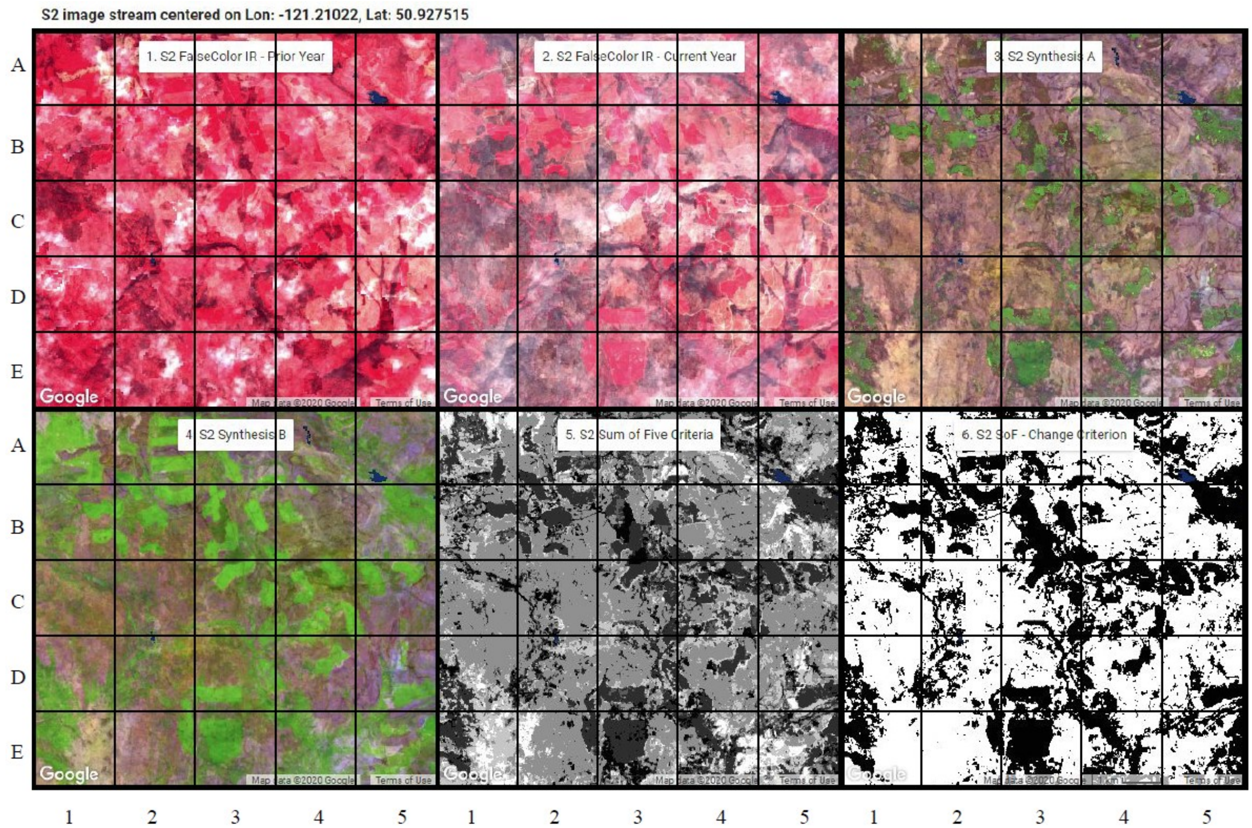

Figure 18 Panels 1 & 2 (top left, top centre): Early Fire area, ***Sentinel-2*** *NIR false colour representative images for the earlier and later years respectively. Panel 3 (top right): RGB composite for Synthesis A. RED: Two-Year Slope inverse values; GREEN: anomalous NBR values from 2017 differenced from 2016; BLUE: Target-Year Slope inverse values. Panel 4 (bottom left): RGB composite for Synthesis B. RED: Two-Year Slope inverse values; GREEN: Target-Year mean NBR values; BLUE: Target-Year Slope inverse values. Panel 5 (bottom centre): summation of the 5 criteria. Panel 6 (bottom right): indicates areas of agreement between 3 or more criteria.*

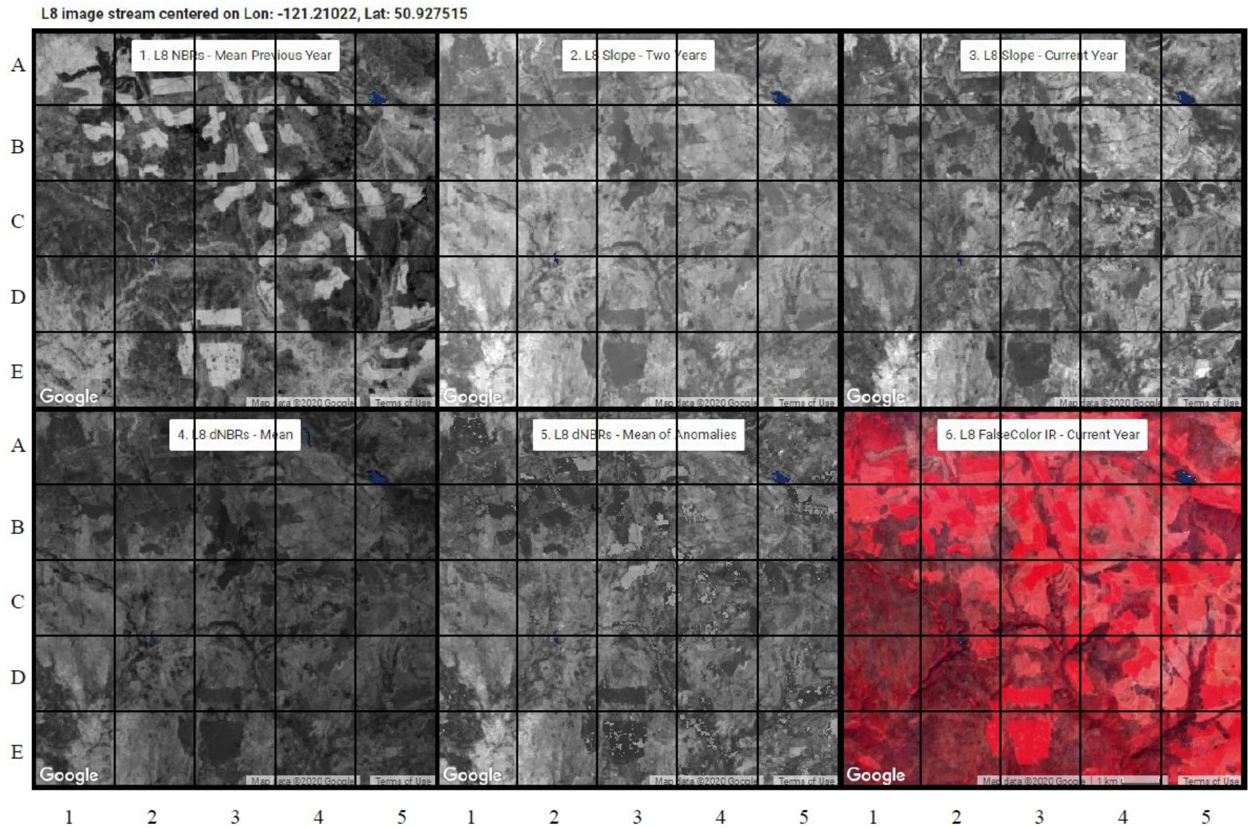

*Figure 19 Five criteria and a false-colour infrared representation of the target year for **Landsat-8** in the Early Fire area. Panel 1 (top left): the NBR for the previous year (2016) with dark areas showing low NBR values. Panel 2 (top centre): slope of the two-year regression line with values inverted such that more negative values are lighter in colour. Panel 3 (top right): slope of the one-year (2017) regression line, also inverted so that positive sloping trend lines are darker. Panel 4 (bottom left): the difference between average NBR values of 2016 and 2017, colour scale inverted such that a negative value (indicating loss of vegetation) is lighter in colour. Panel 5 (bottom centre): the anomalous NBR values of 2017 subtracted from the mean NBR values of 2016. Panel 6 (bottom right): false colour infra-red image of the scene with RGB channels using infrared, red, and green, such that lighter areas are exposed terrain, deeper, brown-tinged red indicated burned areas like cells C1 or E2 and brighter red areas are vegetation cover (e.g., centre of E3).*

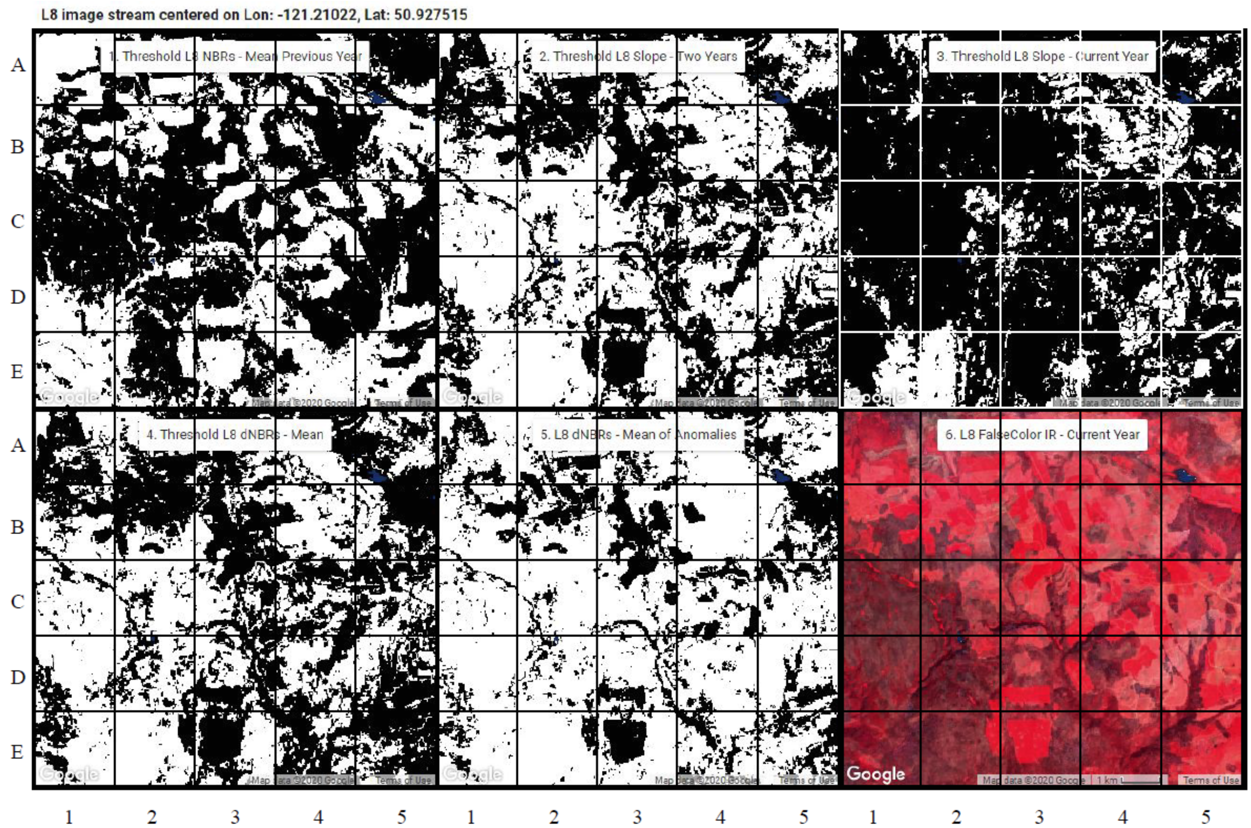

Figure 20 Panels 1 to 5 (bottom centre, left; top left, centre, right): Thresholds of the five criteria (7.5 Table 1) for ***Landsat-8*** *in the Early Fire area. Everywhere the threshold criterion is met the figure is white. Panel 1 (top left): Illustrating NBR values exceed that of a user-adjustable threshold of NBR and can be considered forest land cover. Panel 2 (top centre): the slope of the regression line for two years is sufficiently negative in areas reference data suggest is harvest. Panel 3 (top right): black areas indicate that no change occurs during the year 2017. Panel 4 (bottom left): the differenced Normalized Burn Ratio identifies areas of vegetation loss between prior year and target year, in white. Panel 5 (bottom centre): thresholding the captured anomalous dNBR values. Panel 6 (bottom right): false colour infra-red image of the scene with RGB channels using infrared, red, and green, such that lighter areas are exposed terrain, deeper, brown-tinged red indicated burned areas like cells C1 or E2 and brighter red areas are vegetation cover (e.g., centre of E3).*

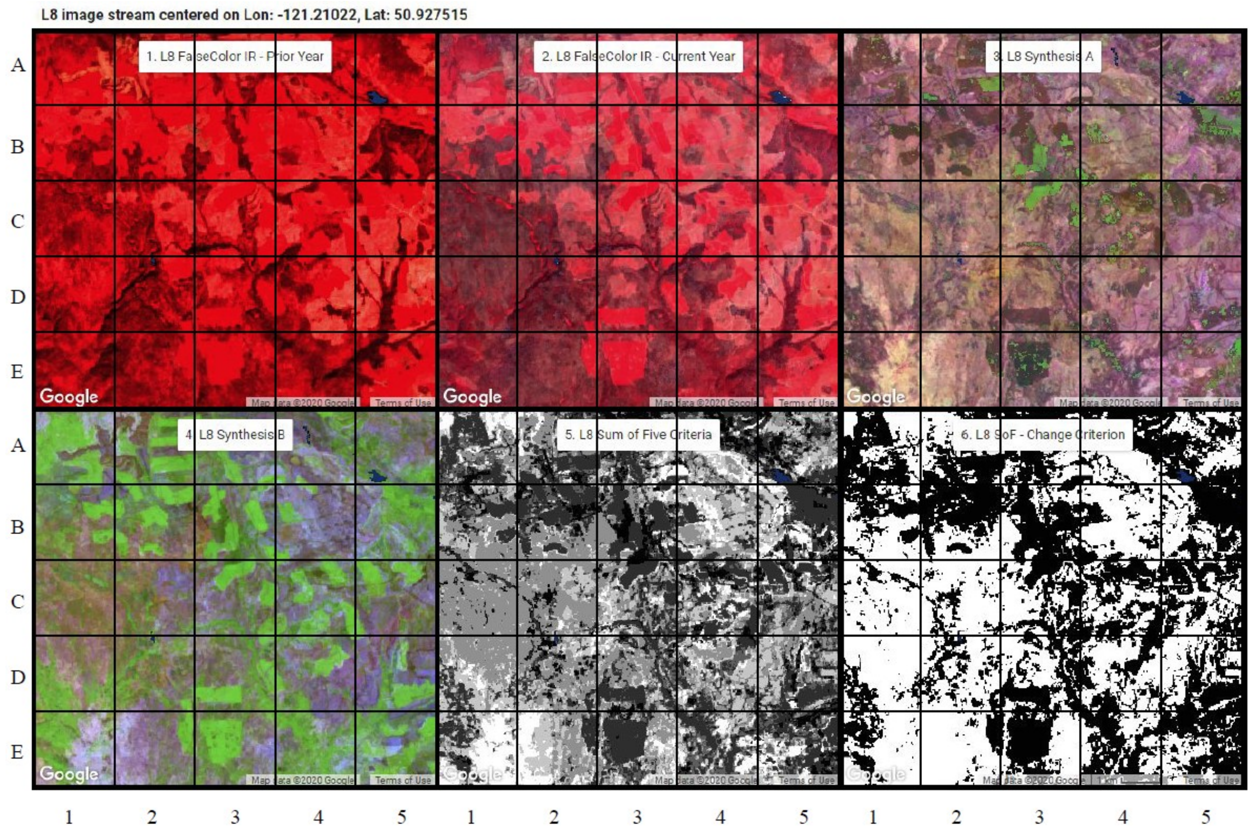

Figure 21 Panels 1 & 2 (top left, top centre): Early Fire area, ***Landsat-8*** *NIR false colour representative images for the earlier and later years respectively. Panel 3 (top right): RGB composite for Synthesis A. RED: Two-Year Slope inverse values; GREEN: anomalous NBR values from 2017 differenced from 2016; BLUE: Target-Year Slope inverse values. Panel 4 (bottom left): RGB composite for Synthesis B. RED: Two-Year Slope inverse values; GREEN: Target-Year mean NBR values; BLUE: Target-Year Slope inverse values. Panel 5 (bottom centre): summation of the 5 criteria. Panel 6 (bottom right): indicates areas of agreement between 3 or more criteria.*

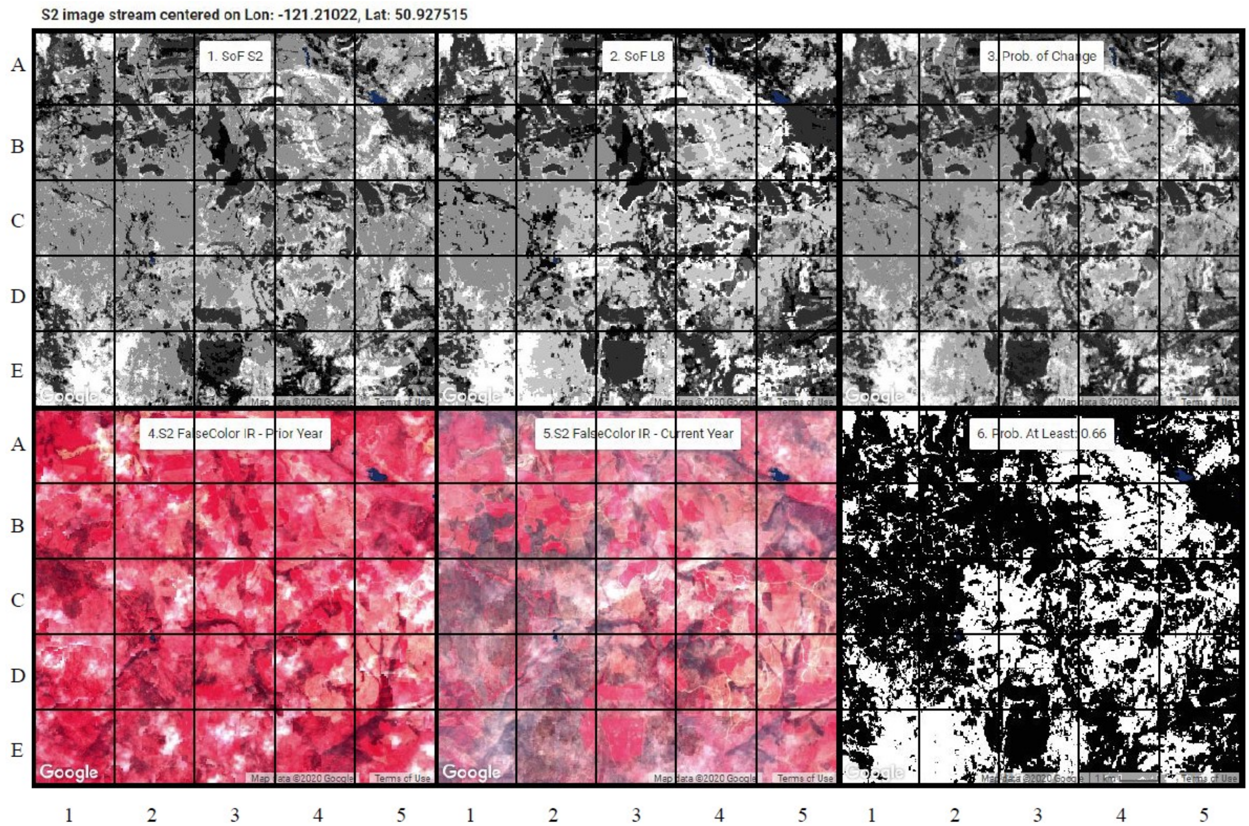

*Figure 22 Panels 1 & 2 (top left, top centre): an estimated probability of change from **Sentinel-2** and **Landsat-8** separately, and in panel 3 (top right) their jointly considered probability of change. Lighter areas are more likely change than darker areas. Panel 6 (bottom right): a 'thresholded' view of said estimate of change at 66% likelihood or greater, that a change has occurred in the Early Fire area (white is disturbed, black is undisturbed). Panels 4 & 5 (bottom left, bottom centre): representative NIR false colour for both years; such that lighter areas are exposed terrain, deeper, brown-tinged red indicated burned areas and brighter red areas are vegetation cover.*

12.2 Late Fire

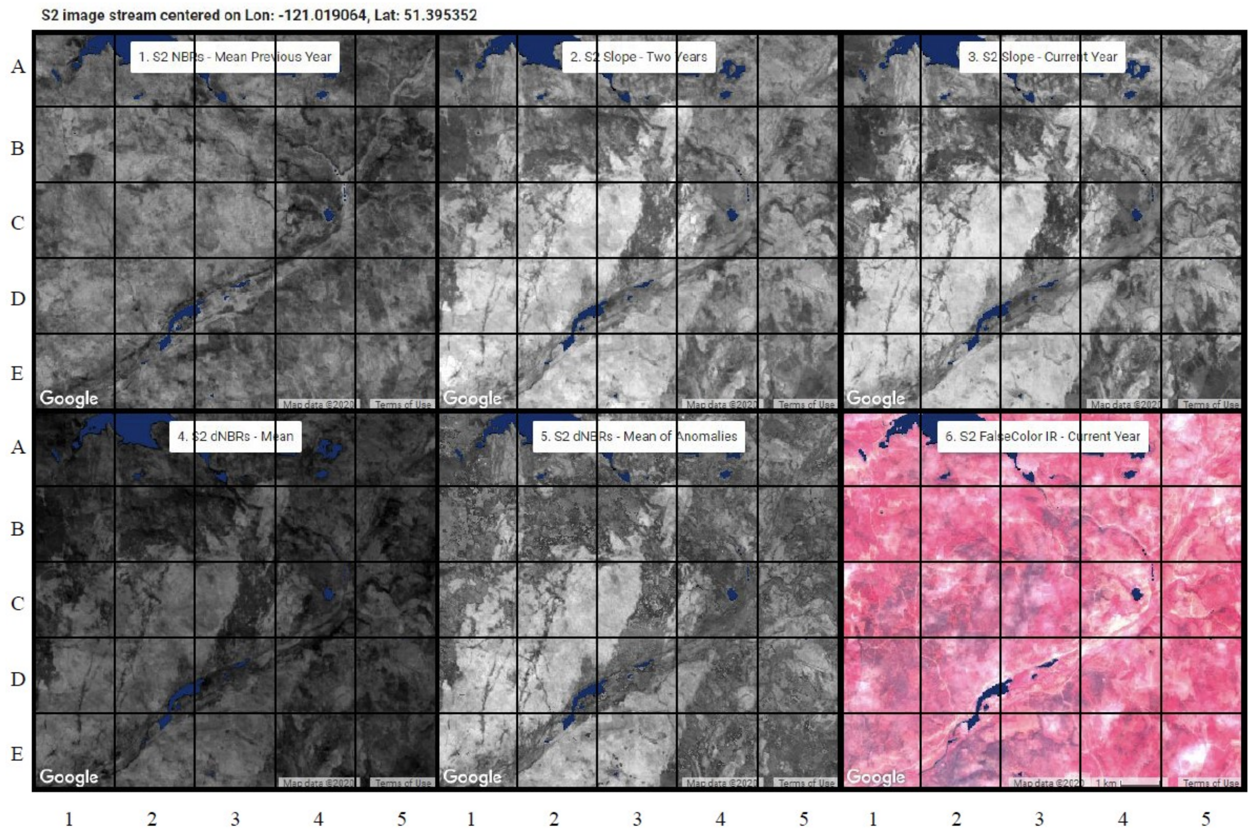

Figure 23 Five criteria and a false-colour infrared representation of the target year for ***Sentinel-2*** *in the Late Fire area. Panel 1 (top left): the NBR for the previous year (2016) with dark areas showing low NBR values. Panel 2 (top centre): slope of the two-year regression line with values inverted such that more negative values are lighter in colour. Panel 3 (top right): slope of the one-year (2017) regression line, also inverted so that positive sloping trend lines are darker. Panel 4 (bottom left): the difference between average NBR values of 2016 and 2017, colour scale inverted such that a negative value (indicating loss of vegetation) is lighter in colour. Panel 5 (bottom centre): the anomalous NBR values of 2017 subtracted from the mean NBR values of 2016. Panel 6 (bottom right): false colour infra-red image of the scene with RGB channels using infrared, red, and green, such that lighter areas are exposed terrain, deeper, brown-tinged red indicated burned areas and brighter red areas are vegetation cover.*

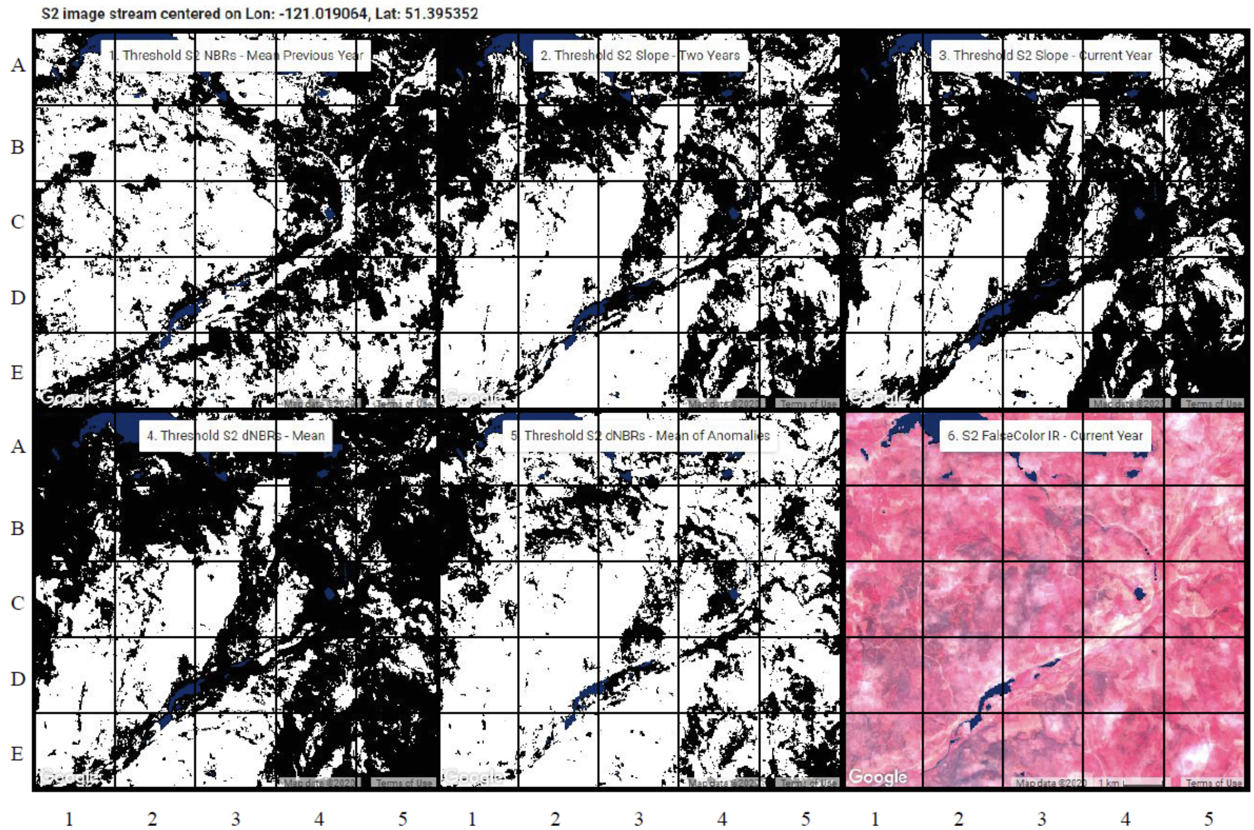

Figure 24 Panels 1 to 5 (bottom centre, left; top left, centre, right): Thresholds of the five criteria (7.5 Table 1) for ***Sentinel-2*** *in the Late Fire area. Everywhere the threshold criterion is met the figure is white. Panel 1 (top left): Illustrating NBR values exceed that of a user-adjustable threshold of NBR and can be considered forest land cover. Panel 2 (top centre): the slope of the regression line for two years is sufficiently negative in areas reference data suggest is harvest. Panel 3 (top right): black areas indicate that no change occurs during the year 2017. Panel 4 (bottom left): the differenced Normalized Burn Ratio identifies areas of vegetation loss between prior year and target year, in white. Panel 5 (bottom centre): thresholding the captured anomalous dNBR values. Panel 6 (bottom right): false colour infra-red image of the scene with RGB channels using infrared, red, and green, such that lighter areas are exposed terrain, deeper, brown-tinged red indicated burned areas and brighter red areas are vegetation cover.*

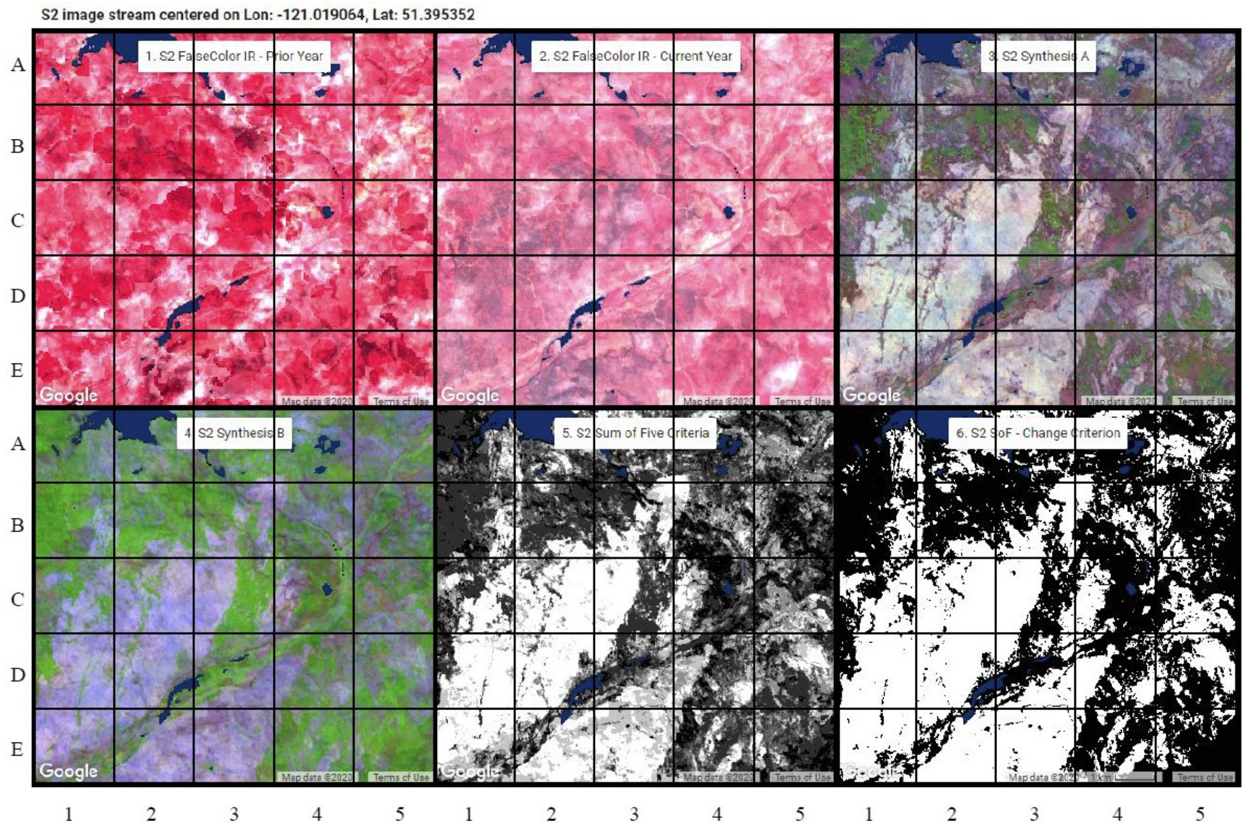

Figure 25 Panels 1 & 2 (top left, top centre): Late Fire area, ***Sentinel-2*** *NIR false colour representative images for the earlier and later years respectively. Panel 3 (top right): RGB composite for Synthesis A. RED: Two-Year Slope inverse values; GREEN: anomalous NBR values from 2017 differenced from 2016; BLUE: Target-Year Slope inverse values. Panel 4 (bottom left): RGB composite for Synthesis B. RED: Two-Year Slope inverse values; GREEN: Target-Year mean NBR values; BLUE: Target-Year Slope inverse values. Panel 5 (bottom centre): summation of the 5 criteria. Panel 6 (bottom right): indicates areas of agreement between 3 or more criteria.*

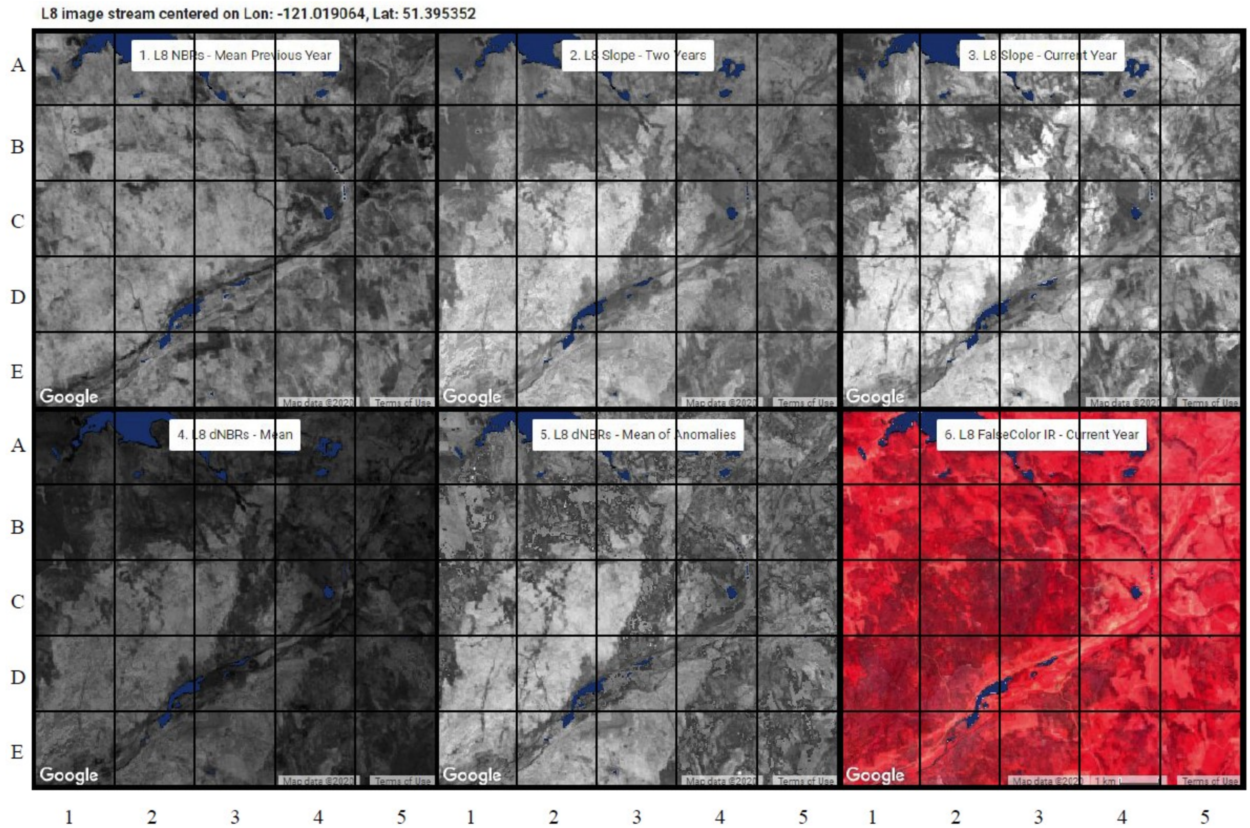

*Figure 26 Five criteria and a false-colour infrared representation of the target year for **Landsat-8** in the Late Fire area. Panel 1 (top left): the NBR for the previous year (2016) with dark areas showing low NBR values. Panel 2 (top centre): slope of the two-year regression line with values inverted such that more negative values are lighter in colour. Panel 3 (top right): slope of the one-year (2017) regression line, also inverted so that positive sloping trend lines are darker. Panel 4 (bottom left): the difference between average NBR values of 2016 and 2017, colour scale inverted such that a negative value (indicating loss of vegetation) is lighter in colour. Panel 5 (bottom centre): the anomalous NBR values of 2017 subtracted from the mean NBR values of 2016. Panel 6 (bottom right): false colour infra-red image of the scene with RGB channels using infrared, red, and green, such that lighter areas are exposed terrain, deeper, brown-tinged red indicated burned areas and brighter red areas are vegetation cover.*

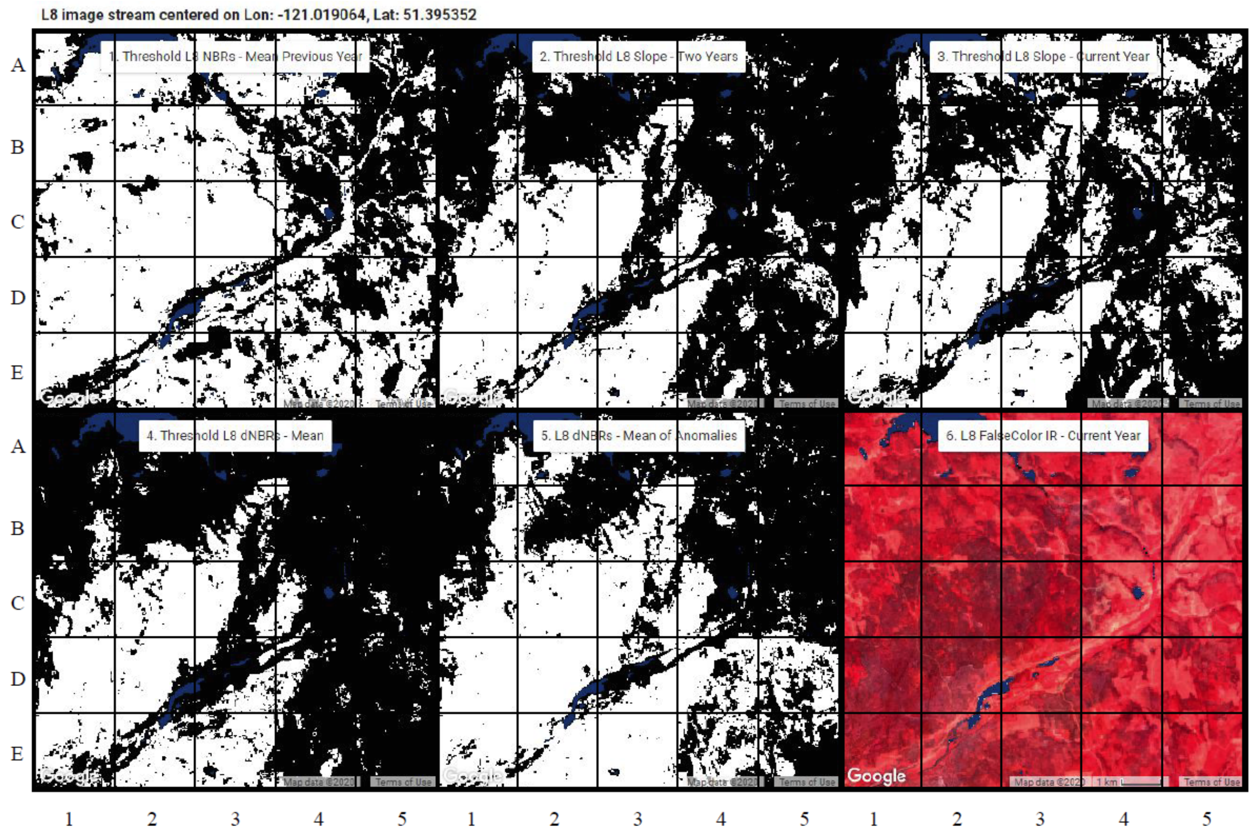

Figure 27 Panels 1 to 5 (bottom centre, left; top left, centre, right): Thresholds of the five criteria (7.5 Table 1) for ***Landsat-8*** *in the Late Fire area. Everywhere the threshold criterion is met the figure is white. Panel 1 (top left): Illustrating NBR values exceed that of a user-adjustable threshold of NBR and can be considered forest land cover. Panel 2 (top centre): the slope of the regression line for two years is sufficiently negative in areas reference data suggest is harvest. Panel 3 (top right): black areas indicate that no change occurs during the year 2017. Panel 4 (bottom left): the differenced Normalized Burn Ratio identifies areas of vegetation loss between prior year and target year, in white. Panel 5 (bottom centre): thresholding the captured anomalous dNBR values. Panel 6 (bottom right): false colour infra-red image of the scene with RGB channels using infrared, red, and green, such that lighter areas are exposed terrain, deeper, brown-tinged red indicated burned areas and brighter red areas are vegetation cover.*

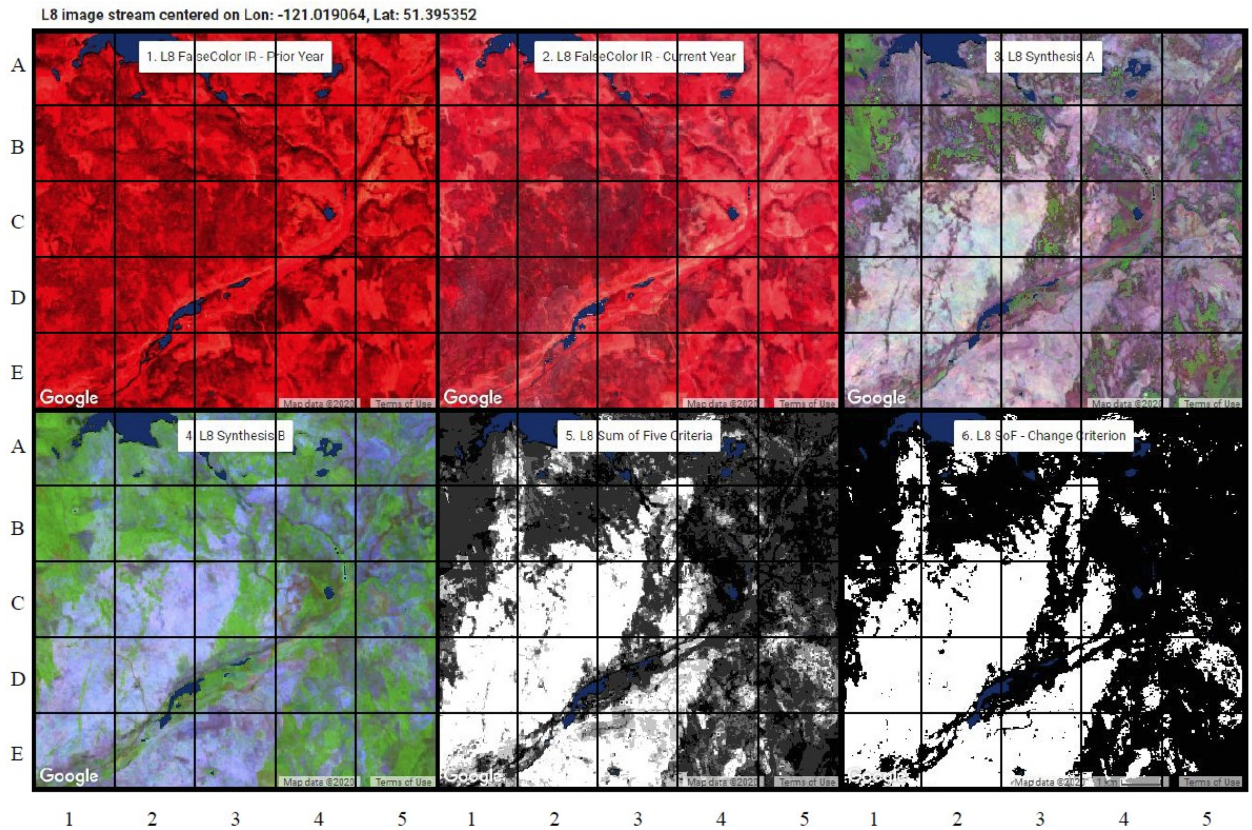

Figure 28 Panels 1 & 2 (top left, top centre): Late Fire area, ***Landsat-8*** *NIR false colour representative images for the earlier and later years respectively. Panel 3 (top right): RGB composite for Synthesis A. RED: Two-Year Slope inverse values; GREEN: anomalous NBR values from 2017 differenced from 2016; BLUE: Target-Year Slope inverse values. Panel 4 (bottom left): RGB composite for Synthesis B. RED: Two-Year Slope inverse values; GREEN: Target-Year mean NBR values; BLUE: Target-Year Slope inverse values. Panel 5 (bottom centre): summation of the 5 criteria. Panel 6 (bottom right): indicates areas of agreement between 3 or more criteria.*

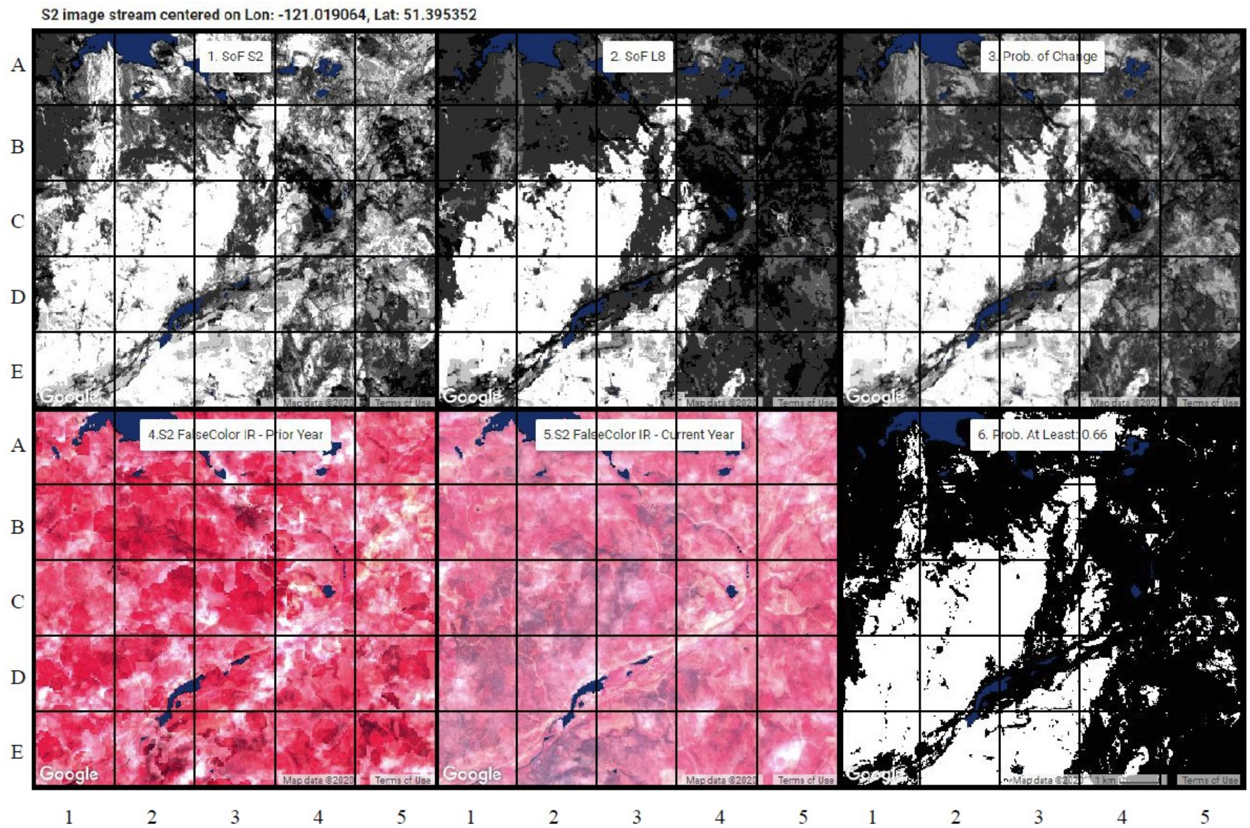

Figure 29 Panels 1 & 2 (top left, top centre): an estimated probability of change from ***Sentinel-2*** *and* ***Landsat-8*** *separately, and in panel 3 (top right) their jointly considered probability of change. Lighter areas are more likely change than darker areas. Panel 6 (bottom right): a 'thresholded' view of said estimate of change at 66% likelihood or greater, that a change has occurred in the Late Fire area (white is disturbed, black is undisturbed). Panels 4 & 5 (bottom left, bottom centre): representative NIR false colour for both years; such that lighter areas are exposed terrain, deeper, brown-tinged red indicated burned areas and brighter red areas are vegetation cover.*

12.3 Stable Forest

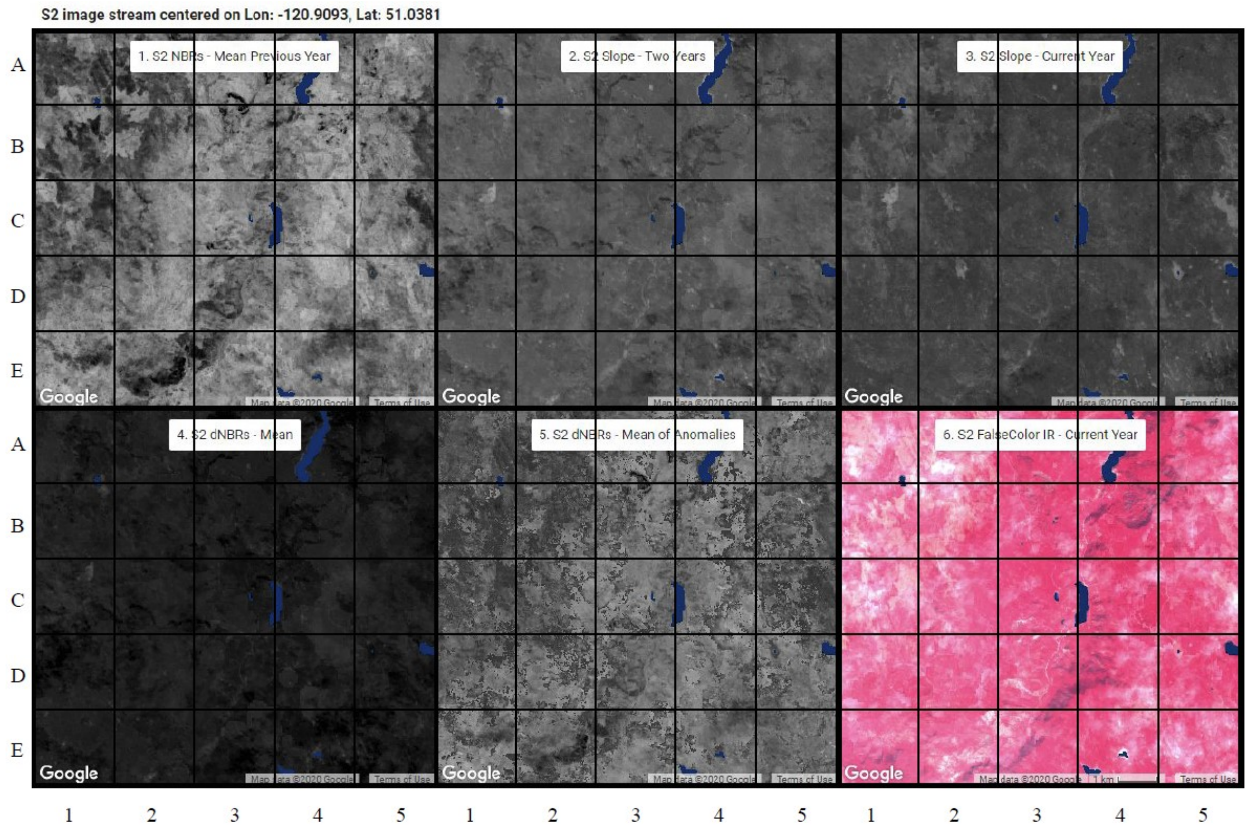

*Figure 30 Five criteria and a false-colour infrared representation of the target year for **Sentinel-2** in the Stable Forest area. Panel 1 (top left): the NBR for the previous year (2016) with dark areas showing low NBR values. Panel 2 (top centre): slope of the two-year regression line with values inverted such that more negative values are lighter in colour. Panel 3 (top right): slope of the one-year (2017) regression line, also inverted so that positive sloping trend lines are darker. Panel 4 (bottom left): the difference between average NBR values of 2016 and 2017, colour scale inverted such that a negative value (indicating loss of vegetation) is lighter in colour. Panel 5 (bottom centre): the anomalous NBR values of 2017 subtracted from the mean NBR values of 2016. Panel 6 (bottom right): false colour infra-red image of the scene with RGB channels using infrared, red, and green, such that lighter areas are thinner vegetation, and brighter red areas are vegetation cover.*

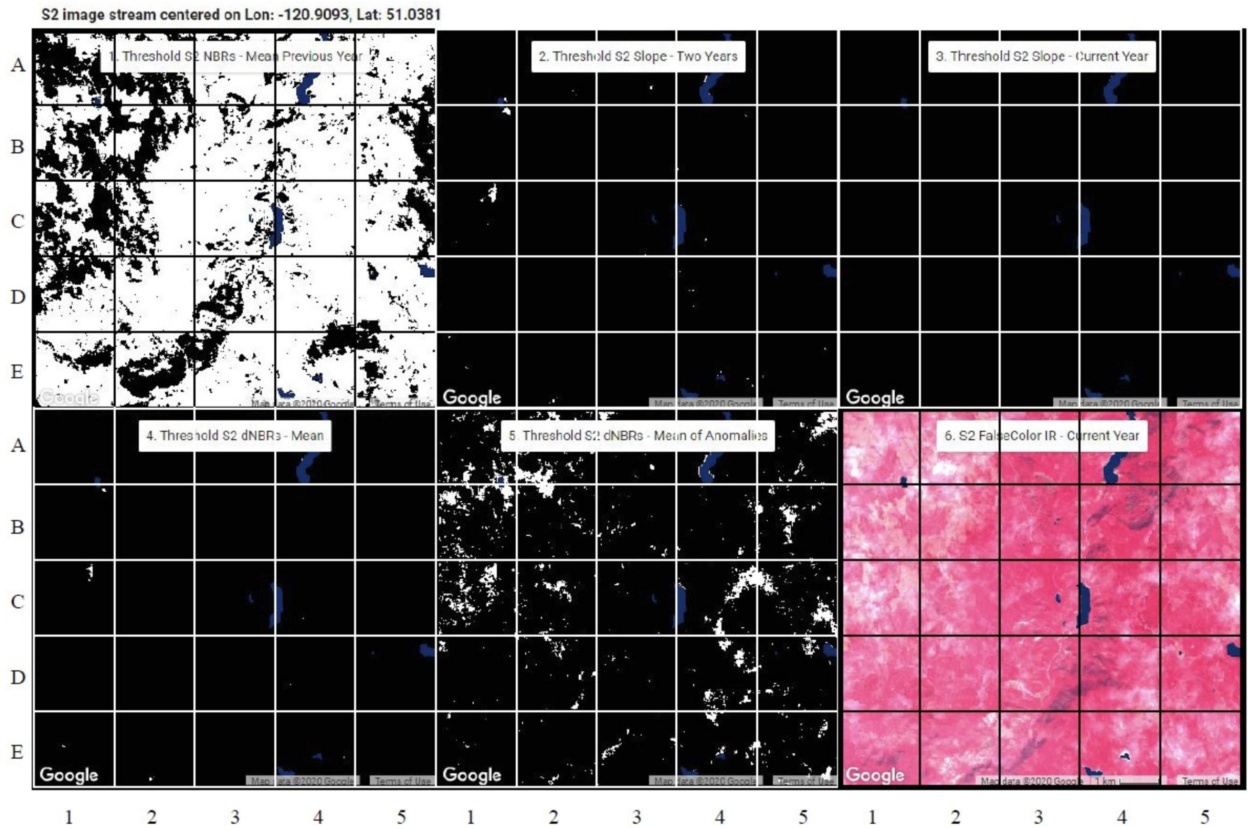

Figure 31 Panels 1 to 5 (bottom centre, left; top left, centre, right): Thresholds of the five criteria (7.5 Table 1) for ***Sentinel-2*** *in the Stable Forest area. Everywhere the threshold criterion is met the figure is white. Panel 1 (top left): Illustrating NBR values exceed that of a user-adjustable threshold of NBR and can be considered forest land cover. Panel 2 (top centre): the slope of the regression line for two years is sufficiently negative in areas reference data suggest is harvest. Panel 3 (top right): black areas indicate that no change occurs during the year 2017. Panel 4 (bottom left): the differenced Normalized Burn Ratio identifies areas of vegetation loss between prior year and target year, in white. Panel 5 (bottom centre): thresholding the captured anomalous dNBR values. Panel 6 (bottom right): false colour infra-red image of the scene with RGB channels using infrared, red, and green, such that lighter areas are thinner vegetation, and brighter red areas are more dense vegetation cover.*

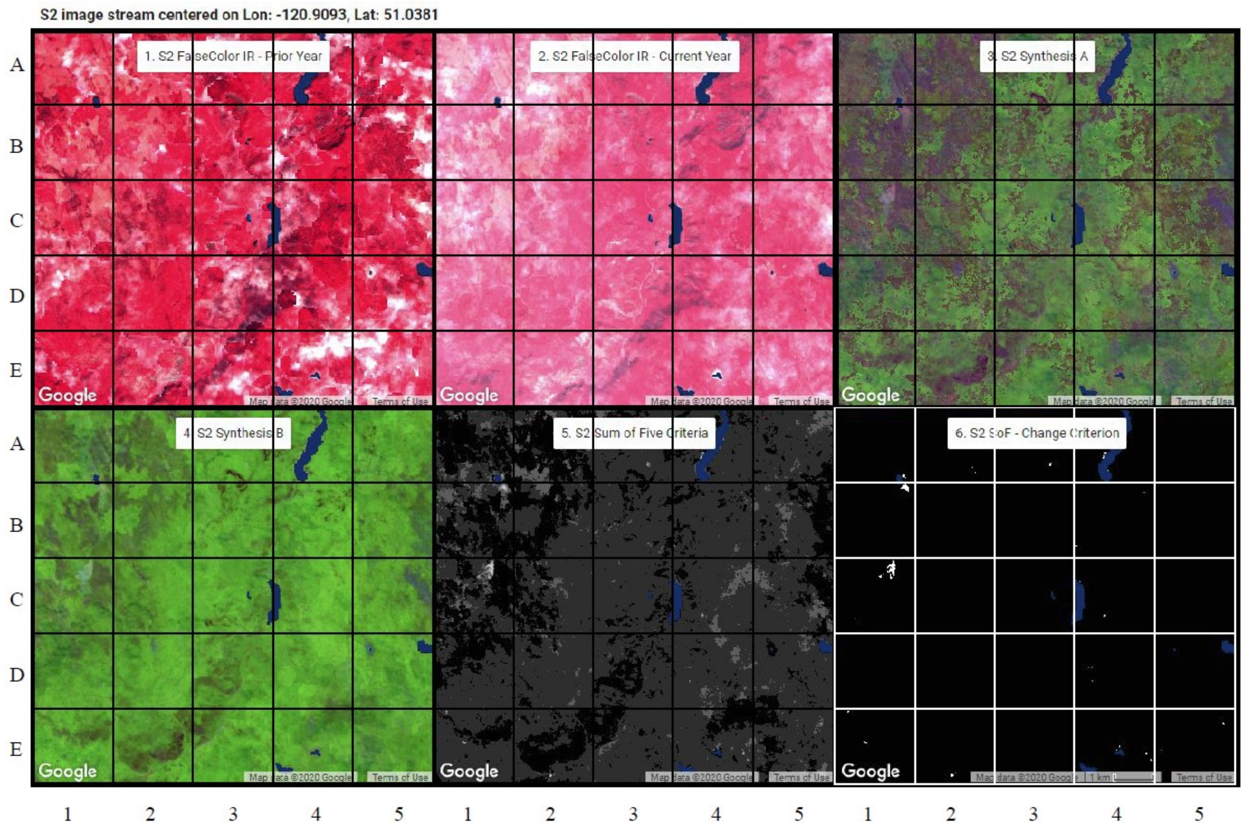

*Figure 32 Panels 1 & 2 (top left, top centre): Stable Forest area, **Sentinel-2** NIR false colour representative images for the earlier and later years respectively. Panel 3 (top right): RGB composite for Synthesis A. RED: Two-Year Slope inverse values; GREEN: anomalous NBR values from 2017 differenced from 2016; BLUE: Target-Year Slope inverse values. Panel 4 (bottom left): RGB composite for Synthesis B. RED: Two-Year Slope inverse values; GREEN: Target-Year mean NBR values; BLUE: Target-Year Slope inverse values. Panel 5 (bottom centre): summation of the 5 criteria. Panel 6 (bottom right): indicates areas of agreement between 3 or more criteria.*

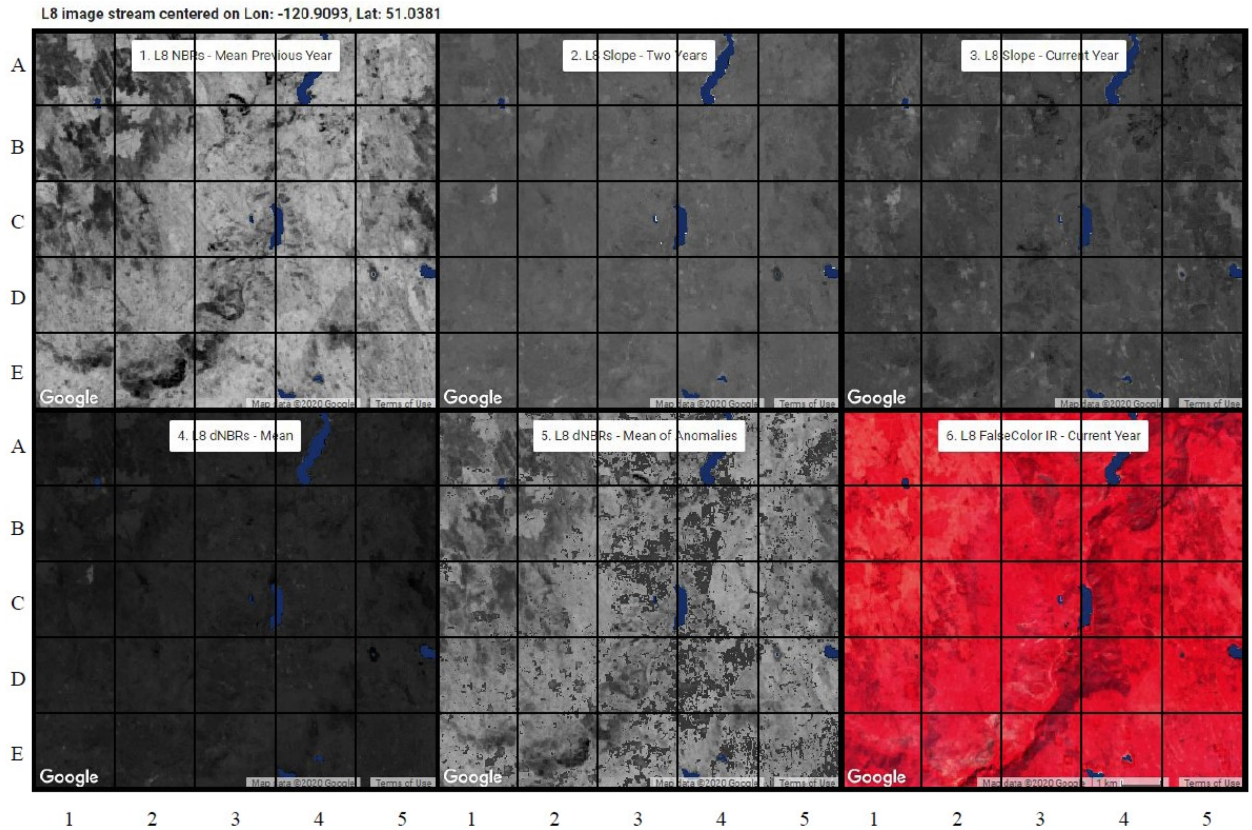

*Figure 33 Five criteria and a false-colour infrared representation of the target year for **Landsat-8** in the Stable Forest area. Panel 1 (top left): the NBR for the previous year (2016) with dark areas showing low NBR values. Panel 2 (top centre): slope of the two-year regression line with values inverted such that more negative values are lighter in colour. Panel 3 (top right): slope of the one-year (2017) regression line, also inverted so that positive sloping trend lines are darker. Panel 4 (bottom left): the difference between average NBR values of 2016 and 2017, colour scale inverted such that a negative value (indicating loss of vegetation) is lighter in colour. Panel 5 (bottom centre): the anomalous NBR values of 2017 subtracted from the mean NBR values of 2016. Panel 6 (bottom right): false colour infra-red image of the scene with RGB channels using infrared, red, and green, such that lighter areas are thinner vegetation and brighter red areas are more dense vegetation cover.*

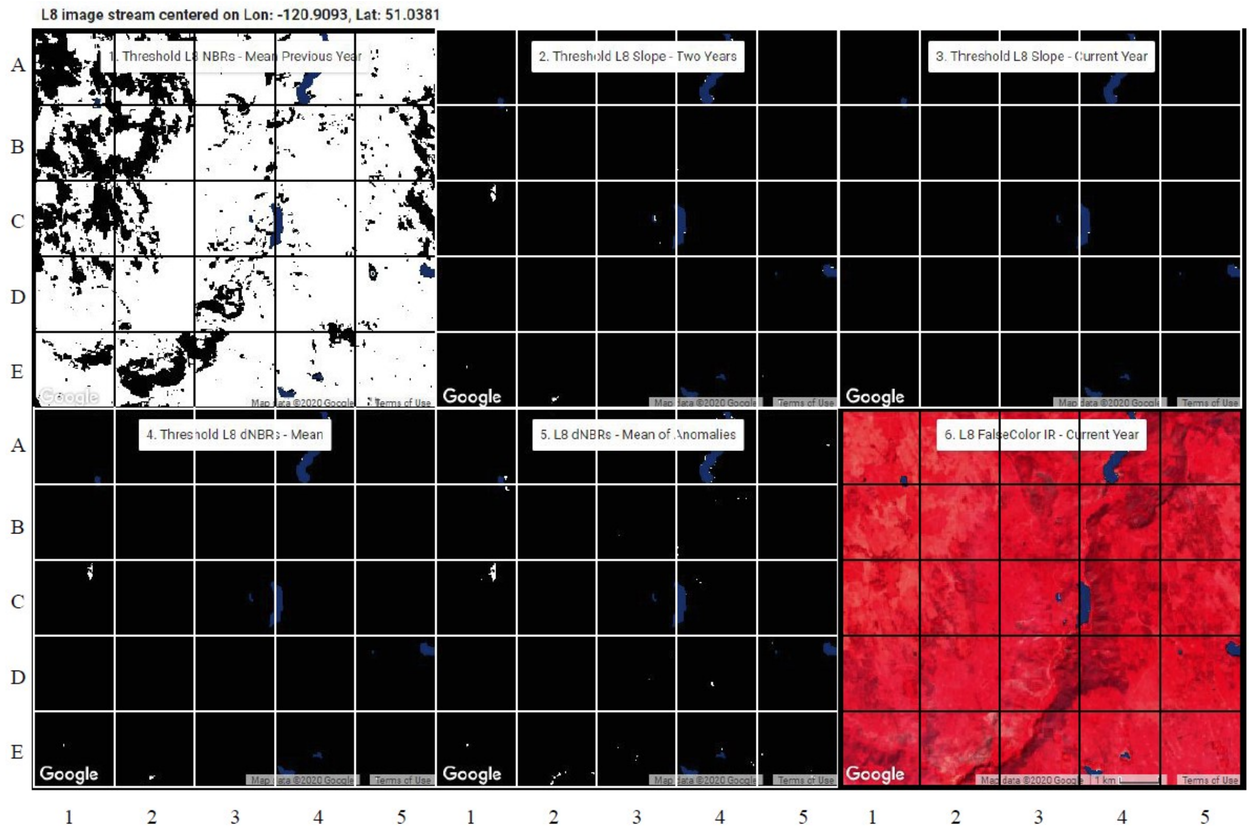

Figure 34 Panels 1 to 5 (bottom centre, left; top left, centre, right): Thresholds of the five criteria (7.5 Table 1) for ***Landsat-8*** *in the Stable Forest area. Everywhere the threshold criterion is met the figure is white. Panel 1 (top left): Illustrating NBR values exceed that of a user-adjustable threshold of NBR and can be considered forest land cover. Panel 2 (top centre): the slope of the regression line for two years is sufficiently negative in areas reference data suggest is harvest. Panel 3 (top right): black areas indicate that no change occurs during the year 2017. Panel 4 (bottom left): the differenced Normalized Burn Ratio identifies areas of vegetation loss between prior year and target year, in white. Panel 5 (bottom centre): thresholding the captured anomalous dNBR values. Panel 6 (bottom right): false colour infra-red image of the scene with RGB channels using infrared, red, and green, such that lighter areas are thinner vegetation and brighter red areas are more dense vegetation cover.*

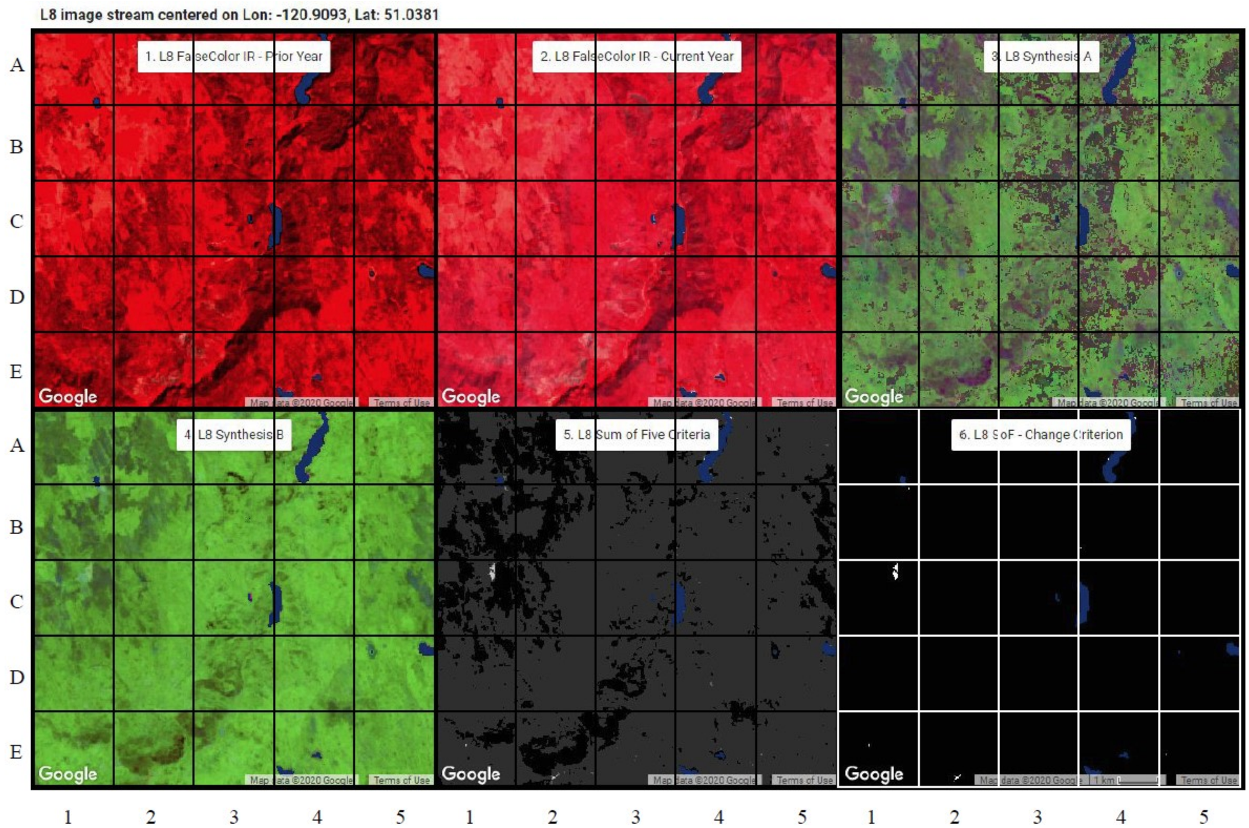

Figure 35 Panels 1 & 2 (top left, top centre): Stable Forest area, ***Landsat-8*** *NIR false colour representative images for the earlier and later years respectively. Panel 3 (top right): RGB composite for Synthesis A. RED: Two-Year Slope inverse values; GREEN: anomalous NBR values from 2017 differenced from 2016; BLUE: Target-Year Slope inverse values. Panel 4 (bottom left): RGB composite for Synthesis B. RED: Two-Year Slope inverse values; GREEN: Target-Year mean NBR values; BLUE: Target-Year Slope inverse values. Panel 5 (bottom centre): summation of the 5 criteria. Panel 6 (bottom right): indicates areas of agreement between 3 or more criteria.*

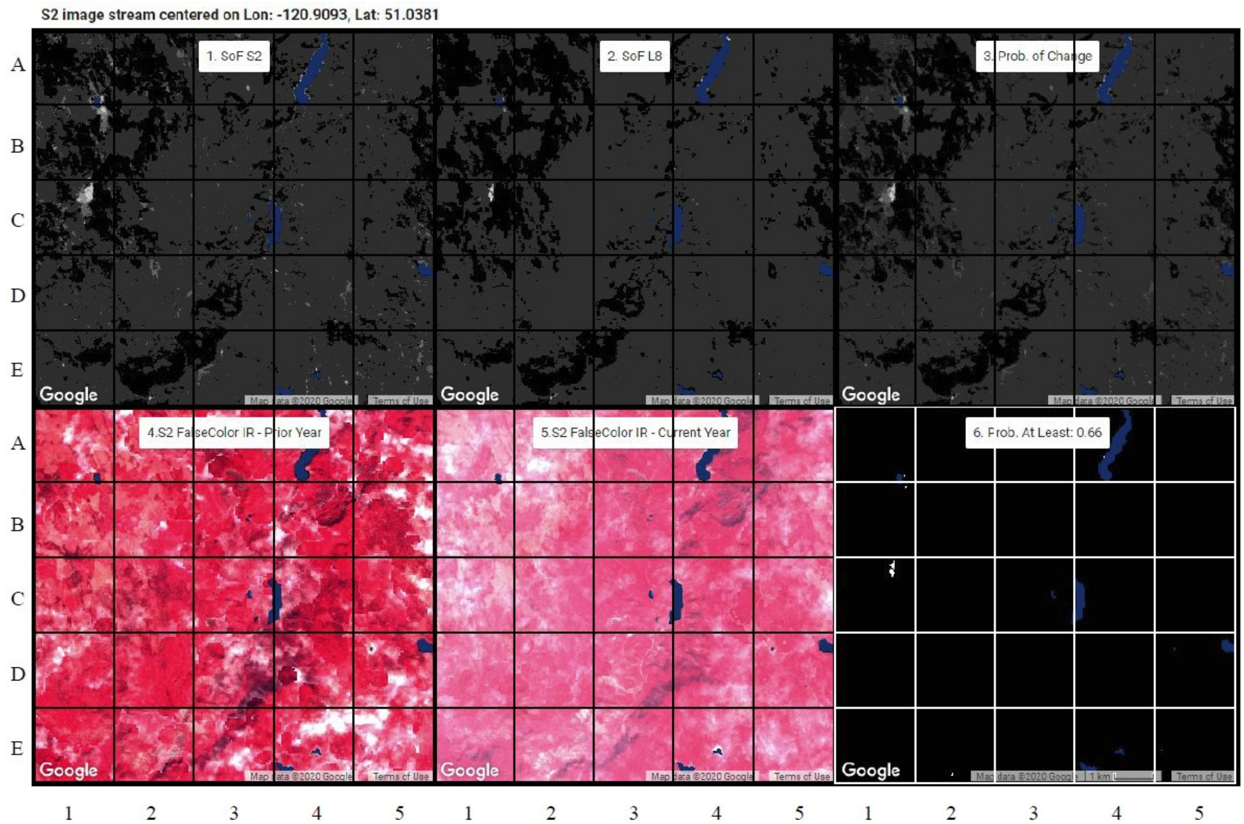

*Figure 36 Panels 1 & 2 (top left, top centre): an estimated probability of change from **Sentinel-2** and **Landsat-8** separately, and in panel 3 (top right) their jointly considered probability of change. Lighter areas are more likely change than darker areas. Panel 6 (bottom right): a 'thresholded' view of said estimate of change at 66% likelihood or greater, that a change has occurred in the Stable Forest area (white is disturbed, black is undisturbed). Panels 4 & 5 (bottom left, bottom centre): representative NIR false colour for both years; such that lighter areas are exposed terrain, deeper, brown-tinged red indicated burned areas and brighter red areas are vegetation cover.*